ACS OMEGA

Open Access

http://pubs.acs.org/journal/acsodf

Review

A Systematic Review of the Contribution of Additive Manufacturing toward Orthopedic Applications

Alphonsa Joseph and Vijayalakshmi Uthirapathy*

Cite This: *ACS Omega* 2024, 9, 44042−44075

Read Online

ACCESS | Metrics & More | Article Recommendations

ABSTRACT: Human bone holds an inherent capacity for repairing itself from trauma and damage, but concerning the severity of the defect, the choice of implant placement is a must. Additive manufacturing has become an elite option due to its various specifications such as patient-specific custom development of implants and its easy fabrication rather than the conventional methods used over the years. Additive manufacturing allows customization of the pore size, porosity, various mechanical properties, and complex structure design and formulation. Selective laser melting, powder bed fusion, electron beam melting, and fused deposition modeling are the various AM methods used extensively for implant fabrication. Metals, polymers, biocrystals, composites, and bio-HEA materials are used for implant fabrication for various applications. A wide variety of polymer implants are fabricated using additive manufacturing for nonload-bearing applications, and β-tricalcium phosphate, hydroxyapatite, bioactive glass, etc. are mainly used as ceramic materials in additive manufacturing due to the biological properties that could be imparted by the latter. For decades metals have played a major role in implant fabrication, and additive manufacturing of metals provides an easy approach to implant fabrication with augmented qualities. Various challenges and setbacks faced in the fabrication need postprocessing such as sintering, coating, surface polishing, etc. The emergence of bio-HEA materials, printing of shape memory implants, and five-dimensional printing are the trends of the era in additive manufacturing.

1. INTRODUCTION

When damage occurs, the human body can repair itself via biological mechanisms within the body.[1] But when the degeneration of bones happens beyond its critical capacity, external assistance is needed. Though traditional approaches like autografts, allografts, and xenografts can eliminate these problems, various unsought scenarios like the rejection of the foreign body and allergic responses and transmission of disease can occur.[2] To counterbalance this, various types of biomaterials are used for the fabrication of scaffolds and implants that can replace human bone such as bioactive glass, various types of ceramics, and metals like titanium (Ti) alloys, stainless steel, cobalt-chromium (Co-Cr) alloys, etc.[3] The main challenge for developing implants using biomaterials is that they should meet many requirements such as biocompatibility, proliferation, a suitable surface for cell attachment, and a porous structure for the transport of nutrients. Also, when a scaffold is used for bone regeneration, the cellular structures must possess adequate strength and capacity to absorb high-impact energy.[4]

Various conventional methods have been used for the fabrication of implants over the years such as casting,[5] electrospinning,[6] injection molding,[7] etc. The mechanical properties, loading of growth factors, and drug-releasing efficiency depend greatly on the porosity and pore structure of the implant fabricated. It is not an easy task to develop implants with precisely controlled pore size and the special distribution of these interconnected pores with desired geometry.[8] It is always a challenge to prepare bioscaffolds and implants using these methods that possess the ability to mimic at least to some extent the properties of an extracellular matrix (ECM) that can prompt cell differentiation and proliferation since the implants have to effectuate the bridging/repairing of damaged bone sites.[9] Implants with fitting biochemistry and nanoscale topology to heal the trauma are also a rigorous task in conventional methods. It is needed to have multistructural and multiple-performance implants with multimaterials that can mimic natural bone structure in all aspects, whose fabrication is a strenuous task in conventional methods.[10] Another problem of conventional methods is the long duration it takes for the fabrication of an implant and its postprocessing. Patient-specific implants are an arduous task,

Received: May 23, 2024
Revised: August 13, 2024
Accepted: September 19, 2024
Published: October 25, 2024

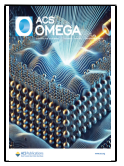

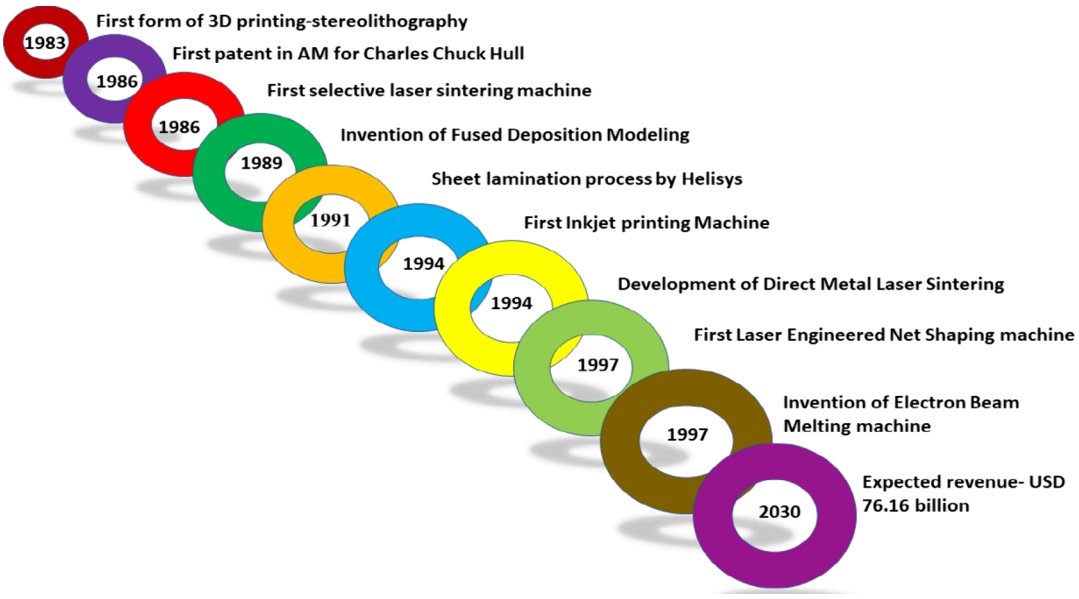

Figure 1. Milestones in the growth of AM.

and their design change can imply the work from scratch.[11] While fabricating the implants using metal alloys for load-bearing application, the latter will be stiffer than the host bone which can induce stress shielding that can instigate osteoporosis at the area of minimum stress.[12] In orthopedic oncology, though modular endoprosthesis is an option for young patients with malignant bone tumors, the availability of custom-made modular implants for unusual sites, such as the pelvis, is not high. Moreover, when limb salvage surgery is done using conventional implants for the tumors at joints or physis, it can lead to arthroplasty sacrifice of the joints.[13] The amount of waste materials formed by various conventional methods, especially subtractive technologies, is huge since it needs a lot of cutting and shaping for a patient-specific implant.[14] For these reasons, additive manufacturing has been preferred for improving surgical results.

Additive manufacturing is the process of layer-by-layer fabrication of structures using metals, polymers, ceramics, or composites with a computer-aided program. ASTM defines additive manufacturing (AM) as a process of joining materials to make objects from 3D model data, usually layer upon layer.[15] In a virtual environment, the surface file is sliced, and the AM machine makes a tool path for structures with the aid of those files, which in turn is added layer by layer to make a three-dimensional structure.[16] The development of functionally graded material is possible in AM, and improvement of certain properties of the desired compound could be done in this way.[17] Without additional tooling or manufacturing costs, greater customization of the product is possible, and a design-to-component direct translation takes place.[18] With an easier method to design even complex structures, with the aid of computer technology, even hollow or lattice structures can be designed.[19] When a correction of the structure is needed, only the design must be changed in the software to optimize the structure. Maximum utilization of the raw material helps to avoid large waste production and makes the process more cost-effective.[20] With quick processing using less manpower, the development of the product is very fast.[21] Considering the medical field, the main challenge we are facing in implantation is patient-to-patient-specific implants with biocompatibility and a high rate of precision.[22] Completely customized products with this specification are produced in additive manufacturing, and the greatest possibility of the preparation of the porous structure is possible which cannot be provided by other conventional methods.[23]

The history of additive manufacturing goes up to 1983 when the first form of additive manufacturing, stereolithography, was introduced by Charles Chunk Hull who used UV light to photocure a liquid polymer in a layer-by-layer manner. As the down layer was hardened, further layers were added in the same manner, and the desired form was produced.[24] Though the patent was granted for this system in 1986, it took years to develop it further, avoiding the limitations faced in the process. The second process that developed further was selective laser sintering (SLS) in 1986 by Dr. Beaman and an undergraduate student Carl Deckard.[25] Around the same time, Scott and his wife Lisa Crump developed a fused deposition modeling (FDM) in which a thermoplastic was heated and deposited on a substrate in a layer-by-layer manner.[26] Inkjet printing was introduced by Roy Sanders in 1994 which was a developed form of stereolithography with the difference that hot thermoplastic wax was used to build the sample. High-resolution models were formed using this new machine which gained popularity in the jewelry industry within no time.[27] Direct metal laser sintering (DMLS) was performed using machinery only by the end of 1994. Dr. Hans J. Langer and Dr. Hans Steinbichler developed this new machine, and they could sinter metal powder such as Cobalt (Co), Aluminum (Al), Nickel (Ni), Stainless steel (SS), and Ti alloys.[28] The growth of AM technology took a new turn when laser-engineered net scanning (LENS) was proposed in New Mexico in the year 1997. A high power laser was used to melt the metal, and it got deposited on the substrate. Since both the base and head are made mobile, only in selected areas will the metal mold get deposited.[27] Electron beam melting (EBM) was also developed around this time. Arcam AB developed this method, and the procedure was to shoot an electron beam only on the selected areas of a powder bed which will eventually melt and a layer is formed. The process is repeated until the desired product is obtained. Ever since. EBM has been used in the production of

https://doi.org/10.1021/acsomega.4c04870
ACS Omega 2024, 9, 44042−44075

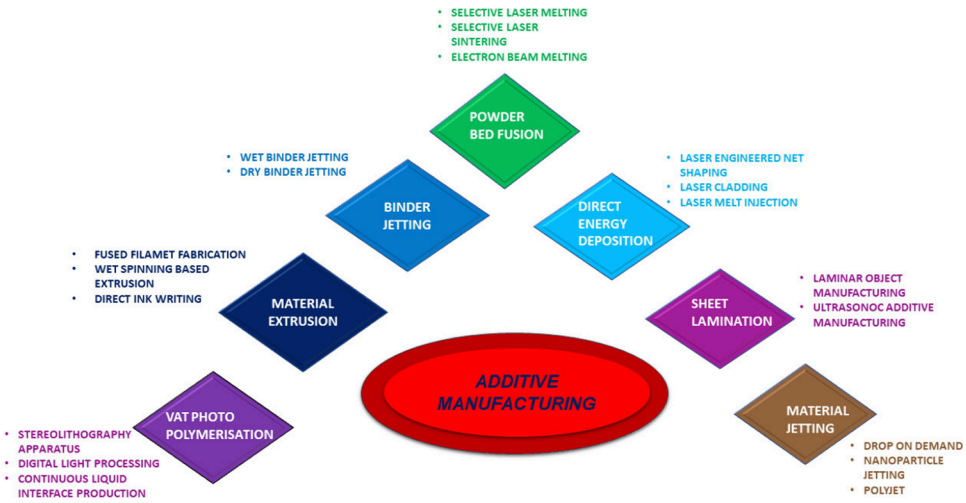

Figure 2. Various additive manufacturing methods.

biomedical implants and the aerospace industry.[29] The journey of additive manufacturing continues with a higher growth rate in the automotive, aerospace, and medical industries.

The general mechanism for the designing and fabrication of complex structures through additive manufacturing[30] is depicted below.

1) A computer aid design is made using the help of a CAD file - generation of the geometry of the part.
2) Conversion of the file formed into a printing format - Standard Tessellation Language (.STL) file format is used for this purpose. This file defines the surface geometry using a no. of triangular facets.
3) Slicing of the model - the STL model is sliced into cross-sectional layers since AM is the layer-by-layer fabrication.
4) Tool path generation and G-code for formation - considering factors such as counters, zigzag, etc. as infill patterns and residual stress evolution, the tool path is created and the tool path is converted into G-code. Thus, the path for fabrication is created.
5) Setting up of the machine into an appropriate printing condition - Many variables need to be taken care such as the layer thickness, traveling speed, the type of material to be used, support type, the temperature of the build plate, etc.
6) Layer by layer of the printing of the material - since the printing is automated, it is very easy to print and less monitoring is needed.
7) Postprocessing of the material prepared - it is not needed for all the AM techniques. When photosensitive resins are used (such as in SLA), curing is needed. If the support form is used, that also gets removed in this step. After the postprocessing, the printed material is ready for application.

2. ADDITIVE MANUFACTURING METHODS

2.1. Vat Photopolymerization. In Vat photopolymerization, the objects are developed by solidifying a liquid photosensitive resin using ultraviolet (UV) light. While securing cohesion from photopolymer, the material gains mechanical and clinical properties desired of a scaffold.[31] Vat polymerization includes various methods such as Stereo Lithography Apparatus (SLA), Digital Light Processing (DLP), and Continuous Liquid Interface Production (CLIP).[32] The surface printed part of the product in this method gives a more finished product since the printed part is dipped in a monomer liquid. This method is mainly used for the production of ceramic-based implants, but the sedimentation of the latter is the main challenge faced, resulting in the nonuniform density of implants.[33]

In SLA, the photopolymer liquid is allowed to be exposed to the laser beam in a nitrogen or argon gas atmosphere. The material, after interacting with the laser undergoes photopolymerization and eventually hardens to become part of the solid layers. A support plate or print bed that is used in the base layer is removed when the first layer is scanned. Material that has not undergone photopolymerization remains in liquid form, and the penetration of the light-treated sample into that of the nonpolymerized sample can cause the production of a distorted structure. Unexposed sample here cannot be reused or treated as supporting material.[34] Allowing the customization of the product, it is a fast and cheaper printing technique and can provide more control of local techniques.[35] The usual thickness of the layer is in the range of 20−100 μm, and this range can provide a fine resolution and powder flowability. If the particle size is large, it results in poor resolution, and if the particle size is small, agglomeration due to van der Waals force takes place. Since sintering and melting temperatures are absent here, this process can provide a rather smooth surface. Another drawback of this method is the lack of available photopolymers for the process. Mixing composites like hydroxyapatite (HAP) in an optimum measurement with photopolymers is widely used now in this method to overcome the above-mentioned problem.[36]

Another Vat Polymerization method is DLP where UV or blue light projections of the object's cross-sectional image are used for polymerization instead of a laser. This method provides a better resolution of around 70 μm, and the processing speed is much faster.[37] With a low consumption of energy and less use of organic solvents, this process can provide sophisticated designs with high printing accuracy.[38] Continuous Digital Light Processing (cDLP) is the better version of DLP because it makes use of a continuous digital projection of images of each layer to create a smoother transition from one layer to the next, which offers the product with a higher resolution and smoother surface and rather easy

https://doi.org/10.1021/acsomega.4c04870
ACS Omega 2024, 9, 44042−44075

manufacturing.[39] In CLIP, the bottom of the container accepts the UV light and the layer gets cured. Though vat photopolymerization provides the product with a good surface finish and high accuracy, the postprocessing is very lengthy.[40] Studies have been done on using CLIP-manufactured biocompatible resins for drug delivery applications,[41] dental occlusal devices,[42] etc.

2.2. Material Extrusion. Material extrusion (ME) uses a single material or a number of materials that are either in a liquid state, viscous gel, or amorphous solid to form a continuous filament. Here, a heated nozzle is used to fill the sample, and the sample gets deposited layer by layer. The main advantage of this method is that there will not be unused powder material since a secondary nozzle is provided to add supporting material with inferior qualities to that of the main model material which could be removed once it serves the purpose.[43] The most used technique of this method is fused filament fabrication (FFF) or the fused deposition method (FDM), where the filaments are squeezed from one or more extruders after heating thermoplastic materials. The molten polymers are then deposited on a platform, which is fused to form a 3D structure. FDM is widely investigated in fabricating ceramic, metal, and polymer composites.[44] When metal or ceramics are used, they must be premixed with polymers, followed by extruding in feedstock filament for additive manufacturing. After the process, the polymer used as a binder must be removed at a high temperature, followed by sintering. The thickness of the layer, its width and orientation, and the air gap between the layers are important parameters that need to be attended to while choosing this method.[45,46] Though the low cost, simplicity of the process, and high speed are the benefits of this method,[47,48] interlayer distortion, layer-by-layer appearance, poor surface quality, very law resolution, and fewer no. of materials to be used in this method are the main drawbacks here.[49] Another disadvantage observed in this method is that the bonding strength in the building direction decreases significantly since the heated material is deposited on the previous layer that has already been cooled off.[50] The anisotropic mechanical behavior is shown by most of the products, since the components used are not melted fully before they undergo additive manufacturing. Another negative impact is the detrimental effect of the high degree of temperature that affects the bioactive sample. To avoid this, the scaffold undergoes bioactive agent postfabrication.[51]

Wet Spinning Based Extrusion is another material extrusion method that uses only very low temperatures, and so it finds a solution to most of the temperature-related challenges brought about by fused filament fabrication. The biological and mechanical properties of the scaffold can be improved by mixing the polymer with bioglass or ceramics.[52]

Direct ink writing (DIW) is also an ME method where liquid-based suspensions are used, and the base material is thinned using water or other suitable solvents before extrusion. Fluid materials like pastes, solutions, and hydrogels are extruded through the nozzle with the help of a piston or a screw system or by pneumatic pressure. The rheological properties and viscosity of the ink used are crucial here.[53] The slurry is carefully selected to target specific mechanical and biological behaviors of the resulting scaffold. The thinning medium plays the double role of transforming the powder into a slurry form and binding the powder particles together. Water can be used as an ideal solvent that does not bring about toxicity for bioactive agents.[54] ME is used for the fabrication of implants widely due to the simplicity in production, ease of development of material, and manufacturing of scaffolds with the finest details within a shorter time even by modulating the porosity.[55] Studies have proved that polycaprolactone (PCL),[56] polylactic acid (PLA),[57] poly(lactic acid-*co*-glycolic acid) (PLGA),[58] bioglass,[59] etc. could be made use of in this method for the successful fabrication of scaffolds.

2.3. Binder Jetting. It is one of the main methods used in AM for the engineering of bone tissue engineering scaffolds. Binder jetting (BJ) uses powder materials and an adhesive for manufacturing implants. In the first step, a uniform thin layer of powder bed consisting of a ceramic, metal, or polymer is formed with the help of a roller. Then a binder in liquid form is printed into a powder bed and then forms a product layer by layer, which acts as a glue that can provide temporary strength to the binding part. At the curing temperature of the binder, further heat treatment is given to provide greater strength for the product.[60] The size of the nozzle, extrusion rate, printing speed, viscosity of the ink, particle size distribution, porosity of the powder, and morphology are the main factors that must be considered here. The usual powder size range is 10−50 μm. The resolution of the product is determined by the precise delivery of the binder.[61] Metals, ceramics, etc. can be used in this method both in the form of wet and dry powder. Since the large particles give greater flowability and low surface area, they are used in dry binder jetting, whereas the small particles are used for wet binder jetting since those particles which are made into slurry provide easy absorption of moisture due to large surface area.[62]

Fast and efficient, this method offers more flexibility and a high tolerance for designing and printing complex implant structures, mostly in ceramics.[63] Without the help of a support structure, a wide range of materials could be printed with higher scalability. This method is mainly used to prepare only large-size implant materials due to its easy fabrication with the help of thousands of jets that can work parallelly.[60] The ability to incorporate functionally graded materials[64] and bioinks loaded with drugs[65] makes this method more acceptable in implant fabrication. The main challenges of this method are low printing resolution, very low precision, surface roughness, and weak binding between layers.[66]

2.4. Powder Bed Fusion. This process consists of thin layers made of very fine powders that are spread well to make a platform. A laser beam or binder is used to make such a film, and subsequent layers are rolled up one above the other. The powder size distribution and packing have to be taken into account since it determines the density of the printed part.[67] The liquid binder can be used for higher temperatures, but the laser method can be applied only to low-melting powders. Selective laser sintering (SLS) can be applied to a variety of metals, alloy powders, and polymers. Selective laser melting (SLM) is done only on a few metals such as aluminum and steel. SLM can provide superior mechanical properties since here the powder is melted at an elated temperature, which leads to a complete fusing. SLS does not give this result since the powder is not melted fully but allows the fusion of the powder only on the surface but not the entire powder. Other advantages offered by SLM methods are the easy fabrication of the product, greater flexibility, and near-net-shape production.[68]

Layer thickness, hatch spacing, scanning speed, and characteristics of laser powder are important parameters to be considered when the SLM method is followed because they

https://doi.org/10.1021/acsomega.4c04870
ACS Omega 2024, 9, 44042−44075

can influence the volumetric energy density that can heat the powder. Balling can take place when the energy is insufficient due to low laser power, large layer thickness, and high scanning speed that cause a lack of wetting of the molten pool.[69] On the other hand, if the scanning speed is low and laser power is high, the result would be extensive material evaporation. Lack of fusing of adjacent species could result from poor hatch spacing which in turn results in the porosity of the product. Another problem faced by this method is the condensation of volatilized materials that prevent the proper delivery of laser power.[70]

An actual melting is not triggered in SLS, but the temperature is raised by using a laser source below the melting point of the powder chosen. The advantage of this method is that avoiding of a temperature up to the melting point helps to preserve the microspace between the powdered particles that can provide a porous structure to the material formed. So careful optimization and choice of apt grain sizes are very important to develop a desired product. Studies have proved that the SLS method can produce structures with macropore resolution of 400 μm and interparticle spacing of 50 μm.[71] Scaffolds produced via this method possess higher density and greater mechanical characteristics.[72]

The Electron Beam Melting (EBM) process works with the same principle as that of the SLM method. The only difference is that the former uses an electron beam as an energy source, while the latter depends upon laser energy. The main advantage of this method is that EBM can provide greater resolution and accuracy.[73]

PBF provides an advantage in printing complex structures since the unused powder can act as a support material that can help to withstand the high temperature during the process. To achieve the desired mechanical and physical properties of the product, the quality of the laser powder, layer thickness, and scan speed are to be optimized. Usually, the process is carried out in a closed environment to avoid oxidation especially when the work is carried out on Ti and Al.[74] Polymers, ceramics, metals, or alloys can be feedstocks for the fabrication of implants using PBF for load-bearing applications. It provides ease of fusing implants and bones because of the option to fabricate implants with a definable degree of surface roughness and desired lattice structure, and it makes this method more acceptable. Though fine resolution and high quality of printing are the advantages of this method, slow process, high cost, and high porosity of the product are the main disadvantages that need to be rectified in this area.[75]

2.5. Sheet Lamination. In the sheet lamination (SL) AM process, instead of metal powder or wire, foil is used as the feedstock. The 3D objects are formed with the help of energy sources, such as lasers or ultrasound. In ultrasonic consolidation, the interfaces of the metal sheet stacks are diffused with the help of ultrasonic waves. The desired geometry via the cutting process is done before treatment with ultrasonic waves (form-then-bond method). In the bond-then-form method, cutting is done after manufacturing. Since the frictional heat is produced at the interface of the sheets, the temperature in the coalesced region increases gradually. To avoid its effect on the product, before each layer is formed, a slight cooling is allowed.[76] SL can be classified into laminated object manufacturing (LOM) and ultrasonic additive manufacturing (UAM). Processing of multimetals is possible in SL.[77] The resolution of the print depends on the printing speed, cross-hatch size, laser power, and temperature applied during the process. Among all the AM processes, SL is the least accurate method and is used for very few applications in the medical field, but the process is fast and cost-effective.[78] Unlike other AM methods, no postprocessing is to be followed, and the parts have high durability. This method has been used for processing simpler prototypes and casting molds without the help of a supporting structure. Metal-filled tapes, papers, ceramics, and polymer composites are usually used in this method.[79]

2.6. Direct Energy Deposition. Direct Energy Deposition (DED) is mainly applied to the preparation of high-performance superalloys. Either a laser or an electron beam is used to melt the implant surface that eventually fuses while cooling. A higher amount of energy is used for this process, and a layer-by-layer fusion of the material takes place which helps to fill the crack effectively that could be formed during manufacturing.[45] The use of multiple materials and multiple-axis deposition is allowed in this method. High-speed and large work envelopes are offered in this method, and this method is applied for the manufacturing of larger components. Less manufacturing time and cost with high mechanical properties can bring about a controlled microstructure and accurate composition control.[80]

There can be three types of processing using the laser beam, such as laser engineered net shaping (LENS), laser cladding, and laser melt injection. LENS is a direct laser deposition technique in which the feedstock could be a powder, wire, or filament to form a three-dimensional unit. A high-power laser of about 4 kW is used which is then focused onto the converging point where the powder sample is delivered using an argon pressurized nozzle.[81] In the laser method, a melt injection powder form is used, and in laser cladding a wire type material is used.

In the electron beam DED process, an electron beam is used to melt the scaffold surface. All of the manufacturing parameters, including the mechanical properties, porosity, surface roughness, and geometrical properties, are optimized and controlled using software that can direct the fabrication of sound parts. Scanning algorithms are created as required for the geometry, and using the software minimum and maximum beam currents are controlled, beam scan repetition time is maintained throughout the manufacturing, the speed of the electron beam and distance between the scan lines are adjusted, and the hatch pattern line order and rotation angle of consecutive hatches are controlled. Studies have proved that the elevated build temperature in this process is responsible for lower residual stresses of the products.[82] Superalloys,[83] Ti-based alloys,[84] Co-based alloys,[85] etc. could be used for implant fabrication via this method. This method gained its acceptance due to the ability to utilize the fabrication of structurally graded materials with varying porosity at various parts of the component.[86]

2.7. Material Jetting. Material jetting (MJ) is a process in additive manufacturing where the liquid materials are sprayed using an extruder, and the tiny droplets thus formed get solidified when light falls into them. The support that is used is removed by using a solvent. The main advantage of this process is that with the help of different extruders, various materials can be used at the same time for the formation of the desired product. The material jetting process can be further classified into drop-on-demand (DOD), nanoparticle jetting (NPJ), and polyjets (PJ). In the DOD, the materials are injected for layer formation. As the name describes, nano-

https://doi.org/10.1021/acsomega.4c04870
ACS Omega 2024, 9, 44042−44075

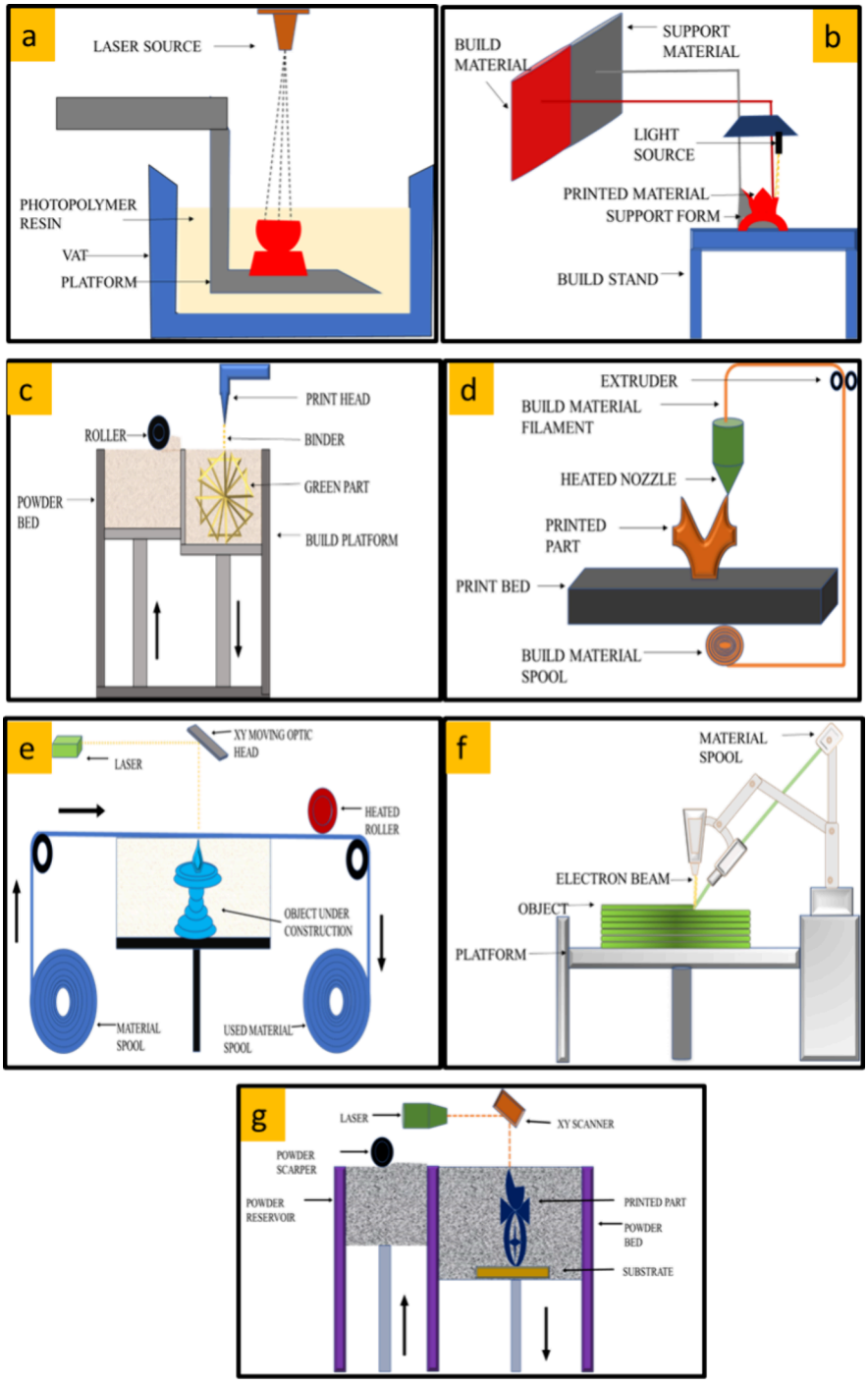

Figure 3. Schematic representations of a) Vat photopolymerization, b) Material jetting, c) Binder jetting, d) Material extrusion, e) Sheet lamination, f) Direct energy deposition, g) Powder bed fusion.

particles are used in NPJ as feedstock, and very thin layers are formed by jetting them. PJ printing is similar to inkjet printing where the materials sprayed get cured immediately with the aid of a UV light source.[87] Usually, photopolymers, metals, and ceramics are used for this method. Though this process provides products with higher accuracy, the mechanical properties are very poor.[88]

Another classification given for MJ is inkjet printing and multijet modeling. In inkjet printing, the liquid droplets follow a predetermined path to be printed and solidified in a layer-by-layer manner. Either a pressurized system or a thermal system can be used for the extrusion of the droplet.[89] Ink viscosity, extrusion temperature, and pulse frequency determine the resolution of the printed sample. The usual nozzle size is 10−30 μm, and the volume of the material deposited could be controlled along with its position. High-speed printing is possible, and the versatility of the printed material is the beauty of this process.[90] The main advantage of this method is that even biological materials like proteins and nucleic acid could be printed along with nanoparticles, ceramics, and various polymers such as biological, structural, and conductive polymers.[91,92]

https://doi.org/10.1021/acsomega.4c04870
ACS Omega 2024, 9, 44042−44075

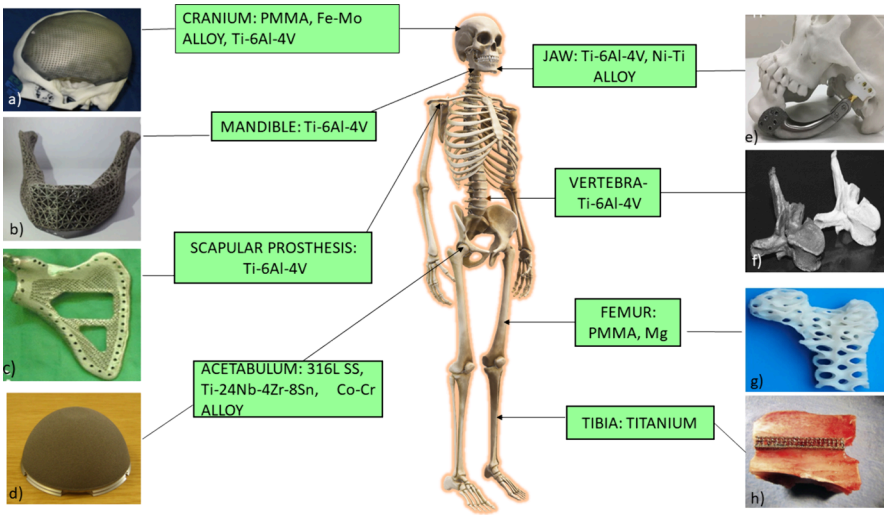

Figure 4. Various materials used in AM and examples for various implants fabricated a) cranial prosthesis fabricated using Ti-6Al-4V. Adapted with permission from ref 98. Copyright 2016, Elsevier, b) mandibular reconstructed using Ti-6Al-4V. Adapted with permission from ref 99. Copyright 2018, Springer Nature, c) scapular prosthesis manufactured with Ti-6Al-4V. Adapted with permission from ref 100. Copyright BioMed Central, d) acetabular cup fabricated using Co-Cr alloy. Adapted with permission from ref 101. Copyright 2013, Elsevier, e) maxillofacial reconstruction with the help of Ti. Adapted with permission from ref 102. Copyright 2022, Springer Nature, f) vertebra fabricated with Ti-6Al-4V. Adapted with permission from ref 103. Copyright 2006, Elsevier, g) Femur bone reconstructed using Mg. Adapted with permission from ref 104. Copyright 2020, Elsevier, h) tibia bone implant fabricated using Ti. Adapted with permission from ref 105. Copyright 2016, Elsevier.

On the other hand, multijet modeling includes multiple numbers of nozzles to extrude the materials, and the simultaneous deposition of these materials is possible to create a printed sample. A support material is needed while printing, which is to be removed using a water jet or by peeling off after the process is done.[93] The peculiarity of this method is that printing complex objects is possible with high resolution and accuracy and with a smooth surface finish. Using mechanical planarization helps maintain the exact layer thickness by removing excess material. The development of controlled bioactive surfaces and cellular scaffolds is the main application of this method.[94] MJ is used nowadays for the preparation of scaffolds for tissue engineering,[22] customized anatomical models,[95] and lifestyle wearable products.[96]

3. MATERIALS USED IN ADDITIVE MANUFACTURING OF ORTHOPEDIC IMPLANTS

On account of patient-specific implants, the material chosen for AM should be able to withstand structural and morphological tailoring. Biofunctionality of the material is another factor that is to be considered along with the mechanical properties that are comparable to human bone.[97]

Figure 4 represents various materials used in additive manufacturing and its applications.

3.1. Polymers. Polymers are used in orthopedic scaffolds for nonload-bearing applications such as craniomaxillofacial scaffolds based on their degradation rate and mechanical properties.[106] They have been mainly used for the replacement of trabecular bone since it has a compressive strength similar to this bone, as well as moderate degradation, and a pore size that can provide interconnectivity with bone tissue.[107] Though widely used, polymers still have a great way to go because of their lack of mechanical stability and controlled porosity. Even though conventional methods such as electrospinning,[106] freeze-drying,[108] laser machining,[109] etc. can enhance the properties of the polymers tailored, a satisfactory improvement cannot be brought about by these methods. For example, in the gas-foaming method, porosity cannot be controlled, while cell seeding becomes inefficient in the freeze-drying method. Wastage of raw materials and a higher processing time are other setbacks for these methods.[110]

AM is sought after today to overcome these challenges. Polymers can be used for additive manufacturing by using various techniques such as BJ, ME, PBF, and vat photopolymerization. In SLA, photopolymer resins are usually used by activating them using UV radiation, which can enhance the polymerization.[111] Dhandapani et al. developed a cortical screw with PLGA using FDM with porous interconnections that could provide a native bone effect, bear the stress-shield effects, and was biodegradable. A 5 ×10 mm screw stem could be printed using AM without any deformities and with 45% fill density and 259 × 207 μm pore dimension that helped the screw to mimic the natural bone in biocompatibility and mineralization studies, and the *in vivo* studies showed less immunogenicity and more neovascularization compared to nonporous screws. The porous interconnectivity provided by the fabrication reduced the Young's modulus to 482.79 MPa in comparison with the usually used Ti (110 GPa).[112]

Patient-specific implants have been proposed by Espalin et al., who prepared scaffolds that could replace femur and cranial bones with the aid of FDM using poly(methyl methacrylate) (PMMA). While varying the porosity from 50 to 70%, it was observed that the compressive strength varied from 7 to 16 MPa and the stiffness decreased from 248 to 165 MPa.[113] Mota et al. attempted to develop scaffolds using subtractive rapid prototyping (SRP) using poly[(*R*)-3-hydroxybutyrate-*co*-(*R*)-3-hydroxy hexanoate) (PHBHH) with a laydown pattern of 0−45°, pore size down to 115 μm, and fiber diameter down to 47 μm that could not be achieved by other conventional methods that possessed a compressive strength of 0.84 MPa, and the tests proved that the aligned fibrous structure with desired porosity showed up to 36% of seeding efficiency in the biological evaluation, and the scaffold proved to enhance bone regeneration.[114] PCL was used by Mazzoli et al. for preparing a

https://doi.org/10.1021/acsomega.4c04870
ACS Omega 2024, 9, 44042−44075

scaffold via SLS that can be used for skeleton damage repair with tailored porosity (500 μm) and interconnectivity that can transfer nutrients and aid in bone development in a controlled manner. The scaffold showed 47.66% porosity that could be obtained by the SLS method and 3.6 MPa strength that falls within the range of trabecular bone.[115] Kosorn et al. incorporated poly(3-hydroxybutyrate-*co*-3-hydroxy valerate) (PHBV) to increase various properties of PCL while preparing scaffolds using FDM for cartilage regeneration. Addition of PHBV to PCL in FDM reduced the pore size from 205 to 191 μm. It was observed that the oxygen plasma treatment of the scaffold increased the surface roughness from 39 to 99 nm, and the hydrophilicity of the scaffold observed via contact angle measurements changed from 86° to 102°, which in turn enhanced cell proliferation, and the compressive strength of the sample was also high with the blending of PHBV (8.34 MPa for 50% PHBV and 15 MPa for 75% PHBV).[116] Polyamide 2200 (PA2200) was used by Sing et al. for fabricating a three-dimensional scaffold, and the *in vitro* studies suggested that the scaffold is a good choice for skull repair. The increase in laser power from 50 to 70%, increased the strength of the porous part, and the compressive strength was observed to be 8.85 MPa, and the scaffold had a desired porosity of 1.2 × 1.2 mm^2.[117]

PCL/Chitosan (Ch) scaffold was introduced by Dong et al. with a pore size of 325 μm and 62.4% porosity with a higher compressive strength of 6.7 MPa that is similar to cancellous bone and was effective in subchondral bone defect repair. The live-dead cell assay showed that the scaffold is effective in cell survival, retention, and even distribution due to the higher hydrophilicity provided by the successful printing of a hybrid scaffold via FDM.[118] Since the matrix can incorporate the properties of the various substituents included, Naghieh et al. experimented with adding electro-spun PCL-gelatin to polylactic acid (PLA) while fabricating the scaffold using FDM, and the pore size of the scaffold was observed to be 350 μm with a porosity of 40% since the addition of the former reduced the hydrophobicity of PLA and improved both the mechanical and biological properties of the scaffold.[119]

Nyberg et al. doped PCL with Bio-Oss (BO) granules and Decellularized Bone Matrix (DBM) and fabricated the scaffold instead of using HAP/β-tricalcium phosphate (β-TCP) that are usually used to increase the biocompatibility and the apatite formation of the implant. The results gave a better apatite formation and osteoinduction than the latter, which is attributed to the presence of the collagen phase and the greater number of BO/DBM on the surface that was possible due to AM printing. Ca/DNA deposition was found to be 60 and 64 ng/ng for BO/DBM, whereas it was 17 and 35 ng/ng for HAP/β-TCP. The samples were fabricated with a strut thickness of 460 μm and pore size of 800 μm with 60% porosity. This porosity range reduced the compressive strength from 250 to 32 MPa for the scaffold.[120] Wang et al. successfully fabricated a polyether ether ketone (PEEK) scaffold to replace the tumor-affected chest wall, and the clinical analysis was done on 18 patients. The success of the study shows the future of AM techniques in the medical field. The tensile strength of the samples was 89 MPa, and the elastic modulus was 2.8 GPa. A reduction in fabrication time was observed (30 h) compared to conventional Ti implants (2 weeks). The patients were under observation for 12 months after the implantation, and the results were satisfactory since the implants performed their functions well. As the tumor area in the chest wall of each patient was different, patient-specific production could be done with the aid of additive manufacturing.[121]

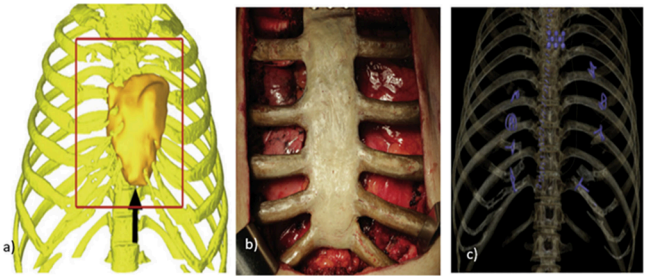

Figure 5. a) 3-D image for the reconstruction of the chest wall affected with a sternum tumor, b) AM fabricated PEEK implant fixed on the patient, and c) image of the chest CT after implantation. Adapted with permission from ref 121. Copyright 2019, Elsevier.

The fused filament fabrication (FFF) method was used by Singh et al. to prepare PLA scaffolds for smaller fracture repair. The apatite formation was observed in the porous structure and the sample with 40% porosity showed maximum apatite formation within 28 days, which was possible due to the pore structure that allowed the transport of nutrients, but it could not withstand the compressive strength studies effectively and showed a reduction in compressive strength by 22.2% within 28 days of incubation which proved that the specimen cannot be used for load-bearing applications but is restricted to small fracture repair.[122] Xiong et al. incorporated different weight % of tantalum (Ta) to PCL to improve the osteoinductive properties of the scaffold using the ME method. The scaffold possessed 450−440 μm porosity, and as the weight % of Ta increased, the porosity slightly changed. The porous structure had evenly distributed Ta particles due to AM fabrication that improved the biological properties of the scaffold, while the 10% Ta incorporated sample showed the best results.[123] The fabrication of a spinal fusion implant using PEEK and silicon nitride (SN) with the aid of FDM was reported by Du et al. where they successfully developed a triply periodic minimal surface structure (TPMS) with a large surface area that can contribute an equal distribution of stress under load-bearing conditions. They observed that the elastic modulus of the 30% porous sample fell in the region of human trabecular bone (734 MPa), and its sheer strength was 8.09 MPa. A study of the damping properties of the implant showed no catastrophic fracture but a remarkable recovery upon unloading. The biological studies provided enhanced biomineralization activity and a positive cellular response.[124] PHBHH and cellulose nanocrystals (CNC) were used by Giuibilini et al. for the preparation of a scaffold with proper control of the macroporosities that cannot be achieved by conventional methods. Good dimensional accuracy (up to 95%) was observed for the scaffold with a macroporosity of around 300 μm, and no delamination or collapsing of layers was observed. Since the degradation studies showed almost no degradation for up to one month, it makes this scaffold a suitable candidate for medium-to-long duration usage.[125] An attempt to fabricate a 3D-printed scaffold using silk fibroin and HAP via ME was done by Milazzo et al. in 2023. The printability of the scaffold with this composition was proven for the first time, and the structural stability was proven by the studies on elastic modulus where the sample showed immediate recovery within 1 s and a minor growth of moduli

https://doi.org/10.1021/acsomega.4c04870
ACS Omega 2024, 9, 44042−44075

Table 1. Various Polymers Used in Additive Manufacturing for Orthopedic Implant Applications

material	year	AM method	application	specification	author
PMMA	2010	Fused deposition modeling	Cranial bones and femur replacement	50−70% porosity to help transport nutrients and biochemical signals	Espalin et al.[113]
PCL	2015	Selective laser sintering	Skeleton damage repairing	Tailored porosity of 500 μm and interconnectivity	Mazzoli et al.[115]
PCL/PHBV	2016	Fused deposition modeling	Cartilage regeneration	Incorporation of PHBV for a faster cartilage regeneration with an increased compressive strength from 8.34 to 15 MPa	Kosorn et al.[116]
PA2200	2016	Selective laser sintering	Skull repairing	1.2 × 1.2 mm^2 porous structure with high compressive strength of 8.85 MPa	Sing et al.[117]
PCL/Chitosan	2017	Fused deposition modeling	Subchondral bone defect repair	Higher compressive strength (6.7 MPa) and porosity of 325 μm than pure PCL	Dong et al.[118]
PHBHH	2017	Subtractive rapid prototyping	Bone regeneration	Aligned fibrous structures with a compressive strength of 84 MPa and good cytocompatibility	Mota et al.[114]
PLA/PCL-Gelatin	2017	Fused deposition modeling	Bone regeneration	Reduction of the hydrophobicity of PLA by the addition of PCL-gelatin mixture.	Naghiesh et al.[119]
PCL doped with BO/DBM	2017	Fused deposition modeling	Bone regeneration	Better Ca/DNA deposition due to the printing of BO/DBM than PCL/HAP and PCL/TCP (60/64 ng/ng compared to 17/35 ng/ng)	Nyberg et al.[120]
PLA	2019	Fused filament fabrication	Small fracture repair	Porous structure with 40% porosity that enhanced cell attachment and tissue growth	Singh et al.[122]
PEEK	2019	Fused deposition modeling	Chest wall reconstruction	Fabrication of implant within 30 h and its successful implantation on 18 patients	Wang et al.[121]
PLGA	2020	Fused deposition modeling	Cortical screws	Porous interconnections with 45% fill density that provided biodegradability to samples	Dhandapani et al.[112]
PCL	2021	Material extrusion	Bone tissue engineering	Incorporation of evenly distributed Ta for better osteoinductive properties	Xiong et al.[123]
PEEK/SN	2023	Fused deposition modeling	Spinal fusion implant	TPMS structure with a sheer strength of 8.09 MPa	Du et al.[124]
PHBH/CNC	2023	Fused filament fabrication	Scaffold fabrication	Controlled macroporosity of 300 μm with no degradation for up to one month	Guibilini et al.[125]
Silk fibroin/HAP	2023	Direct ink writing	Microprosthetic applications	The first attempt to fabricate a scaffold with 3D-printed SF	Milazzo et al.[126]
PAEK polymer composites	2023	Fused filament fabrication and Selective laser sintering	Biomedical applications	Superior surface quality by SLS method compared to FFF	Yap et al.[127]

over time. The addition of silk increased the compressive strength of the sample from 1.3 to 10.1 MPa and a Young's modulus from 58 to 189 MPa.[126] Various PAEK composites, including carbon fiber reinforced polymers, were taken into consideration for AM fabrication by Yap et al. They used FFF and SLS for the fabrication of these, and the increased properties of the implants were reported. It was observed by them that SLS could provide better polymer interdiffusion and provided better polymer chain mobility, which in turn elevated the bond strength of the product. Infusing of carbon fibers into polymer matrix resulted in the increased porosity of the scaffold.[127]

Table 1 summarizes some of the studies performed over the years using additive manufacturing of polymers for orthopedic applications.

3.2. Ceramics. Though metal implants are a permanent solution for the critical size defect, wear resistance, corrosion, and leaching of toxic metal ions are the main challenges that could be caused by these implants. The choice of ceramics is a better alternative for this problem since it shows tissue tolerance, biocompatibility, and resistance to wear. Moreover, ceramics could even induce a biological response to the scaffold mainly due to its capacity for apatite formation.[128] AM allows the fabrication of ceramic implants with a porous structure and sufficient strength that can provide a better biological response.[129] Following are various ceramic materials used in AM for orthopedics.

3.2.1. β-Tricalcium Phosphate. β-Tricalcium phosphate (β-TCP) is one of the ceramics used widely for bone regeneration applications since it is bioresorbable, can be replaced by new bone formed, and has a high osteoinductive potential. Since β-TCP is brittle, it is used only for nonload-bearing applications. Moreover, the resorption rate is very high, which makes the scaffold useful only for short-term applications.[130] To counterbalance these problems additive manufacturing has been used.[131]

Cipitria et al. used FDM for the additive manufacturing of scaffolds using PCL with β-TCP. Bone morphogenetic proteins were added to it, and the studies proved that these new scaffolds effectively help in bone regeneration and site-specific distribution of proteins due to the presence of 70% porosity and the results were exactly equivalent to autografts transplantation.[132] To overcome the less mechanical strength of β-TCP, Fielding et al. proposed a new way by doping silica and zinc oxide to β-TCP. The structure with interconnected macropores with a pore size of 500 μm and compressive strength of 10.21 was fabricated. The doping process was found to increase the compressive strength of the latter to 250% more, and it had better biological properties for effective use in bone regeneration applications.[133] Park et al. incorporated β-TCP with PCL to prepare dental bone implants with a pore size of 400 μm and pore distance of 300 μm via rapid prototyping (RP), and the addition of 70% β-TCP reduced the compressive strength from 9 to 3 MPa, which made it a good candidate for dental application and increased the biological activity and wettability of the scaffold which in turn enhanced the cellular activity. The osteogenic differentiation was higher for the β-TCP-added scaffold, and the mechanical properties were similar to natural teeth.[134] Davila et al. used FDM for the fabrication of a β-TCP/PCL bone scaffold with 54% porosity and 447 μm pore size with the addition of 30% of β-TCP. The presence of β-TCP increased

https://doi.org/10.1021/acsomega.4c04870
ACS Omega 2024, 9, 44042−44075

the compressive strength from 40.72 to 84.3 MPa for 20% and 78.2 MPa for 30% of β-TCP respectively, which proved that it could be used for cancellous bone regeneration applications.[135] Shim et al. in the year 2017 printed a "guided bone regeneration membrane" using β-TCP and PCL for patients suffering from alveolar bone defects. It showed a higher elastic modulus (213 MPa) than collagen (12 MPa), which was usually used for this application. Better bone regeneration than collagen membrane (1.5 times higher) which was observed both *in vitro* and *in vivo* makes the AM fabricated sample a good replacement for collagen.[136] For mandibular reconstruction, Lee et al. proposed a DED-modeled scaffold with a double porous layer using PCL/β-TCP composite that showed acceptable potential for bone regeneration, and the design of the scaffold was done in a way that increased the rigidity of fixation to native bone. The results were proven *in vivo*, and even the wing structure that kept the scaffold in place could be customized according to the defect of the bone. The bilayer provided the mechanical support cortical bone-like layer (300 μm pore size) and allowed new bone growth from native bone into the other layer that acted like a cancellous bone layer (600 μm pore size), thus achieving both mechanical properties as well as osteogenesis. Though the studies faced many shortcomings such as the absolute volume of the new bone formed was remarkably less than the previous studies, the mechanical defects could be covered with this new approach.[137]

3.2.2. Hydroxyapatite. HAP has been the choice of scientists for bone grafts due to its excellent biocompatibility, osteoconductive nature, and nontoxicity. It possesses a lower solubility than other calcium phosphate ceramics like β-TCP. However, it has a lower fracture toughness and lower load-bearing capacity.[138] AM methods can improve the mechanical properties of the HAP.

The incorporation of polypropylene fumarate (PPF) into PCL/HAP was done by Buyuksungur et al. to increase the compressive strength and cell adhesion. The scaffold developed had a pore size of 350 μm with 35% porosity, which was easily achieved using FDM. HAP addition increased the compressive strength of the scaffold from 22.8 to 33.7 MPa. So, the successful fabrication of the scaffold that could replace the human trabecular bone was done. By the addition of mesenchymal stem cells from rabbit bone marrow, the *in vitro* and *in vivo* studies showed better osteochondral tissue formation than a pure PCL/HAP scaffold with a 14-fold increase in cell viability than the latter.[139] Since apatite and wollastonite can provide excellent biocompatibility, Tcacencu et al. made the scaffold using AW/PLA by the combination of two AM methods BJ and FFF. First, they binder jetted AW, and then PLA discs were formed using FFF followed by thermal bonding of the two discs. The composite structures were thus formed, and the studies proved that the scaffold could replace cortical and cancellous bones. Excellent vascularization and osseointegration were shown in both *in vitro* and *in vivo* studies. No delamination was observed, and the new bone formed was bound together in and around the scaffold inserted.[140] Ramu et al. proved that human femur bone repairing can be done using a polyamide/HAP implant fabricated using SLS with up to 70% porosity, and the implant could withstand the physical activities of a normal person. The tensile strength (24.3 MPa) and compressive strength (28.1) tests also were satisfactory.[141] A poly(vinyl alcohol) (PVA)/HAP hybrid structure with a rough and porous surface was fabricated for fast osseointegration. Deposition of the subsequent layers that are 0.3 mm thick was possible via FDM, and the compressive strength studies gave values (2−12 MPa for various concentrations of HAP) similar to that of human trabecular bone.[142]

Oledapo et al. introduced a poly ether-ether-ketone (PEEK)/HAP scaffold modeled using FDM which showed better differentiation and proliferation than the pure PEEK scaffolds when tested with an alkaline phosphatase solution. Osseointegration and bioactivity also showed a higher resulting rate. The pore structure of the scaffold could help in body fluid transport as well as to retain mechanical robustness under load-bearing conditions, and it was observed that the complex lattice structures were retained even after 40 cycles, which increases its acceptance in the medical device industry.[143] To improve the properties of PLA and to make it more biocompatible and bioactive, Nazeer et al. developed a scaffold with a PLA/Chitosan/HAP composite scaffold using FDM. The surface activity of the scaffold increased eventually, which was observed with a substantial decrease of the water contact angle (from 80.2 to 38.1°) and a higher rate of proliferation of bone cells was observe, and the samples were proven to be noncytotoxic.[144] Manzoor et al. developed an FDM-printed PEEK/HAP scaffold and another scaffold with doped HAP (Zn and Sr) that could be used for dental applications. Reductions in tensile strength (67.9 to 51.5/47.9 MPa) and percentage elongation (12.8 to 8.9/8.4) due to doped (Sr/Zn) HAP addition were observed. The results proved that the *in vitro* bioactivity of the inert PEEK-modeled scaffold increased with the addition of HAP and its doping. Since the printed samples showed good print quality, patient-specific implants for orthopedic and dental applications could be custom-prepared using the parameters mentioned in the study.[145] Zhang et al. proposed a scaffold made of PLA/HAP using FDM, which showed both the properties of PLA and HAP where the addition of HAP reduced the compressive strength from 45 to 15 MPa and increased the bioactivity of PLA. Since the brittleness of HAP reduces its acceptability in clinical applications, incorporation of PLA with it in AM fabrication reduced the brittleness, and it showed 4.44% of postbreak shrinkage which showed the sample is mechanically compatible. Biological evaluations showed cell attachment on the rough surface, and *in vivo* studies showed that all the micropores of the composite scaffolds were filled with bone tissues that developed anew. Maturation of bone tissues was observed within the scaffold, and the discovery of the haversian canal indicated the success of the AM-fabricated scaffold.[146]

Park et al. in the year 2021 introduced a PCL/HAP scaffold with a higher protein adsorption and cell adhesion. The printed scaffold showed a smooth surface, while the oxygen plasma and NaOH treatment provided a rougher surface. Reduction in strut dimension due to the addition of HAP increased the pore size of the sample, and the bone-like microenvironment provided by HAP nanoparticles induced osteogenic differentiation.[147] For the rapid regeneration of the damaged bone, a HAP/Chitosan/Genipin hybrid scaffold was developed by Zafeiris et al. using DIW for the first time. The pore size of the sample was 600 μm, and the scaffolds with various print speeds could achieve an open porosity similar to that of human cancellous bone (50−90%). The inflammatory response that is usually caused by traditional implants could be avoided using this scaffold. The microporous surface could improve the cell-scaffold interaction, and the modulus values

https://doi.org/10.1021/acsomega.4c04870
ACS Omega 2024, 9, 44042−44075

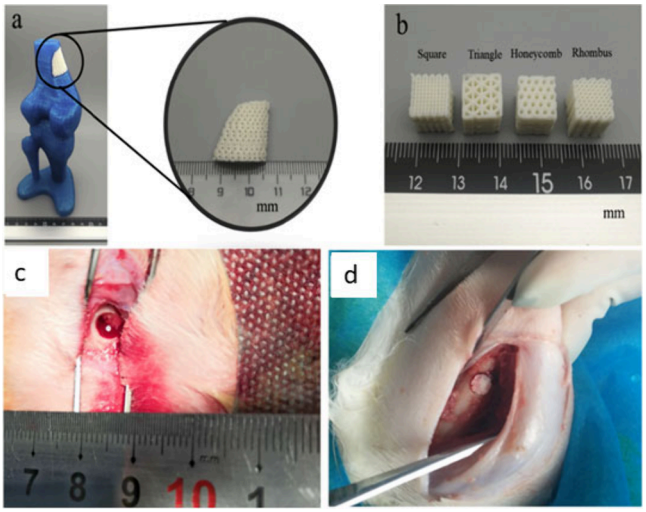

Figure 6. a) PLA/HAP bone scaffold fabricated using FDM, b) scaffolds with various pore structures, c) implantation of the scaffold at the bone defect, d) scaffold after a month. Adapted with permission from ref 146. Copyright 2021, Elsevier.

were higher than 0.6 GPa (for cancellous bone it is between 0.1 and 2 GPa), and the hardness was observed to be 0.25 GPa which was obtained through the 3D printing of the microporous structure.[148] The studies reported by Xia et al. proposed a scaffold with HAP/PCL using the SLS method with 70% porosity. The microporous structure formed showed a pore size of 600 μm and a compressive strength of 3.17 MPa had a higher degree of cell proliferation up to 109% even on day 1, which increased significantly as the day passed which was possible because of the successful printing of HAP with PCL, and the scaffold could be used for nonload bearing applications.[149] The fabrication of a vancomycin microsphere incorporated PLA/HAP scaffold by Li et al. proved the efficiency of AM in scaffold fabrication. FDM was used for the fabrication of the scaffold, and an even and accurate distribution of drug-loaded microsphere avoided ineffective bacteriostatic concentration which was possible due to the double nozzle 3-D printing technology. The experimental study on the animal proved the scaffold to be bone regenerative and without any fibrosis, inflammatory cell infiltration, or necrosis, and the regenerated bone gradually replaced the scaffold.[150]

3.2.3. Bioactive Glass. Various types of bioactive glasses have been used for tissue engineering and drug delivery applications due to their easier bone-bonding ability (apatite formation) and biocompatibility.[151] Though bioactive glass can form a strong interfacial bond with the bone, its fracture toughness is still high which it makes less applicable for load-bearing sites.[152]

A successful development of mesoporous bioglass (MBG)/PHBHH was done by Yang et al. using inkjet printing, and the printability of the material provided symmetrical microporous struts with a pore size of 423 μm, and mesoporous interfaces also were observed. The average porosity was 63.8%, and bioactivity studies gave a successful result in the formation of apatite within 7 days of immersion of the scaffold in the simulated body fluid (SBF). The addition of MBG gave a larger surface area due to which the cell adhesion capacity is also increased, which is attributed to the hydrophilicity and roughness provided by MBG.[153] Sun et al. doped Mg to wollastonite and a 3D printed scaffold for the first time with a 400 μm pore size and 63% porosity. The scaffold showed a compressive strength of 65 MPa, and the *in vitro* studies proved that the 3D porous biostructure showed the attachment of cells into pore struts. The real-time *in vivo* analysis resulted in new bone formation within 6 weeks with the presence of the haversian canal and blood vessels, which indicates the accomplishment of desired results via AM.[154] A well-ordered, mesoporous scaffold using bioglass and PVA binder was suggested by Wu et al. The scaffold prepared using the BJ method showed controlled drug delivery and excellent apatite formation with 60% porosity. The compressive strength (16.10 MPa) and toughness (155.13 MPa) of the scaffold were satisfactory, and the 3D printed scaffold retained the bulk scaffold morphology even after the compressive strength test, which is attributed to the AM method that could provide a continuous uniform pore structure and binding of MBG particles and PVA together. Another advantage of AM was observed in the increase in compressive strength 200-fold to the scaffold prepared via polyurethane foam templating. The bioactivity was observed within 3 days in SBF, and the presence of a 5 nm-sized mesoporous channel provided an opportunity for controlled drug delivery.[155] The interconnected porous structure incorporating magnesium hydroxide ($Mg(OH)_2$) into a PCL scaffold was proposed by Abdal-hay et al. for osteoporotic fracture fixation, and it was the first attempt to incorporate $Mg(OH)_2$ into AM. The scaffold had a 700 μm pore size and the dispersion of $Mg(OH)_2$ nanoparticles not only acted as a nanofiller but also provided a rigid morphology that determined the mechanical properties of the implant. The increase in the efficiency of apatite formation that can lead to enhanced osteoblast activity has been attributed to the bioactive $Mg(OH)_2$ release.[156] The scaffold with 500 μm pore size prepared by Wu et al. incorporated calcium silicate (CS) into PCL with an excellent result on cell adhesion and viability. The decellularization resulted in a higher rate of cell proliferation and differentiation than the untreated one as well as providing a more uniform alignment of the seeded cells.[157] Table 2 summarizes various additive manufacturing works performed on ceramics.

3.3. Ti-6Al-4V. A greater paradigm in the use of additive manufacturing products in the medical field is the application of meta-biomaterials which are produced at the micro or nano level for enhanced results in mimicking mechanical, morphological, and biological characteristics of native bone tissue for bone tissue regeneration, osseointegration, and tissue implant interface stability.[159] The experimental study proved that these meta-biomaterials can show a better elastic modulus, most likely that of cortical bone and a better flexural stiffness and strength than human bone. These characteristics were closely related to the pore size and the specific surface area.[160] Ti and its alloys are highly used in additive manufacturing since they can be prepared with less cost and minimum waste, while the commercially available implants are very costly.[161] Since it can provide a good strength to weight ratio and perfect cytocompatibility, it is used widely for implant fabrication in AM.[162] It was observed that the cooling rate can affect the formation of the α'-martensitic phase because, after the heat treatment procedure when the solution is cooled, the faster cooling rate gives a greater amount of this phase, and a full α' phase is formed when the water cooling method at 650 °C/s is used. The peculiarity of this product was that it possessed a greater strengthening effect in material but less ductility.[163]

https://doi.org/10.1021/acsomega.4c04870
ACS Omega 2024, 9, 44042−44075

Table 2. Various Ceramics Used in Additive Manufacturing for Orthopedic Implant Applications

material	year	AM method	application	specification	author
Bio glass/PVA	2011	Binder jetting	Bone regeneration	Multifunctional scaffold with hierarchical pore architecture	Wu et al.[155]
β-TCP/SiO_2/ZnO	2012	Binder jetting	Nonload bearing implants	Increase in compressive strength up to 250% due to the addition of SiO_2/ZnO	Fielding et al.[133]
β-TCP/PCL	2013	Fused deposition modeling	Bone regeneration	70% porosity with controlled release of proteins	Cipitria et al.[132]
HAP/PCL	2013	Selective laser sintering	Bone scaffold	Microporous and interconnected structure with 70% porosity	Xia et al.[149]
MBG/PHBHH	2014	Inkjet printing	Bone regeneration	Mesoporous interfaces with Improved bioactivity within 7 days	Yang et al.[153]
β-TCP/PCL	2016	Rapid prototyping	Dental bone tissue engineering	The addition of 70% β-TCP with a pore size of 400 μm to provide increased hydrophilicity and bioactivity	Park et al.[134]
β-TCP/PCL	2016	Fused deposition modeling	Bone tissue regeneration	Improved compressive strength of 84.3 MPa	Davila et al.[135]
Mg-doped wollastonite	2016	Material extrusion	Skull defect repair	Scaffold with 400 μm pore size and 65 MPa compressive strength	Sun et al.[154]
β-TCP/PCL	2017	Material extrusion	Regeneration of the damage caused by the alveolar bone defect	Better bone regeneration (1.5 times higher) than usually used collagen membrane	Shim et al.[136]
PCL/HAP/PPF	2017	Fused deposition modeling	Bone regeneration	Enhanced compressive modulus (22.8 to 33.7 MPa) and a 14-fold increase in cell viability	Buyuksungur et al.[139]
Apatite-Wollastanite/PLA scaffold	2018	Fused filament fabrication and binder jetting	Cortical and cancellous bone replacement	Fusing of two scaffolds developed via two AM methods to impart the characteristics of both materials	Tcacencu et al.[140]
PA/HAP	2018	Selective laser sintering	Femur bone repairing	70% porous scaffold to withstand mechanical stress	Ramu et al.[141]
PLA/HAP	2019	Fused deposition modeling	Bone regeneration	Rough and porous surface structure to improve cell adhesion	Oladapo et al.[142]
Calcium silicate/PCL	2019	Material extrusion	Bone regeneration	3D printed scaffold with decellularisation properties that allowed cell proliferation and differentiation	Wu et al.[157]
PEEK/HAP	2020	Fused deposition modeling	Orthopedic applications	Better adhesion and proliferation	Oladapo et al.[143]
PLA/Chitosan/HAP	2020	Fused deposition modeling	Bone scaffold	Improved performance for tissue engineering due to the reduction in water contact angle from 80.2 to 38.1°	Nazeer et al.[144]
PCL/$Mg(OH)_2$	2020	Material extrusion	Osteoporotic fracture fixation	Rigid morphology of the 3D printed sample with the incorporation of nanoparticles and enhanced osteoblast activity due to $Mg(OH)_2$ release	Abdal-hay et al.[156]
PCL/ β- TCP	2020	Direct energy deposition	mandibular reconstruction	Potential to reconstruct canine mandible	Lee et al.[137]
PEEK/HAP	2021	Fused deposition modeling	Orthopedic and maxillofacial applications	Reduction in tensile strength (67.9 to 47.9 MPa) and improved *in vitro* bioactivity for PEEK	Manzoor et al.[145]
PLA/HAP	2021	Fused deposition modeling	Cancellous bone regeneration	4.44% of postbreak shrinkage and osteo-regeneration *in vivo* with the formation of Haversian canal	Zhang et al.[146]
PCL/HAP	2021	Fused deposition modeling	Bone replacement	Reduction in strut dimension and higher protein adsorption and cell adhesion	Park et al.[147]
HAP/Chitosan/Genipin	2021	Fused deposition modeling	Cancellous bone replacement	600 μm porous structure that provided no inflammation response with the implant	Zafeiris et al.[148]
Vancomycin/PLA/HAP	2023	Fused deposition modeling	Femur bone regeneration	Accurate and even distribution of the microsphere in the pores of the scaffold	Li et al.[150]
Strontium incorporated β-TCP	2023	Digital light processing	Bone regeneration	Scaffold with 80% porosity and 1.44 MPa compressive strength	Shan et al.[158]

A lower elastic modulus (13 GPa) is shown by the Ti-6Al-4V alloys fabricated by Nune et al. into open cellular three-dimensional structures using EBM which are much more similar to human cortical bone. These open cellular structures enhanced the cell growth rather than its counterpart and were observed to be conducive for cell proliferation, differentiation, and protein synthesis, which could be due to the topography of the surface of the strut provided by AM. The higher seeding efficiency was attributed to the gradient mesh structure with a 600 μm pore size that provided a greater interaction of the cells. The greater observation of the study was that the different stages of cell maturity could coexist in the mesh structure.[164] Studies done by Van Bael et al. proved that the porous Ti-6Al-4V structure allowed the cells to proliferate more densely at the corners. When the DNA studies and metabolic activities were conducted, it was proven that the scaffolds with 1000 μm porosity had a higher living cell density, and the compressive stiffness of the samples of various porosities ranged from 454 MPa to 2.7 GPa. From their finding, it was observed that the larger pores avoid cell occlusion, and the small pore size (500 μm) helps in initial cell attachment, and it was proven that the latter is beneficial for cell growth.[165]

Though the highly porous structure allows a smooth flow of nutrients, as the porosity increases, it affects the mechanical strength, cell seeding efficiency, and absorption capacity of the structure. Manufacturing of the 3D gradient structures could overcome the above-mentioned disadvantages.[166] An extensive study done by S. A. Yavari et al. proved that various surface modifications on the AM fabricated Ti-6Al-4V structure including acidic, alkali, and anionic modifications can improve the apatite formation and enhance the properties of the 3D structure such as modulation of mechanotransduction and stimulation of differentiation of cells toward the osteogenic lineage with improved cell proliferation, and thus a higher rate of bone regeneration is easily observed.[167] It is also noted by

https://doi.org/10.1021/acsomega.4c04870
ACS Omega 2024, 9, 44042−44075

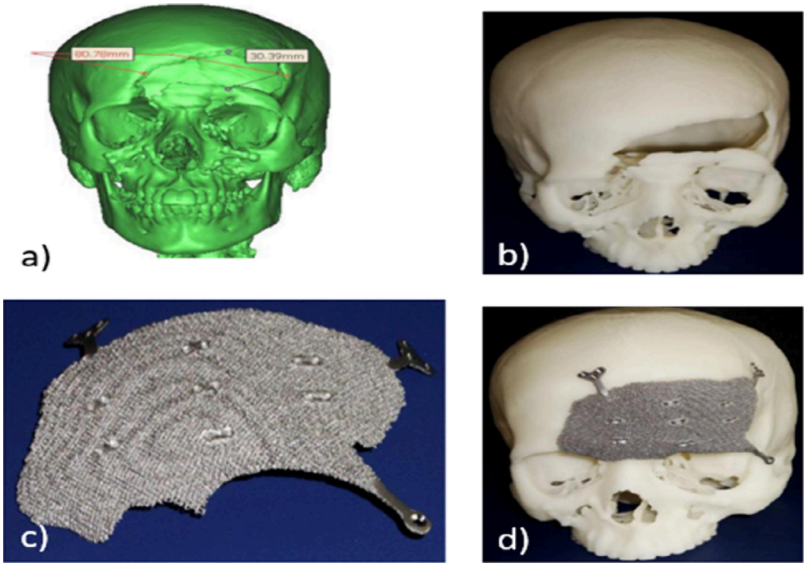

Figure 7. Porous Ti fragment fabricated to treat a skull defect. a) Computer model of the defect, b) skull model to be treated, c) fabricated portion using Electron Beam Melting, d) EBM implanted sample. Adapted with permission from ref 177. Copyright 2011, Elsevier.

scientists that the affinity of Ti alloys toward gases like Nitrogen, Oxygen, Hydrogen, etc. makes the AM product more brittle. Since we desire to achieve implants that can replace human bone, this case has to be taken care of during manufacturing to avoid a reduction in ductility. Chemical surface modifications could avoid this problem to keep the structure intact.[168] Though the AM fabricated porous structure helps bone regeneration, the inaccuracy in manufacturing leads to the reduction of porosity and pore size which can negatively affect the desired result, and this conclusion was proved by S. Arabnejad et al.[169] Another criterion to facilitate the pore-structured AM products is that the pore size should be at least three times greater than the grain size of the powder used. While making a study of the relationship between the grain size and the porosity using the SLM process in additive manufacturing, Zhang et al. fabricated samples with porosities ranging from 200 to 450 μm and a Young's modulus of 16−85 GPa. Though SLM provided the microstructure with a martensitic phase containing both α and β phases, the high cooling rate of SLM caused the increase in β phase, and they encountered the problem of adiabatic shear band fracture.[170]

Though Ti-6Al-4V is highly acceptable for implant fabrication due to its biocompatibility, the high modulus of the material becomes a hindrance at some points to choosing it for bone regeneration applications. If β stabilizing elements such as Ta, Nb, Zr, and Mo are added, Young's modulus could be reduced, thus making the implant patient-specific.[171] Results have been reported with such alloys which exhibit good biocompatibility and lower modulus for Ti13Nb13Zr,[172] Ti29Nb13Ta4.6Zr,[173] and Ti35Nb5Ta7Zr.[174] Another study performed by Chai et al. proved that using a 6-channel perfusion electrodeposition system, it is possible to produce three-dimensional calcium phosphate (CaP)/Ti-6Al-4V hybrids exhibiting distinctive physicochemical properties that can enhance *in vitro* osteoprogenitor cells and *in vivo* ectopic bone formation capabilities that can facilitate a successful skeletal repairing because the coating of CaP can get dissolved into and become converted into biological apatite.[175] It was observed that the tensile properties of the Ti-6Al-4V samples were greatly affected by the stress relief heat treatment because the slip transfer that takes place during heat treatment in the manufacturing process increases the ductility of the sample. The directionality of the product during AM also has a great impact on the fracture mechanism due to the different build orientations.[176]

Synthesis of products with a minimal surface area was a leap in the production of implants, especially using Ti-6Al-4V, because various properties of bone could be mimicked by using this method. Bobbert et al. successfully prepared such compounds using SLM and observed that the product has a relatively low elastic modulus similar to that of trabecular bone and a higher yield stress than cortical bone. These characteristics would help the implant avoid stress shielding and provide strong mechanical support for the desired bone regeneration and osseointegration. Another observation was that the biomaterials developed by them showed extremely high fatigue resistance which could withstand up to 1×10^6 load cycles, and the permeability values measured for it (4.9×10^{-11} to 4.8×10^{-10} m^2 at a pressure difference of 9000 Pa) were in the range of normal trabecular bone.[159]

The study done by Croes et al. proved that Ti-6Al-4V implants fabricated using direct metal printing which was further coated with chitosan (Ch) using electrophoretic deposition provided a better bone regeneration capacity. The research was done by loading chitosan with silver (Ag) and vancomycin. Because Ag has antibacterial properties, though they developed Ch/Ag-coated implants, the results were not satisfactory since the sample could not reduce the infection effectively, rather promoting osteoclast formation and bone remodeling which is a clear example that the biofunctionalization of the AM fabricated implants always do not give a positive result, and the choice of materials for biofunctionalization of AM fabricated samples is a crucial step to take.[178] Ben et al. used Ti-6Al-4V and Co-Cr-Mo alloys to prepare dental prostheses with an accurate fit between implant and framework with greater mechanical properties (for e.g.; tensile yield strength 1050−1200 MPa). It was observed that as the porosity decreased, the hardness of the implant increased, and the hardness of the SLM fabricated sample was higher than that of the cast sample due to the rapid cooling taking place

https://doi.org/10.1021/acsomega.4c04870
ACS Omega 2024, 9, 44042−44075

Table 3. Ti-6Al-4V Used in Additive Manufacturing for Orthopedic Implant Applications

metal alloy	year	AM method	application	specification	author
Ti-6Al-4V	2012	Electron beam melting	Total hip replacement	High specific strength	Murr et al.[29]
Ti-6Al-4V	2012	Selective laser melting	Bone scaffold	Porous scaffolds that proved that larger pores reduce cell occlusion and smaller pores allow initial cell attachment	Van Bael et al.[165]
Ti-6Al-4V	2017	Selective laser melting	Femoral bone	Avoids bone resorption secondary to stress shielding	Arabnejad et al.[184]
Ti-6Al-4V	2017	Electron beam melting	Tibia and femoral bone replacement	Gradient mesh structure with elastic modulus similar to human cortical bones that are conducive to calcium deposition, cell adhesion, and proliferation	Nune et al.[164]
Ti-6Al-4V	2017	Electron beam melting	Trabecular bone replacement	Gradient cellular structures with 60−21% porosity and 0.9−3.6 GPa elastic modulus for tissue engineering	Surmeneva et al.[168]
Ti-6Al-4V	2017	Selective laser melting	Trabecular bone replacement	Exceptionally high fatigue life (no specific damage up to 1×10^6 load cycles) and large fatigue resistance due to the topology of internal structure and notches created via the AM process	Bobbert et al.[159]
Ti-6Al-4V	2019	Electron beam melting	Bone screw	Microrough surface that provided higher osteogenesis	Lee et al.[180]
Ti-6Al-4V	2020	Selective laser melting	Auxetic bone screw	Improved bone screw fixation with the screw that had no interlayer differentiation indicating complete melting of the powder	Yao et al.[182]
Ti-6Al-4V incorporated with Ag and Zn nanoparticles	2020	Selective laser melting	Orthopedic implants	Prevention of bacterial infection and strengthening of implant fixation at a faster rate due to the large surface area provided by the implant	Van Hengel et al.[181]
Ti-6Al-4V	2021	Selective laser melting	Pedicle screw	Possibility of the radical expansion of screw body when tensile strength increases and the increase in pull-out force from 6.29% to 14.46%	Yao et al.[183]
Ti-6Al-4V	2020	Electron beam melting	Bone replacement	Large wall space for the transport of nutrients	Wang et al.[187]
Ti-6Al-4V	2023	Selective Laser Melting	Orthopedic plate screw	Greater bending strength medium (3.07 N m) than conventionally constructed (2.57 N m)	Polak et al.[185]
Ti-6Al-4V	2023	Direct Metal Laser Sintering	Dental implant	An increase in porosity increased the peri-implant microstrain to 51.67%	Chakraborty et al.[186]

https://doi.org/10.1021/acsomega.4c04870
ACS Omega 2024, 9, 44042−44075

during the process. It was also noted that the additive manufacturing of the alloy reduced the corrosion rate than the cast sample.[179] Murr et al. could develop a total hip replacement component with various specific characteristics such as high specific strength. The femoral hip stem they fabricated contained a lower-density central foam core and higher-density outer foam, and the studies proved that the porosity is closely related to Young's modulus since the sample with 83% porosity had a Young's modulus of 1 GPa where that of 56% porosity showed a Young's modulus of 10 GPa.[29] The animal studies done by Lee et al. proved that the screws they AM fabricated using Ti-6Al-4V showed higher osteogenesis and microroughness. It was observed that the failure load of AM fabricated screw increased three times higher within 2 weeks of implantation, and the shear stress of the screw after 2 weeks was 1.27 MPa which was much higher than a conventional screw (0.27 MPa). The new bones developed at a faster rate, and the bonding force was higher which was attributed to the surface roughness brought about by AM.[180] Biofunctionalization of Ti-6Al-4V implants using Ag nanoparticles was done by van Hengel et al. to improve bacterial infection prevention and the longevity of the implant. One of the reasons for these results was the substantial increase in the surface area to a factor of 3.75 through SLM fabrication and without inducing any cytotoxicity; the implant prevented the colony formation of bacteria both *in vitro* and *ex vivo*. The release of Ag particles seemed to take place at a faster rate within 24 h which eventually reduced to smaller doses over a month.[181] SLM was used by Yao et al. in 2020 to prepare auxetic bone screws, and they observed that the change in auxetic structure changed the mechanical properties rapidly. So, the patient-specific design of the screw is possible with the help of AM parameters, and the printed screw did not show any interlayer differentiation stipulating complete melting of the powder material used. As the wall thickening varied from 0.8 to 1.6 mm, the tensile strength varied from 81 to 621.56 MPa.[182] Pedicle screws developed using the same method, and materials also showed the novel property of expanding under greater tensile strength, which shows that the implant can avoid pulling out under similar conditions, and the pull-out force increased from 6.29% to 14.46%. The sample could resume the distortion once unloading was done, which could minimize the damage to the bone. The porosity provided by the AM method was a factor for osseointegration and increased fixation stability.[183] Arabnejad et al. introduced a new structure that could mimic the femoral bond effectively, avoiding the secondary shielding and improving mechanical strength. It was noted that as the porosity increased, the strength of the structure also increased, and a 70% porous structure showed 87.85 MPa strength. This fully porous material could mimic the bone tissues, and mechanical properties could be tuned. The *in vivo* studies they had done proved that the bone implant built had only less amount of femur surface strain.[184] Polak et al. fabricated an orthopedic plate screw via conventional as well as AM methods to compare the results. The findings emphasized that the SLM fabricated screws had greater bending strength (3.07 N m) than the conventionally fabricated screws (2.57 N m). The implant-maintained fracture stability and underwent a shorter plastic deformation.[185] Fabrication of dental implants with the help of DMLS using Ti-6Al-4V illustrated the characteristics of a good implant when the pore size of the sample fabricated was 1000 μm rather than 650 μm. The stiffness of the implants was reduced as the porosity increased, and this resulted in a lesser defect volume of the sample with 1000 μm porosity that also can be attributed to the higher rate of cell attachment and proliferation obtained in the latter. When the porosity of the implant increased from 30 to 35%, the peri-implant microstrain increased up to 51.67%, which provided a favorable biomechanical environment to the implant.[186] Table 3 summarizes different additive manufacturing methods used in the fabrication of implants using Ti-6Al-4V.

3.4. Magnesium Alloys. Since Mg is a bioresorbable and biocompatible material with the lightest weight structure and a density closer to that of natural bone (1.74 g cm^{-3}), this alkaline earth metal has been used in AM. The Young's modulus of Mg alloy ranges between 41 and 45 GPa, which is similar to the human bone that helps in avoiding the stress-shield effect.[188] However, the higher corrosion rate of Mg has been an unsolved problem for scientists over the years. Introducing rare earth elements into Mg alloy can avoid the negative impacts that Mg could produce due to corrosion and make it a more suitable candidate for additive manufacturing since it can improve mechanical properties.[189] AM of Mg alloys is still not developed fully, because it is not easy to prepare the Mg alloy powder for the fabrication of Mg implants. Moreover, Mg alloys possess a high tendency to oxidize and have high vapor pressure and low vapor temperature.[190] Wang et al. performed a study about these problems and developed a new Mg alloy which includes Mg-Nd-Zn-Zr metals (JDBM alloy); the additive manufacturing of the latter could overcome the above-mentioned problems, and the compressive strength and Young's modulus of the samples fell within the region of human cancellous bone (0.2−80 MPa and 0.01−2 GPa). Clinical application of the samples could be proven by the biodegradation studies, and the surface treatment with dicalcium phosphate dihydrate increased the biological capacity of the sample.[191]

Farag et al. developed a bone scaffold with the addition of gelatin on magnesium phosphate (MgP) using the paste extrusion deposition (PED) method to increase the mechanical properties, and the studies proved that the addition of <6% of gelatin gave a compressive strength of 16.7 MPa. The samples also showed more hydrophilicity with enhanced cell affinity (spreading out of cells within 30 min of incubation) and drug release kinetics with a sustained drug release throughout 30 days.[192] One of the studies done on magnesium electron (WE43) powder after manufacturing using the SLM method proved that the structure formed could be biodegradable, and the porous structure was built with a pore size of 600 μm. The higher cooling rate provided by SLM allowed the formation of smaller grain sizes. The mechanical studies (Young's modulus: 700−800 MPa) and the cytotoxicity studies proved it to be a better alternative for natural bone. Though corrosion was observed in the sample, hydrogen evolution was observed to be less than the other conventionally fabricated samples, which is attributed to the topology of the AM sample and the formation of a passive layer of $Mg(OH)_2$ on the surface was observed which could act as a protective layer.[193] An anterior cruciate ligament screw was developed by Antoniac et al. with the help of FFF using Mg/PLA/vitamin E composite. The printing provided perfect adhesion between the layers and a well-maintained interconnection between the layers. Without any agglomerations of the particles, desired morphology was observed.[194] Ho et al. used the friction stir process to prepare Mg and nanoscale HAP to make a

https://doi.org/10.1021/acsomega.4c04870
ACS Omega 2024, 9, 44042−44075

Table 4. Various Mg Alloys Used in Additive Manufacturing for Orthopedic Implant Applications

metal alloy	year	AM method	applications	specifications	author
MgP	2014	Paste extrusion deposition	Bone scaffold	Samples with 16.7 MPa compressive strength and sustained drug release for 30 days	Farag et al.[192]
MgP	2014	Paste extrusion deposition	Bone scaffold	Effective drug delivery carrier (utilizing 93% of the drug with a slow release) with a pore size of 400 μm and 4.8 MPa compressive strength	Lee et al.[199]
WE43	2018	Selective laser melting	Bone substitution	Biodegradable and porous structure with a pore size of 600 μm	Li et al.[193]
Sr substituted MgP	2019	Binder jetting	Bone scaffold	Improved biological response and clinical applicability with a porosity of 23% that could be achieved from LPBF	Meininger et al.[200]
WE43	2019	Laser powder bed fusion	Bone scaffold	Microporous structure with long-term stability	Kopp et al.[201]
Mg/PLA/vitamin E (α-tocopherol)	2019	Fused filament fabrication	anterior cruciate ligament screws	Perfect adhesion between the layers without any agglomeration of particles.	Antoniac et al.[194]
Mg-HAP composite	2020	Friction stir processing	Bone substitute	Significant grain refinement from 7.76 to 2.2 μm that provided better resistance with Rp: 5.18×10^4 ohm and I_{CORR}: 1.95 $\mu A/cm^2$	Ho et al.[195]
MgP/Sr/PCL	2020	Material extrusion	Bone defect curing	Bone growth at the periphery as well as the center of the scaffold and the change in elastic properties were <5% over 50 cycles	Golafshan et al.[196]
Mg-Nd-Zn-Zr alloy	2020	Selective laser melting	Bone tissue engineering	Fully interconnected structures with compressive properties	Wang et al.[203]
Mg-Nd-Zn-Zr	2022	Selective laser melting	Bone replacement	Ability to prevent implant-related infection and higher biocompatibility due to the biodegradation of sample (0.039 g/day) and increase in compressive strength to 54.8 MPa	Xie et al.[197]
Mg-Zn alloy	2022	Direct ink writing	Degradable trabecular bone scaffold	81% reduction in corrosion rate than pure Mg scaffold	Dong et al.[198]
PLA-Mg alloy	2023	Fused deposition modeling	Bone tissue engineering	Implants with interconnected pore structure with a pore size of 779 μm that could provide biodegradation and cell proliferation	Bakhshi et al.[202]

https://doi.org/10.1021/acsomega.4c04870
ACS Omega 2024, 9, 44042−44075

Table 5. Various Fe Alloys Used in Additive Manufacturing for Orthopedic Implant Applications

Metal alloy	Year	AM method	applications	specifications	author
Fe-Mn	2013	Inkjet printing	Craniofacial scaffold	Cytocompatibility and pore infiltration of cells with 36.3% porosity and reduction of yield strength from 239 to 106 MPa	Chou et al.[206]
Fe_3O_4/ MBG/ PCL	2014	Binder jetting	Trabecular bone replacement	Excellent hyperthermia and anticancer drug delivery (30% within a day)	Zhang et al.[207]
Fe scaffold with HAP nanocoating	2018	Binder jetting	bone tissue engineering for load-bearing applications	67.5% porosity with young's modulus and compressive strength within the range of human bone making it usable for load-bearing cases	Yang et al.[208]
Fe	2018	Direct metal printing	Trabecular bone replacement	Interconnected pore structure with cytocompatibility and biodegradation of the sample with 3.1% reduction within 28 days with a corrosion rate of 1.18 mm/ year	Li et al.[209]
Fe	2021	Material extrusion	Trabecular bone replacement	Porous iron scaffold with 7.2 MPa yield strength and 0.6 GPa elastic modulus	Putra et al.[210]

composite, and they achieved a significant grain size refinement reducing from 7.76 to 2.2 μm, and the *in vitro* studies using SBF proved that they could achieve corrosion resistance with an I_{CORR} value 1.95 $\mu A/cm^2$ and Rp 5.18×10^4 ohm that is attributed to the reduced grain size.[195] The introduction of a strontium (Sr) substituted MgP/PCL implant was done by Golafshan et al., and the printing procedure avoided nucleation of cracks, and fusing of struts at the junctions also was observed owing to the printability of the composite, and the change in elastic properties was less than 5% over 50 cycles making the sample a good implant for tough areas. The *in vivo* studies proved bone regeneration properties of the implant with higher durability and toughness. Bone growth was observed even at the center of the scaffold with 12% of new bone tissue and 15% of degradation of the implant observed over six months.[196] To reduce the mechanical imbalance of the pure Mg implants, Xie et al. introduced a new implant using Mg-Nd-Zn-Zr alloy designed and developed using SLM, which showed a compressive yield strength value of 54.80 MPa. The implant had a large surface area-to-volume ratio due to 3D printing which provided a degradation rate of 0.039 g/day, so the antibacterial properties could be observed with higher bacterial inhibition and greater resistance to implant-related infections.[197] Dong et al. introduced a new Mg-Zn bone scaffold fabricated using the DIW method with a microporous structure, and the corrosion studies showed that the Mg-Zn alloy's corrosion rate was 81% less than pure Mg scaffold. However, the elastic modulus (448.8 MPa) and yield strength (14.5 MPa) were higher than those of the latter. The mechanical properties were similar to that of the trabecular bone, and the cytocompatibility results were satisfactory.[198] MgP scaffold produced by Lee et al. was reported to give a good drug delivery response, bioactivity, and load-bearing capacity with greater cell proliferation and osteogenic differentiation. The scaffolds with a 400 μm pore size showed a compressive modulus of 30 MPa and compressive strength of 4.8 MPa which fall into the range of human cancellous bone, and it was observed that these values were achieved without any postprocessing. It was also proven that this sample had greater loading and release of the drug than other conventionally fabricated and sintered samples since it allowed 93% loading of the sample and slow release of it, while the other samples had less loading (26%), and its faster release (88.5% was released over a month while the 3D printed sample's drug release was 60% at the same time).[199] The studies done by Meininger et al. proved that the incorporation of Sr^{2+} ions into the MgP composite gave an increase in the porosity from 20 to 23%, which is near the maximum porosity that could be achieved in LPBF and improved osteoblast activity and cell growth and bone ingrowth.[200] Another study reported by Kopp et al. was on WE43 alloy where they fabricated a microporous scaffold with the aid of LPBF that showed long-term stability with an increase in the percentage of content of rare earth alloy from 7.6 to 8.6%.[201] PLA-Mg composite implant fabrication was suggested by Bakshi et al. for hard tissue engineering and with the aid of FDM, and implants with varying concentrations of Mg were obtained with a pore size of 779 μm, and interconnected pores were observed. Though the 3D printed implants showed superior mechanical properties, the biodegradation of the scaffolds was satisfactory which could be obtained by the controlled porosity achieved in FDM. It also allowed maintenance of the cell integrity and proliferation observed after 24 h.[202] Table 4 summarizes various Mg implants fabricated using AM methods.

3.5. Iron Alloys. Additively manufactured iron implants have been used for potential biodegradable applications compared to Mg and Zn because of their ability to design porous structures and patient-specific implants.[204] They also possess better mechanical properties and a longer life frame which make them an apt candidate for load-bearing applications.[205] In 2013 Chou et al. successfully printed a craniofacial scaffold using Fe-Mn alloy, and the biological studies based on it proved that the scaffold could be used for biological applications. 36.3% open porosity obtained by the sample through AM helped in stress relaxation, and the yield strength of the 3D printed sample reduced from 239 to 106.07 MPa than the sintered and rolled sample made using the same composition. The live dead cell assay showed not only a high density of cells attached to the surface but also the infiltration of cells within the porous parts.[206] Zhang et al. produced a Fe_3O_4/MBG/PCL composite scaffold for bone regeneration with 400 μm pore size and 60% porosity, and the inclusion of Fe induced excellent hyperthermia, and apatite formation could be observed due to the presence of bioglass. The compressive strength was observed to be 13−16 MPa similar to human trabecular bone, and even after treatment with SBF, the samples retained the compressive strength. It also showed excellent anticancer drug delivery in a controlled manner with 30% of drug release within a day and slow release within up to 10 days.[207] Fe scaffolds coated with HAP nanoparticles were prepared by Yang et al. in 2018, and the studies proved that the high porosity (67.5%) of the scaffold and its cytocompatibility make it a novel scaffold for bone tissue engineering without the leaching of Fe ions. The Young's modulus (1.25 GPa) and compressive strength (141.25 MPa) values of the implant show its load-bearing applicability.[208] In the same year, Li et al. used

https://doi.org/10.1021/acsomega.4c04870
ACS Omega 2024, 9, 44042−44075

Table 6. Various Zn Alloys Used in Additive Manufacturing for Orthopedic Implant Applications

metal	year	AM method	applications	specifications	author
Pure Zn	2018	Selective laser melting	Cardiovascular stents	Higher mechanical properties such as hardness (42 HV), elastic modulus (23 GPa), ultimate strength (114 MPa), elongation (10.1%)	Wen et al.[211]
Zn	2019	Laser powder bed fusion	Trochanter bone replacement	Densified porous scaffold (almost 100%) with a rough surface	Wen et al.[213]
Zn-WE43 composite	2019	Laser powder bed fusion	Porous bone scaffold	High densification (over 99.47%) and tensile strength (335.4 MPa)	Qin et al.[214]
Zn	2020	Fused deposition modeling	Trabecular bone replacement	Porous scaffold (65% porosity) with high biocompatibility and cell viability	Cockerill et al.[212]
Zn-Mg alloy	2022	Laser powder bed fusion	Bone scaffold	Relative density greater than 99.5% and formation of brittle phase due to the incorporation of Mg	Voshage et al.[215]

the direct metal printing method for the fabrication of porous iron scaffolds with a controlled topology, 749 μm pore size, 73% porosity, and a smooth surface which showed the mechanical properties of trabecular bone with desired cytocompatibility. The biodegradability of the sample (3.1% reduction within 28 days with a corrosion rate of 1.18 mm/year) was attributed to the grain refinement topological design obtained via AM.[209] The porous iron scaffold prepared by Putra et al. in 2021 showed a higher biodegradability, yield strength (7.2 MPa), and elastic modulus (0.6 GPa) than that of the conventionally prepared scaffold with a static corrosion rate of 0.05 mm/year.[210] Table 5 summarizes various AM used for the fabrication of Fe implants.

3.6. Zinc Alloys. Zinc is an essential element of the human body. Zinc has been used for biomedical applications due to its high biocompatibility and degradability. Using the SLM method, the cardiovascular stents prepared by Wen et al. had higher mechanical properties such as higher hardness (42HV), elastic modulus (23 GPa), and elongation (10.1%) properties. Good densification (over 99.50) was produced due to the optimized laser energy and overlap remelting that happened during AM fabrication. When the top part had a smooth surface, the side surfaces were more rough,and solidified balling particles were observed. Sandblasting was used as postprocessing.[211] The near-net-shaped zinc scaffolds produced by Cockerill et al. were seen to be highly biocompatible, and cell proliferation and adhesion were observed at a faster rate with high cell viability due to the intercellular connection. As the pore size of the samples varied (from 900 μm to 2 mm with 22 and 65% porosity), yield strength also varied (11 to 6 MPa). Corrosion products were observed only on the surface and were not intruded into the pores, and the corrosion rate was 85 μm/year. The scaffold could mimic trabecular bone and avoid the stress-shield effects of the surroundings.[212] Wen et al. introduced the LPBF method for the preparation of the zinc scaffold for the replacement of trochanter bone. Though they could achieve printing the densified scaffold (almost 100%) with a pore size of 300 μm and 43.8 HV hardness, many problems were encountered in the process. The surface quality of the samples was very poor due to overheating and recoil force of evaporation, and postprocessing was required for a uniform and smooth surface.[213] To avoid these drawbacks, another attempt was made by Qin et al. to prepare a porous zinc scaffold for bone replacement using Zn-WE43 composites. It was observed that they showed a high densification (over 99.47%) and tensile strength (335.4 MPa). Though the compressive strength (73.2 MPa) and Young's modulus (2.48 GPa) were satisfactory, the elongation was only 1%. The reason for this was the rapid cooling which resulted in the formation of fine grains.[214] Voshage et al. incorporated Mg alloys to Zn and using LPBF fabricated the scaffold which showed significant differences from pure Zn scaffolds due to the addition of Mg. The relative density increased to 99.5% with 381 MPa tensile strength and 4.2% elongation, and the samples showed approximately no plastic deformation after breakage. The compressive strength (19.12 MPa) and Young's modulus (0.65 GPa) of the scaffold show that this AM process could be used for the fabrication of Zn implants.[215] Table 6 summarizes various AM methods used in the fabrication of Zn implants for biomedical applications.

3.7. Additive Manufacturing of bio-HEA Implants. Though various metals and their alloys like Ti-6Al-4V have been used in implant fabrication over the years, the main disadvantages of these materials are the corrosion of the metal, leaching of ions from the metal alloy, and high stress shielding.[216] High Entropy Alloys (HEA) were first reported by Yeh et al. in 2004 which are composed of five or more (up to 13) metals in near to equimolar ratio for advanced properties and applications.[217] HEAs result in lattice distortion that can reduce the microstructure to a substantial amount, which in turn can affect the physical chemical and mechanical properties. Easier to understand and analyze, these have proposed a novel approach to conventional alloy formation.[218] Bio-HEAs are an answer to alloys with both biocompatibility and desired mechanical properties for the fabrication of implants. Mo-Ta-Nb-Ti-Zr,[219] Ti-Zr-Hf-Cr-Mo, and Ti-Zr-Hf-Co-Cr-Mo HEAs[220] are some of the alloys of these types used in implant fabrication.

Ishimoto et al. used SLM for the development of Ti-Nb-Ta-Zr-Mo alloy for the implant fabrication, and the use of AM helped in avoiding elemental segregation due to the high cooling rate that could be provided by SLM that is unable to be achieved with other conventional methods. A unique solidified microstructure was obtained without any cracks, and the dense structure was with <0.5% porosity. The proof stress was shown to be 1690 MPa, which is remarkably higher than other cast alloys. The Young's modulus 140 GPa and all these benefits are attributed to the rapid cooling effect that can be provided by the SLM process. The biocompatibility results also were satisfactory.[221] A coating on Ti-6Al-4V using Co-Cr-Fe-Ni-Mo HEA with the aid of laser cladding was provided by Deng et al. Using of the AM method provided a nonuniform microstructure and the grain refinement provided an increased microhardness of 885.5 $HV_{0.2}$ which was 1.66 times greater than the arc-melted alloy. Laser cladding of the sample provided an increased wear and corrosion resistance to the substrate with better I_{CORR} (9.87×10^{-8} A·cm^{-2}) and E_{CORR} (−0.329 V vs SCE) values.[222] Ti-Nb-Ta-Zr-Mo HEA was fabricated by Feng et al. via SLM, and the method used allowed the suppression of elemental segregation and

https://doi.org/10.1021/acsomega.4c04870
ACS Omega 2024, 9, 44042−44075

Table 7. Various bio-HEA used in AM for Implant Fabrication

alloy	year	AM method	application	specification	author
Ti-Nb-Ta-Zr-Mo	2021	Selective laser melting	Implant fabrication	Biocompatible alloy with proof strength of 1690 MPa	Ishimoto et al.[221]
Co-Cr-Fe-Ni-Mo	2022	Laser cladding	Implant coating	Increased microhardness of 885.5$HV_{0.2}$ due to strain refinement strengthening	Deng et al.[222]
Ti-Nb-Ta-Zr-Mo	2023	Selective laser melting	Implant fabrication	93% BCC phase composition with suppressed elemental segregation	Feng et al.[223]
Ti-Ta-Nb-Mo-Zr	2023	μ-plasma arc additive manufacturing	Knee implant applications	A substantial decrease in leaching of ions to 57 ppb with a corrosion rate of 12 mm/year at a pH of 7.4 SBF solution	Kumar et al.[224]
Ti-Zr-Hf-Nb-Ta-Mo	2023	Laser powder bed fusion	Implant formation	Higher yield stress (1355−1426 MPa) and lower Young's modulus (88.6 GPa) with suppressed elemental segregation	Gokcekaya et al.[225]
Ta-Ti-Nb-Zr	2023	Direct ink writing	Scaffold fabrication	Higher mechanical strength (149.98 MPa) and lower elastic modulus (0.64 GPa) than Ta scaffolds fabricated using conventional methods	Zhao et al.[226]

fabrication of alloy with a fine grain size of 5.14 μm. The samples had 93% BCC phase composition and the Young's modulus of the sample was observed to be near to human trabecular bone.[223] Kumar et al. developed Ti-Ta-Nb-Mo-Zr HEA using μ-plasma arc AM for knee implant applications, and the studies proved the sample to be corrosion resistant with excellent biocompatibility having a cell viability of 92% even after 72 h. The samples formed had two body-centered cubic (BCC) microstructures and two minor interdendritic structures, and the use of AM technique prevented the formation of other phases as well as the decomposition of the BCC phase. The leaching of ions was reduced considerably up to 57 ppb, which was reported as 10000 ppb in previous studies.[224] Gokcekaya et al. fabricated Ti-Zr-Hf-Nb-Ta-Mo HEA using LPBF, and the ultracooling provided by the AM method suppressed the elemental segregation, and only the BCC phase could be observed in XRD analysis with a single crystalline-like structure. Higher yield stress (1355−1426 MPa) and lower Young's modulus (88.6 GPa) were observed in the LPBF sample than in the cast sample owing to the advantages of AM methods. Excellent cytocompatibility of the sample makes it a good candidate for orthopedic applications.[225] Ta-Ti-Nb-Zr HEA was proposed by Zhao et al. for the scaffold fabrication, and DIW was used to achieve the same. Varying the Zr content resulted in decreasing the pore size from 51.1% to 46.9% and the density from 78.6 to 88%. The mechanical properties also could be regulated in the same manner, and it was observed that it possessed higher mechanical strength (149.98 MPa) and lower elastic modulus (0.64 GPa) than Ta scaffolds prepared by conventional methods. the cell proliferation study and live−dead cell assay proved the samples to be biocompatible, and the method provided a low-cost fabrication of implants with these properties.[226] Table 7 summarizes various bio-HEA implants fabricated by using AM.

3.8. Additive Manufacturing of Other Metal Implants and Composites. Ti-24Nb-4Zr-8Sn alloy was used by Zhang et al. in 2014 for the fabrication of an acetabular hip cup using selective laser melting which was the first one to be reported of the kind using SLM. By adjusting the laser scan speed, the density and the hardness of the implant could attain the desired values, and it was observed that by decreasing the scan speed, density could be increased, and the sample was fabricated with 99.3% density and 10% ductility. Due to the high oxygen content of the starting powder, the implant could avoid pronounced super elastic discomfort.[161] Porous Ta implants prepared by Ballla et al. with the aid of LENS showed superior biocompatibility than Ti implants with a similar porous structure, so the bone cell adhesion was easier and more effective. The porosity of the implant was tailored by varying the laser energy input. The localized melting followed by solidification during the process effectively provided the particle bonding and reduced the brittleness of the sample, and the elastic modulus was observed between 2 and 20 GPa which could not be achieved by other conventional methods. Since the surface energy of these implants was higher, the early integration of the bone tissues was observed.[227] Habijan et al. in 2013 proposed a Nickel-Titanium (Ni-Ti) alloy implant using SLM, and the studies proved that the porous implant is a good carrier of mesenchymal stem cells, and the nickel ion leaching was much very less for the additively manufactured implant, and a reduction of 258 ng/mL to 101 ng/mL was obtained by reducing the laser beam diameter to 61 μm from 128 μm.[228]

To increase the implant stability and bone anchorage, Stenlund et al. fabricated the implant with Co-Cr-Mo alloy by doping Zr to it. The sample had high surface roughness, and the surface thickness appeared to be 50 nm. In the *in vivo* studies, it was observed that there was a condensation of bone cells at the surface of the implant placed in the femur and in the tibia, and remodeling of the cortex at the top and endosteal bone growth was obvious.[229] Instead of Ti-6Al-4V alloy which is usually used for the fabrication of implants, Jahadakbar et al. designed the implant for mandibular reconstruction using Ni-Ti alloy, and the results showed that allowing 45.7% porosity gave the stiffness of the implant equivalent to the surrounding bones and the implant was a better solution for vascularization and rapid healing than the former. The study was done by preparing the implants using both the material by maintaining the same Young's modulus (12 GPa), and the porous structure of the Ti-6Al-4V sample failed when the stress shield study was done.[230] To compare the osseointegration response of Co-Cr alloy implant to Ti-6Al-4V, Shah et al. designed Co-Cr implants using EBM. The observations showed that bone ingrowth in both implants was similar, which confirmed that EBM did not reduce the biological capacity of the Co-Cr alloy, but the Co-Cr implants had rougher surfaces. Due to this, a higher osteocyte density also was observed at the periphery of the implant in the *in vivo* studies.[231] It was a novel invention to prepare the scaffold using calcium sulfate hemihydrate (plaster) by incorporating RBC3200 epoxy resin into the porous implant formed using powder bed binder jetting. The elastic modulus of the scaffold was 6.2 MPa and 0.31 mm^2/s thermal diffusivity. But it remains as a concept, not a final product, since many of the parameters that concern the bone could not be achieved with this model (for e.g. compressive strength was only 11.7 MPa).[232] Though scientists still

https://doi.org/10.1021/acsomega.4c04870
ACS Omega 2024, 9, 44042−44075

consider Ti-6Al-4V as a better choice for total hip replacement, it usually faces some disadvantages, such as stiffness mismatch and poor wear resistance. It was a novel attempt to incorporate Ti-6Al-4V into the Ni-Ti alloy to fabricate a single hip implant so that the former could overcome the limitations and achieve a shape memory effect, wear resistance, and super elasticity. These dissimilar materials gave an interconnected porous structure with a 400 μm pore size, and the shear stress studies showed a value of 33.2 MPa, which shows a good mechanical interlocking between them.[233]

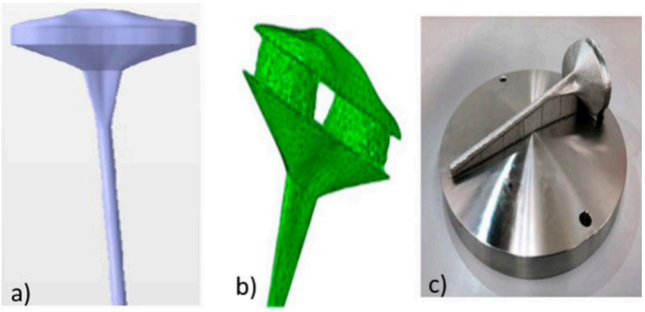

Figure 8. Various steps of tibia implant formation using 316L SS; a) design of tibia intramedullary implant, b) optimized form, and c) implant after selective laser melting. Adapted with permission from ref 234. Copyright 2019, Elsevier.

Tilton et al. proposed the fabrication of proximal humerus fracture fixation plates using stainless steel with the help of LPBF. The new implant reduced the risk of screw cut-out and varus collapse (tibial loosening). Higher hardness (49%) was observed for the implant than the forged 316L SS due to the fast cooling during LPBF, which leads to increased microhardness and refined microstructure. They could develop the design considering the patient's anatomy, fracture type, and bone quality within a short period of 24 h, which shows the advantage of AM.[235] To increase the biocompatibility and mechanical properties of the PEEK scaffold, Jung et al. coated the 3D-printed sample with Ti. The enhanced tensile strength (84.1 MPa) of the scaffold was ascribed to the higher crystallinity provided to the scaffold due to the elevated temperature during AM fabrication, and this value was higher than the scaffolds prepared by other conventional methods. The larger surface area created via AM and the surface chemical composition helped in an early initial cell attachment of the scaffold to the body, which led to faster proliferation and differentiation due to the possibility of direct cell-cell-cell communication. The results were proved *in vivo* which showed that the modified topography and chemical composition of the surface helped in faster cell proliferation and differentiation, and after 12 weeks of implantation, the new bond formation could be observed.[236]

Graphene is a two-dimensional nanoscale material that could be synthesized via chemical vapor deposition and electrochemical and mechanical exfoliation methods.[237] Though conventional methods such as soft lithography and direct writing are used to make 2D structures, they face a lot of drawbacks such as limitations in using a variety of substrates, high operational costs, high defect density, and additional etching process make these methods less desirable. AM can overcome these difficulties in a more desirable way, where a computer-aided program directs the process, and even the complex structures could be developed which otherwise would be very difficult to achieve. With high resolution, effective products could be developed that can be fabricated according to the needs of the end-user requirements with superior mechanical properties. Among various additive manufacturing methods, the PBF method is the most accepted method for graphene-based synthesis compared to the others. The composites thus formed possess a higher amount of mechanical, thermal, and optical properties with greater chemical stability that is not possessed by individual components.[238] With excellent biocompatibility, cell seeding, viability, and mobility, Chen et al. prepared 3D thermoplastic polyurethane (TPU)/PLA/graphene oxide (GO) nanocomposites with 3D structures using additive manufacturing methods.[239]

Studies have proved that a double deposition of the filament can improve the interaction between the matrix and the composite, and thus higher mechanical properties are shown that are more related to the bone tissue.[240] Arif et al. in the year 2020 successfully developed scaffolds with PEEK, carbon nanotubes, and graphene, and the results showed that the product formed had better dimensional stability, and the tensile strength could be modified by varying the nanostructures' weight ratio. It was also noted that the printing dimensions can greatly affect the mechanical properties. The density of vertically fabricated samples (1.27 g/cm^3) was higher than horizontally fabricated ones (1.15 g/cm^3). It is because of the good degree of compaction of layers in the vertical phase due to the less deposition time in the XY plane that is still in a molten state.[241] It was suggested by Larsson et al. in 2022 that Zr-based bioglass ($Zr_{59.3}Cu_{28.8}Al_{10.4}Nb_{1.5}$) could show biocompatibility similar to that of Ti alloys, and the fabrication of the bone implant with the former was done. When the laser power was higher (95 W), crystalline phases were formed in the samples, and the surface roughness was reduced from 11.6 to 4.6 μm. Higher laser power also caused a reduction in unmelted powder particles on the surface thus providing a better spreading of powder bed over the melted one. The cytocompatibility studies showed no significant toxicity, and irrespective of the surface roughness, proliferation of the cells was observed.[242] A novel metal composition Ti-35Nb-7Zr-5Ta was suggested by Nadammal et al. where they fabricated the scaffold with the aid of L-PBF with more than 98.5% of theoretical density. The samples fabricated could obtain the elongation to break at a higher rate as 25%. The samples could employ a passivation behavior while undergoing corrosion studies, and the values were much better than commercially pure Ti (E_{CORR}: −0.16 to −0.25 and I_{CORR}:0.25 to 0.033) implying that the samples can be a potential replacement for various metal alloys in AM for future applications in orthopedics. The cytotoxicity analysis of the metal composites indicated that the samples could enhance the cell growth without any toxicity even after 7 days, and fluorescence analysis exhibited a large number of live cells.[243] Another paper published by Gurbova et al. conducting a theoretical study of the above-mentioned metal composites proved that this composite is a good candidate for the fabrication of orthopedic internal fixation devices.[244] Corona-Castuera et al. were able to fabricate a partial hip prosthesis with the aid of DMLS using stainless steel powder following the patient's anatomy. The sample fabricated possessed a density of 0.72 g/cm^3, and the elastic modulus was observed to 0.25 GPa for a simple gyroid structure and 0.95 GPa for double gyroid structure.[245]

https://doi.org/10.1021/acsomega.4c04870
ACS Omega 2024, 9, 44042−44075

Table 8. Various Metal Alloys Used in AM for Orthopedic Implant Applications

metal alloy	year	AM method	applications	specifications	author
Ta	2010	Laser engineered net shaping	Cortical bone replacement	Localized melting of the sample provided particle bonding and reduced brittleness	Balla et al.[227]
Ti-24Nb-4Zr-8Sn	2011	Selective laser melting	Acetabular hip cup	99.3% dense sample by adjusting the scan speed	Zhang et al.[161]
Ni-Ti	2013	Selective laser melting	Bone replacement	Efficient carrier for human mesenchymal stem cells and reduction of Ni leaching from 258 ng/mL to 101 ng/mL by varying laser scan diameter	Habijan et al.[228]
Zr doped Co-Cr-Mo alloy	2015	Electron beam melting	Trabecular and femur bone replacement	High implant stability and bone response	Stenlund et al.[229]
Ni-Ti	2016	Selective laser melting	Mandibular Reconstruction	Porous structure with stiffness related to the surrounding bone	Jahadakbar et al.[230]
Co-Cr alloy	2016	Electron beam melting	Bone implant	Bone in-growth in the interconnected porous structure similar to that of Ti-6Al-4V	Shah et al.[231]
calcium sulfate hemihydrate/ RBC3200 epoxy resin	2018	Binder jetting	Cortical bone repair	Though the elastic modulus was 6.2 MPa, other mechanical properties of bones were lacking	Tai et al.[232]
PEEK/TiO_2	2019	Fused deposition modeling	Bone screw	Faster proliferation and differentiation due to the large surface area provided by AM fabrication	Jung et al.[236]
316L SS	2020	Laser powder bed fusion	Proximal humerus fracture fixation plates	Reduced possibility for screw cut-out and varus collapse and fabrication of implants within 23 h	Tilton et al.[235]
CNT/GNP/PEEK	2020	Fused filament fabrication	scaffold	The dimensional stability and density of the samples depended on the print direction	Arif et al.[241]
Stainless steel	2021	Direct metal laser sintering	Partial hip prosthesis	Prosthesis with 0.72 g/cm^3 density	Corona-Castuera et al.[245]
$Zr_{59.3}Cu_{28.8}Al_{10.4}Nb_{1.5}$ bioglass	2022	Selective laser melting	Bone implant	As the laser power increased (55−95 W), surface roughness decreased (11.6 to 4.6 μm)	Larsson et al.[242]
Ti-35Nb-7Zr-5Ta	2022	Laser powder bed fusion	Patient specific orthopedic implants	More corrosion resistance and better cell proliferation than existing pure Ti	Nadammal et al.[243]

https://doi.org/10.1021/acsomega.4c04870
ACS Omega 2024, 9, 44042−44075

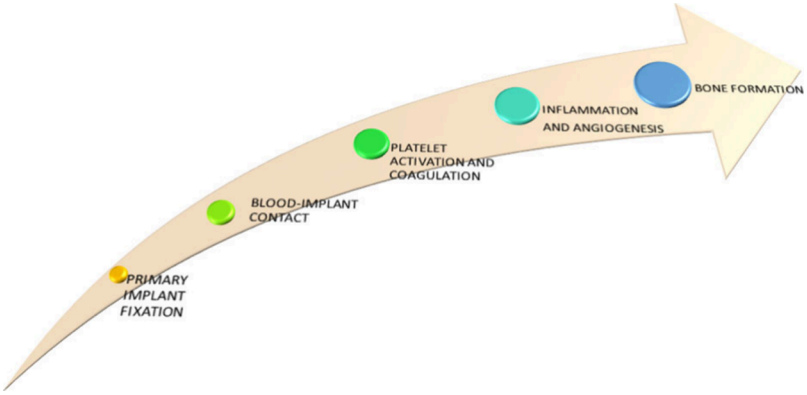

Figure 9. Various steps in bone healing with the aid of implants.

Electrospinning has been used over the years for the fabrication of scaffolds with the aid of polymer composites and ceramic materials. It allows the fabrication of porous scaffolds that can enhance osteogenesis.[246] Though it is said that all polymers can be electrospun, in an actual scenario this is not possible always. Another problem faced in electrospinning is the use of various polymer composites, which will not give a desired result if the composites are not completely miscible. Electrospinning is also a time bound task, and the scaffold fabricated usually lacks tensile strength which minimizes its application to nonload bearing implants.[247] Usage of polymer composites in AM can overcome these limitations. Mushtaq Alam et al. reported various PLA-ceramic composite implants fabricated with the aid of ME. Biphasic calcium phosphate,[248] β-TCP/α-Al_2O_3,[249] ZrO_2,[250] ZrO_2/Al_2O_3,[251] $DyPO_4$,[252] etc. had been used to reinforce PLA. Usage of 5% biphasic calcium phosphate gave a stable product with good cell viability and biocompatibility. Reinforcement of β-TCP with alumina allowed its usage up to 20% which was not possible in the previous experiment with biphasic calcium phosphate, and they could achieve an infill density of 100%. Even the tensile strength of the samples was improved to a higher extent. ZrO_2 added PLA implants were fabricated with uniform dispersion of the former, and defect-free shapes could be obtained via FDM. Though the addition of ZrO_2 reduced the mechanical properties, bonelike characteristics were maintained by the samples to a great extent. ZrO_2 reinforcement with alumina gave the structure with an infill pattern of 350−450 μm, and an increment in the hardness was observed. The better results obtained by the studies encouraged them to fabricate various prototypes of clavicle bone, clavicle hook plate, and various screws, which shows the success of fabrication of the implant via FDM. Addition of $DyPO_4$ not only enhanced the various mechanical properties but allowed the bioimaging of the AM fabricated sample that would be a breakthrough in the real-time analysis. Table 8 summarizes various metal implants and composites fabricated by using AM.

4. DISCUSSION

Bone consists of both organic (collagen types I, III, and IV and fibrillin) and inorganic (HAP) components. Human bones are of two types: compact bone (cortical bone), which is almost solid with less porosity (10−30%), and trabecular bone (cancellous bone), which has a porosity between 50 and 90%. Accordingly, their mechanical properties also differ.[73] The compressive strength of cancellous bone is 5−10 MPa, but for cortical bone it is 100−230 MPa. Young's modulus of both bones also differ to a large extent. Trabecular bone possesses very little Young's modulus (0.05−0.10 GPa), whereas it is 17−20 GPa for cortical bone.[253] Polymers, metals, ceramics, or biocomposites can be used for implant fabrication for orthopedic trauma. With personalization and precision implants are to be fabricated that have the potential for nutrient and cell permeability and bone growth along with mechanical properties similar to that of human bone to avoid the stress-shield effect.[254,246] Bone healing with the aid of implants goes through various steps as follows.[255]

AM is used for the fabrication of implants due to its unique features in printing patient-specific implants with mechanical properties similar to those of human bone. Varying the scan speed and other parameters while printing can alter the characteristics of the fabricated materials. Freedom of design, controlled porosity, and printing complex structures with microarchitecture give more opportunities for the fabrication of desired products with more precision.[256] Though there are various types of methods in AM fabrication, only a few are widely used in implant fabrication. SLS and SLM are mainly used for the fabrication of metal implants. SLS can provide high material utilization without any support structure with a high print speed. However, it lacks a powder surface finish, and postprocessing is needed before using the structure implant applications.[257] SLM provides a more accurate product with smooth surfaces, and a variety of materials can be used for the fabrication of even complex structures. Misalignment of the layers due to high temperature during the fabrication and low speed for printing are the difficulties faced during the fabrication.[258] EBM has also been used widely in manufacturing implants, since the production of dense materials is possible via EBM with high efficiency and product strength. Postprocessing is needed after the fabrication of implants since the surface finish is very poor and it takes a long time to print the material.[259] Another fabrication method widely used in AM implants is FDM due to its ability to have scalable products with high surface finish, better mechanical strength and with low investment cost and cost-to-size ratio a wide range of materials can be printed using simple manufacturing techniques.[8]

Among the materials used for AM, metal AM of Ti-6Al-4V, Fe, Zn, Mg, 316L SS are most widely used (about 75%) since these can provide long-term stability and mechanical properties such as elasticity and high strength similar to the human bone adjusting the parameters of 3D printing.[22] However, the lack of tribological properties can cause inflammation of the implanted area, and the leaching of toxic ions can have a

https://doi.org/10.1021/acsomega.4c04870
ACS Omega 2024, 9, 44042−44075

negative impact on metal implant surgery. Incorporation of biomaterials during printing or coating can induce biochemical properties to these implants that can reduce rejection of implants and the leaching of metal ions and corrosion.[260] Since ceramics can offer biocompatibility, bone conductivity, resorption, and corrosion resistance, HAP, β-TCP, bioglass, etc. have been used for AM implant fabrication and coating of metal fabricated implants. Yet they have high elastic modulus, insufficient fracture strength, and inadequate fracture toughness.[261] The choice of polymers for scaffold fabrication is due to their biodegradability, biocompatibility, nontoxicity, cell affinity, ease of availability, and bioactivity (for natural polymers). However, they are used for nonload bearing applications or need to be incorporated with metals or ceramics to improve their properties since the main drawback of polymers is the lack of mechanical properties that match human bone.[262]

5. CHALLENGES AND FUTURE PERSPECTIVES OF ADDITIVE MANUFACTURING OF ORTHOPEDIC IMPLANTS

Though orthopedics has gained much from the area of additive manufacturing both economically and medically, there are many difficulties encountered while developing an implant through this procedure. It is challenging to prepare a patient-specific implant for load-bearing application without any flaws from start to postprocessing. The main challenges that are faced in AM are lack of resolution, surface finish, and layer bonding in microscale manufacturing, which require post-processing techniques such as sintering. The limited materials available for 3D printing also make it less usable for utilizing this technology in various industries. Since each of the parameters used can affect the finishing of the structure and both mechanical as well as biological properties, the optimization consumes a lot of time with the option to increase the mechanical properties.[45] Columnar grains and periodic cracks may form during the heating and eventual cooling in AM methods, which can affect the nanostructure properties of the materials that are used in additive manufacturing with the preferred topological shape of the scaffold.[73] Another problem experienced by the additive manufacturing process is the deformation that could be formed due to repeated treatment of the scaffold with high energy and successive sudden cooling. As a solution for this problem, scientists suggest postheat treatment after the additive manufacturing process. This helps to modify and stabilize the microstructure and improve its performance by relieving stress.[263] Nonequilibrium solidification in the procedure needs to be attended to by formulating new compositions of the material matrix rather than depending on the powder metallurgy industry to buy metal powder compositions.[264] Since the test standards for the comparison of the manufactured implants are still limited, it is difficult to compare the printed parts by various additive manufacturing techniques. Standards are to be developed in the areas of design, development, and experimental parts.[265] Fabrication of thin-walled and hollow structures also is still at stake since the deformation of the structure can take place on layer-by-layer formation due to the difference in temperature of the successive layers. It can also lead to the formation of a void in the structure resulting in reduced interconnection.[45] Dimensional correctness is another area that needs attention while fabricating the implants. Studies have reported that it is an arduous task to do the precision in the Z-direction since the control of various parameters such as powder densification, solidification evaporation, etc. can affect the desired outcome.[266] Measures are to be taken to scale up the production of implants with better resolution and precision via AM.

Once these problems have been rectified, AM could provide implants for even larger bone defects that are patient-specific, and its intraoperative guidance would help to avoid implant failure. Since AM-fabricated products can provide strength and elastic properties similar to that of human bone, AM products can improve human life to a greater extent.[267] Including antibiotics, carbonaceous materials, antimicrobial polymers, etc. can increase the clinical application of scaffolds.[8] Fabrication of a porous scaffold providing new bone infiltration can increase implant stability. Incorporating finite element analysis and image mapping in AM opens new areas for the orthopedic implant industry.[268] To date, only single-cell print implant products have been developed, and the development of implants that can replace physiologically functional bone marrow will be a crucial step in this area. Incorporating artificial intelligence in topology optimization of the internal structure of bone can be a powerful tool in AM.[269] Research works have been started on 3D printing of anatomical models and other materials from biomass[270,271] and other natural products.[272,273] More development and studies in this area can lead to the development of implants using biomass. Though in its infancy, studies have emerged on the development of 4-dimensional shape memory smart scaffolds[274] and complex and curved 5-dimensional scaffolds.[275] Advancement of these technologies could bring about a solution for complex and stronger implant fabrication and can open up the path for next-generation biomaterials.

5.1. Melt Electro Writing (MEW). It is one of the newest AM methods used in biomedical applications, where the three-dimensional structure is fabricated with the aid of an electric field that melts the polymer under consideration. Intricate structures are created with the precise control of the scaffold's geometry. Application of the electrodynamic forces onto the nozzle that contains molten polymer creates charged droplets that are deposited on to the surface according to the designed structure.[276] Unlike the electrospinning method, there is no formation of a Taylor cone, and no whipping of droplets takes place, whereas the layer formation in MEW begins only when the molten polymer connects to the collector. Applied voltage and the viscosity of the polymer play a crucial role in the fabrication process along with the nozzle to collector distance.[277] The superiority of this technique toward FDM is that ultrafine fibers can be created that can fabricate complex structures with precision.[278] This method has been successfully used in the development of drug delivery systems and implant fabrication. PCL[279] and its various composites,[280] PLA,[281,282] poly(dioxanone)[283] etc. have been used in MEW.

5.2. Two-Photon Polymerization. Two-Photon Polymerization (multiphoton lithography) (TPP) is the AM method that utilizes the possibility of two photon absorption.[284] The photosensitive liquid resin absorbs two photons simultaneously that are emitted via laser or infrared rays and excited to higher state wherein the polymerization occurs. The main peculiarity of this method is the fast and precise printing of complex three-dimensional structures.[285] Liquid polymeric acrylates and epoxides etc. are the main feedstocks in TPP.[286] Submicron sized scaffolds and microneedle arrays[287] have been prepared via this method, and ossicular prostheses[288] also have been

https://doi.org/10.1021/acsomega.4c04870
ACS Omega 2024, 9, 44042−44075

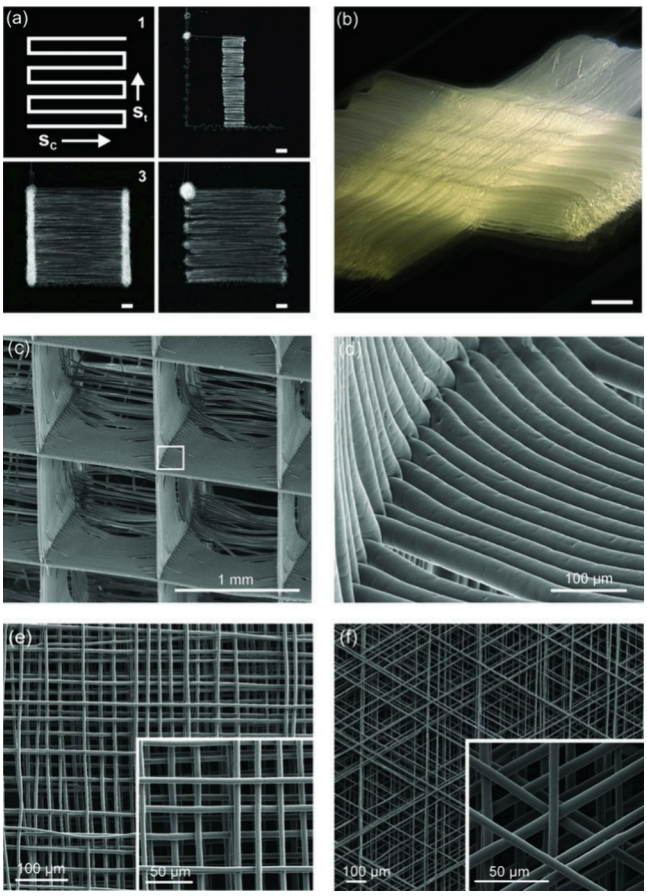

Figure 10. Various stages of PCL MEW: a) the square wave pattern in the XY direction at various time durations (2:0.1, 3:0.002, 4:0.005 m min^{-1} and S_C - straight line speed, S_T - turning speed), b) scaffold fabricated via MEW, c) stacked fibers, d) intertwined fibers, e) scaffold with 90° orientation, f) scaffold with 60° orientations. Reproduced with permission from ref 276. Copyright 2011, John Wiley and Sons.

reported fabricated via this method. Kampleitner et al. reported a TPP fabricated scaffold using methacrylated poly(D,L-lactide-*co*-ε caprolactone), and both the *in vitro* as well as *in vivo* evaluations were successful. The tailor-made scaffolds possessed a 20% of compression recovery and were observed to be a good candidate for biodegradable scaffold.[289]

5.3. 4-D Printing. 4-D printing is considered to be "3-D printing and time" where the fabrication of implants take place with the aid of computer fabricated design, 3-D printing, and smart materials. In 3-D printing where the focus is on XYZ planes, 4-D printing takes into consideration the time dimension too. Dynamic structures are built incorporating smart materials that can transform its shape when external stimuli such as heat, light, electric field, or humidity are applied.[290] The 4-D printed products can have various properties such as self-adaptability, expandability as well as shrinkage, and self-assembling ability. 3-D digital data are used for smart design, and shape-memory polymers or alloys are used to create dynamic structures that can switch shape for self-repairing and self-regeneration.[291] After the images are captured and the required format is converted into a CAD file, the smart material is printed which can grow over time on the human body. This provides endless possibilities in fabrication of custom-made implants that can offer intelligent materials to deal with bone-related problems, and it can reduce the materials needed and its difficulty in assembling the parts.[292] 4-D printing is the advanced version of 3-D printing to fabricate complex and flexible structures by keeping time as the fourth dimension. The same printing methods and devices can be used for layer-by-layer fabrication of implants that are responsive to stimuli to expand and reshape in human body.[293] The materials used for fabrication include polymers that are temperature sensitive, photoresponsive, and ionic interactive. It was reported by Grinberg et al. that the 4-D printed implant prosthesis using barium titanate and polyamide 11 can respond to an electromagnetic stimulus. Studies proved that the prosthesis could withstand the mechanical strain that a human knee can go through.[294] Ghalayaniesfahani et al. developed a shape memory structure using PLA and poly(butyl succinate), and this biobased sandwich structure could withstand greater elongation at break had a 96% recovery ratio.[295] Liu et al. developed a 4-D printed craniofacial implant, and the guided bone regenerative membrane they developed using PCL and poly(glycerol sebacate) (PGS) and coated with polydopamine (PDA) for mussel adhesion was a success both *in vitro* and *in vivo*. The vertical bone defect was treated effectively since flexibility of the implant helped in maintaining the curvature of the alveolar bone. Since the vertical bone defect could be treated effectively these types of implants indicate a promising future in bone defect treatments.[296]

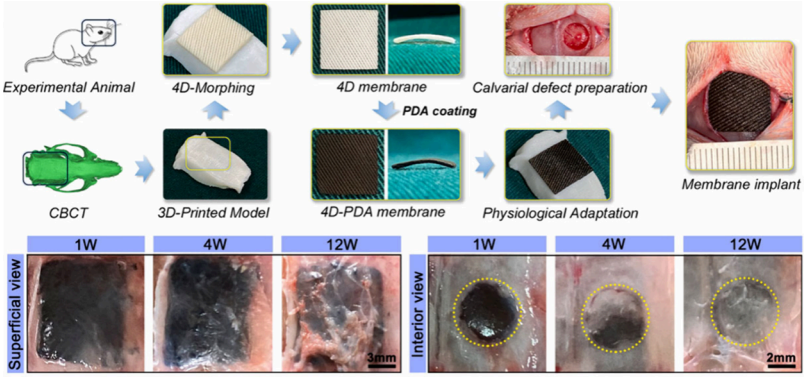

Figure 11. Various stages of the *in vivo* analysis of a 4-D printed PCL-PGS implant coated with PDA for vertical bone defects. Reproduced with permission from ref 296. Copyright 2021, Elsevier.

https://doi.org/10.1021/acsomega.4c04870
ACS Omega 2024, 9, 44042−44075

The main challenges faced in this area are the lack of availability of the smart materials and its compatibility in the human body. Moreover, all of the available smart materials cannot be used in all of the printing procedures due to its response to external stimuli like temperature. It was reported that the usual AM methods used for implant fabrication such as FDM, DLP, DIW, SLA, and SLS could be used in 4-D implant fabrication. But the difficulties faced while using these methods are the environmental response of the material printed. Since FDM like methods can impart a high temperature, this can affect the fabrication of the smart material. Another negative impact of using these methods is that the low resolution of the products fabricated via these methods may affect the applicability of these 4-D printed implants. Since the actuation of the smart materials depends on printing parameters too, introducing a multistimuli response also is difficult. Fabrication of multimaterials as well as composites responding to various stimulus can really open up a new chapter in implant fabrication.[297]

5.4. 5-D Printing. 5-D printing is the most advanced version of AM which is still in its development stage. 5-D printing offers the possibility of printing in five axes by moving the printhead in five different angles along with the plateau on which the structure is printed. This helps in printing most complex structures with curved layers that cannot be achieved via 3-D printing. Creating weak points are avoided by curved layers and stronger structures that are three to five times stronger than 3-D printed structures built in this manner with 25% less materials.[298] The 5-D printing machine is reported to have five degrees of freedom (two rotational axes along with three axis of movement).[299] This method can make use of the 3-D CAD file and design and printing materials but should be provided with a dynamic plateau instead of static one. It has the potential to fabricate human bone that has complex and curved structures with more strength than 3-D printing since both the print head as well as the plateau are moving.[300] But the actualization of this procedure is rather at its infancy due to the high cost of the printing machine as well as difficulties in maintenance and lack of personnel trained for this. By tackling this problem in an effective manner, 5-D printed scaffolds can be available to patients in an easier way.[301]

5.5. 6-D Printing. Another future work that could be looked forward to is the combination of 4-D and 5-D printing. It would be printing of the curve-shaped scaffolds making use of the five-dimensional technology that also can provide intelligent surfaces with a shape response that could be provided according to the environmental stimuli. This can help the fabrication of a well-designed implant that really is efficient to meet the patient's requirements. The materials using for this fabrication are smart materials that contain multiple intelligences, and this method can provide greater accuracy to the implants.[302] This concept was introduced by Georgantzinos et al., and they believe the actualization of this procedure could bring about stronger products within minimal manufacturing time and greater adaptability. They propose that this method can help in printing of even the most complicated structures with minimal raw materials and greater flexibility. 6-D printing using nanoreinforced polymers can aid in more applicability.[303]

6. CONCLUSION

This review briefly discusses the most promising additive manufacturing technology in the area of orthopedics. For the past few decades, the contribution of additive manufacturing toward the development of various implants and scaffolds has been noteworthy. Among the various additive manufacturing methods, the most used ones for manufacturing orthopedic implants are binder jetting, fused deposition modeling, selective laser melting, selective laser sintering, and electron beam melting. Various materials such as metals, polymers, and ceramics have been used for the fabrication of implants; depending upon the specificity of the patient, the choice of raw materials diversifies. For the scaffolds that are to be bioresorbable, the most used raw materials are bioceramics/polymer composite, and for nonload bearing applications polymers are the best choice. For load-bearing applications like knee joints, hip replacements, etc. metal alloys like Ti-6Al-4V, stainless steel, etc. are the most preferred implants. Since every parameter used in additive manufacturing can directly decide the features of the implant, the correct choice of each parameter is of utmost importance. Manufacturing of implants using fused deposition modeling, direct ink writing, material extrusion etc. have reported to reduce the corrosion of implants and control the tensile strength and Young's modulus of the metal implants. Fused deposition modeling is an extensively used manufacturing method for polymer implants that enhances the properties of polymers and controls the bioresorbability and drug delivery. Functionalized implants to avoid undesired bacterial and other microbial infections and enhanced bioactivity can offer a long life to the AM fabricated implants. Bio-HEA implants are one of the fast-growing areas in recent years, and the implants developed show better mechanical as well as biological properties, and this type of implant can avoid many of the problems faced by implants fabricated using other metal alloys. New composite systems are yet to be developed that can handle both the biological and mechanical properties of human bone in the closest proximity. The development of materials with tunable interfaces can bring about smart implants with improved degradation resistance.

AUTHOR INFORMATION

Corresponding Author

Vijayalakshmi Uthirapathy − *Department of Chemistry, School of Advanced Sciences, Vellore Institute of Technology, Vellore 632014, India;* orcid.org/0000-0003-0727-4277; Email: vijayalakshmi.u@vit.ac.in

Author

Alphonsa Joseph − *Department of Chemistry, School of Advanced Sciences, Vellore Institute of Technology, Vellore 632014, India*

Complete contact information is available at: https://pubs.acs.org/10.1021/acsomega.4c04870

Notes

The authors declare no competing financial interest.

ACKNOWLEDGMENTS

The authors would like to thank the Vellore Institute of Technology for all the help and support provided for carrying out the research work.

ABBREVIATIONS

AM - Additive manufacturing
BJ - Binder jetting

https://doi.org/10.1021/acsomega.4c04870
ACS Omega 2024, 9, 44042−44075

BO - Bio-Oss
β-TCP - β-Tricalcium phosphate
CLIP - Continuous Liquid Interface Production
DBM - Decellularized Bone Matrix
DED - Direct Energy Deposition
DIW - Direct ink writing
DLP - Digital Light Processing
DMLS - Direct metal laser sintering
DOD - Drop-on-demand
ECM - Extracellular matrix
EBM - Electron beam melting
FDM - Fused deposition modeling
FFF - Fused filament fabrication
HAP - Hydroxyapatite
LOM - Laminated object manufacturing
LENS - Laser Engineered Net Shaping
LPBF - Laser powder bed fusion
ME - Material extrusion
WE43 - Magnesium Elektron
$Mg(OH)_2$ - Magnesium hydroxide
MgP - Magnesium phosphate
(MJ) - Material jetting
MBG - mesoporous bio glass
NPJ - Nanoparticle jetting
PA2200 - Polyamide 2200
PBF - Powder bed fusion
PCL - Polycaprolactone
PHBHH - Poly[(*R*)-3-hydroxybutyrate-*co*-(*R*)-3-hydroxy hexanoate)
PJ - Polyjets
PLA - Polylactic acid
PDLGA - Poly(lactic acid-*co*-glycolic acid)
PEEK - Poly ether-ether-ketone
PHBV - Poly(3-hydroxybutyrate-*co*-3-hydroxy valerate)
PMMA - Poly(methyl methacrylate)
PPF - Polypropylene fumarate
SLA - Selective laser apparatus
SLS - Selective laser sintering
SBF - Simulated body fluid
SRP - Subtractive rapid prototyping
UAM - Ultrasonic additive manufacturing
316L SS - 316L stainless steel

REFERENCES

(1) Rama, M.; Vijayalakshmi, U. Influence of silk fibroin on the preparation of nanofibrous scaffolds for the effective use in osteoregenerative applications. *J. Drug Delivery Sci. Technol.* **2021**, *61*, No. 102182.
(2) Rama, M.; Vijayalakshmi, U. Biological and mechanical investigation of novel flax/silk protein-based nanofibrous scaffold for bone regeneration. *Progr. Nat. Sci.: Mater. Inter.* **2022**, *32*, 443−455.
(3) Priyadarshini, B.; Ramya, S.; Shinyjoy, E.; Kavitha, L.; Gopi, D.; Vijayalakshmi, U. Structural, morphological and biological evaluations of Cerium incorporated Hydroxyapatite sol-gel coatings on Ti-6Al-4V for orthopaedic applications. *J. Mater. Res. Technol.* **2021**, *12*, 1319−1338.
(4) Kim, T.; See, C. W.; Li, X.; Zhu, D. Orthopedic implants and devices for bone fractures and defects: Past, present and perspective. *Eng. Regen.* **2020**, *1*, 6−18.
(5) Wang, S. P.; Xu, J. TiZrNbTaMo high-entropy alloy designed for orthopedic implants: As-cast microstructure and mechanical properties. *Mater. Sci. Eng., C* **2017**, *73*, 80−89.
(6) Murugapandian, R.; Clement, S.; Uthirapathy, V. Fabrication and in vitro drug delivery evaluation of Cephalexin Monohydrate-loaded PLA:PVA/HAP:TiO_2 fibrous scaffolds for bone regeneration. *ACS Omega* **2023**, *8*, 5017−5032.
(7) Chen, L. J.; Li, T.; Li, Y. M.; He, H.; Hu, Y. H. Porous Titanium implants fabricated by metal injection molding. *Trans. Nonferrous Met. Soc. China* **2009**, *19*, 1174−1179.
(8) Dubey, A.; Vahabi, H.; Kumaravel, V. Antimicrobial and biodegradable 3D printed scaffolds for orthopedic infections. *ACS Biomater. Sci. Eng.* **2023**, *9*, 4020−4044.
(9) Anavadya, K. K.; Vijayalakshmi, U. A comprehensive review of fabrication techniques and their impact on mechanical behaviour and osteoregenerative applications of bioactive inorganic substituents. *Mater. Res. Lett.* **2023**, *11*, 821−855.
(10) Shuai, C.; Li, D.; Yao, X.; Li, X.; Gao, C. Additive manufacturing of promising heterostructure for biomedical applications. *Inter. J. Extrem. Manuf.* **2023**, *5*, No. 032012.
(11) Haleem, A.; Javaid, M. 3D printed medical parts with different materials using additive manufacturing. *Clin. Epidemiol. Glob. Health* **2020**, *8*, 215−223.
(12) Abdullah, M.; Mubashar, A.; Uddin, E. Structural optimization of orthopedic hip implant using parametric and non-parametric optimization techniques. *Biomed. Phys. Eng. Express* **2023**, *9*, No. 055026.
(13) Park, J. W.; Kang, H. G. Application of 3-dimensional printing implants for bone umors. *Clin. Exp. Pediatr.* **2022**, *65*, 476−482.
(14) Pal, A. K.; Mohanty, A. K.; Misra, M. Additive manufacturing technology of polymeric materials for customized products: Recent developments and future prospective. *RSC Adv.* **2021**, *11*, 36398−36438.
(15) Standard ASTM. *Standard Terminology for Additive Manufacturing Technologies*; ASTM International, 2012; F2792-12a.
(16) Bose, S.; Ke, D.; Sahasrabudhe, H.; Bandyopadhyay, A. Additive manufacturing of biomaterials. *Prog. Mater. Sci.* **2018**, *93*, 45−111.
(17) Lu, Y.; Chi, B.; Liu, D.; Gao, S.; Gao, P.; Huang, Y.; Yang, J.; Yin, Z.; Deng, G. Wideband metamaterial absorbers based on conductive plastic with additive manufacturing technology. *ACS Omega* **2018**, *3*, 11144−11150.
(18) Ghosh, A.; Orasugh, J. T.; Ray, S. S.; Chattopadhyay, D. Integration of 3D printing-coelectrospinning: Concept shifting in biomedical applications. *ACS Omega* **2023**, *8*, 28002−28025.
(19) Xu, S.; Fang, M.; Yan, X. Research on rheology and formability of SiO_2 ceramic slurry based on additive manufacturing technology via a light curing method. *ACS Omega* **2022**, *7*, 32754−32763.
(20) Huner, B.; Kısı, M.; Uysal, S.; Uzgoren, I. N.; Ozdogan, E.; Suzen, Y. O.; Demir, N.; Kaya, M. F. An overview of various additive manufacturing technologies and materials for electrochemical energy conversion applications. *ACS Omega* **2022**, *7*, 40638−40658.
(21) Bourell, D. L. Perspectives on additive manufacturing. *Annu. Rev. Mater. Res.* **2016**, *46*, 1−18.
(22) Mobarak, M. H.; Islam, M. A.; Hossain, N.; Al Mahmud, M. Z.; Rayhan, M. T.; Nishi, N. J.; Chowdhury, M. A. Recent advances of additive manufacturing in implant fabrication − a review. *Appl. Surf. Sci. Adv.* **2023**, *18*, No. 100462.
(23) Haleem, A.; Javaid, M. 3D printed medical parts with different materials using additive manufacturing. *Clin. Epidemiol. Glob. Health* **2020**, *8*, 215−223.
(24) Charles, W. H. Apparatus for Production of Three-Dimensional Objects by Stereolithography. United States Patent, Appl. No. US638905, Filed 1984.
(25) Juster, N. P. Rapid prototyping using selective laser sintering process. *Assem. Autom.* **1994**, *14*, 14−17.
(26) Crump, S. S. Apparatus and method for creating three-dimensional objects. United States Patent, Appl. No. US5121329, Filed 1992.
(27) Bandyopadhyay, A.; Gualtieri, T.; Bose, S. Global Engineering and Additive Manufacturing. In *Additive Manufacturing*. Bandyopadhyay, A., Bose, S., Eds.; CRC Press: New York, 2015; pp 9−11.

https://doi.org/10.1021/acsomega.4c04870
ACS Omega 2024, 9, 44042−44075

(28) Glasser, M. *Case Studies: Innovative Solutions from EOS for E-Manufacturing to Cope with Current Market Trends*; European Congress and Exhibition on Powder Metallurgy, European PM Conference Proceedings; The European Powder Metallurgy Association 2003, 2:1−6.
(29) Murr, L. E.; Gaytan, S. M.; Martinez, E.; Medina, F.; Wicker, R. B. Next generation orthopaedic implants by additive manufacturing using electron beam melting. *Int. J. Biomater.* **2012**, *2012*, No. 245727.
(30) González-Henríquez, C. M.; Sarabia-Vallejos, M. A.; Rodriguez-Hernandez, J. Polymers for additive manufacturing and 4D-printing: Materials, methodologies, and biomedical applications. *Prog. Polym. Sci.* **2019**, *94*, 57−116.
(31) Edgar, J.; Tint, S. Additive manufacturing technologies: 3D printing, rapid prototyping, and direct digital manufacturing. *Johnson Matthey Technol. Rev.* **2015**, *59*, 193−198.
(32) Pagac, M.; Hajnys, J.; Ma, Q. P.; Jancar, L.; Jansa, J.; Stefek, P.; Mesicek, J. A review of vat photopolymerization technology: Materials, applications, challenges, and future trends of 3D printing. *Polymer* **2021**, *13*, 598.
(33) Bandyopadhyay, A.; Mitra, I.; Bose, S. 3D printing for bone regeneration. *Curr. Osteoporos. Rep.* **2020**, *18*, 505−514.
(34) van Bochove, B.; Hannink, G.; Buma, P.; Grijpma, D. W. Preparation of designed Poly(Trimethylene Carbonate) meniscus implants by stereolithography: challenges in stereolithography. *Macromol. Biosci.* **2016**, *16*, 1853−1863.
(35) Protick, F. K.; Amit, S. K.; Amar, K.; Nath, S. D.; Akand, R.; Davis, V. A.; Nilufar, S.; Chowdhury, F. Additive manufacturing of viscoelastic polyacrylamide substrates for mechanosensing studies. *ACS Omega* **2022**, *7*, 24384−24395.
(36) Geven, M. A. *Additive Manufacturing of Bone-Forming Composite Implants Using Photo-Curable Poly(Trimethylene Carbonate)-Based Resins*. PhD Dissertation, University of Twente, 2018.
(37) Tesavibul, P.; Chantaweroad, S.; Laohaprapanon, A.; Channasanon, S.; Uppanan, P.; Tanodekaew, S.; Chalermkarnnon, P.; Sitthiseripratip, K. Biocompatibility of hydroxyapatite scaffolds processed by lithography-based additive manufacturing. *Biomed. Mater. Eng.* **2015**, *26*, 31−38.
(38) Tessanan, W.; Daniel, P.; Phinyocheep, P. Development of photosensitive natural rubber as a mechanical modifier for ultraviolet-curable resin applied in digital light processing-based three-dimensional printing technology. *ACS Omega* **2021**, *6*, 14838−14847.
(39) Dean, D.; Mott, E.; Luo, X.; Busso, M.; Wang, M. O.; Vorwald, C.; Siblani, A.; Fisher, J. P. Multiple initiators and dyes for continuous digital light processing (cdlp) additive manufacture of resorbable bone tissue engineering scaffolds: a new method and new material to fabricate resorbable scaffold for bone tissue engineering via continuous digital light processing. *Virtual Phys. Prototyp.* **2014**, *9*, 3−9.
(40) Medellin, A.; Du, W.; Miao, G.; Zou, J.; Pei, Z.; Ma, C. Vat photopolymerization 3D printing of nanocomposites: A literature review. *J. Micro Nano-Manuf.* **2019**, *7*, No. 031006.
(41) Bloomquist, C. J.; Mecham, M. B.; Paradzinsky, M. D.; Januszewicz, R.; Warner, S. B.; Luft, J. C.; Mecham, S. J.; Wang, A. Z.; DeSimone, J. M. Controlling release from 3D printed medical devices using CLIP and drug-loaded liquid resins. *J. Controlled Release* **2018**, *278*, 9−23.
(42) Piedra-Cascón, W.; Sadeghpour, M.; Att, W.; Revilla-León, M. A vat-polymerized 3-dimensionally printed dual-material occlusal device: a dental technique. *J. Prosthet. Dent.* **2021**, *126*, 271−275.
(43) Park, S. I.; Rosen, D. W.; Choi, S.; Duty, C. E. Effective mechanical properties of lattice material fabricated by material extrusion additive manufacturing. *Addit. Manuf.* **2014**, *1*, 12−23.
(44) Chakraborty, R.; Anoop, A. G.; Thakur, A.; Mohanta, G. C.; Kumar, P. Strategies to modify the surface and bulk properties of 3d-printed solid scaffolds for tissue engineering applications. *ACS Omega* **2023**, *8*, 5139−5156.
(45) Ngo, T. D.; Kashani, A.; Imbalzano, G.; Nguyen, K. T. Q.; Hui, D. Additive manufacturing (3D Printing): A Review of materials, methods, applications and challenges. *Composites, Part B* **2018**, *143*, 172−196.
(46) Lolla, R.; Srinath, A.; Govindarajan, M.; Murugan, M.; Perumal Venkatesan, E.; Hasan, N. Effect of infill patterns with machine learning techniques on the tensile properties of polylactic acid-based ceramic materials with fused filament fabrication. *ACS Omega* **2023**, *8*, 24786−24796.
(47) León-Becerra, J.; González-Estrada, O. A.; Quiroga, J. Effect of relative density in in-plane mechanical properties of common 3d-printed polylactic acid lattice structures. *ACS Omega* **2021**, *6*, 29830−29838.
(48) Mohankumar, H. R.; Benal, M. G. M.; Pradeepkumar, G. S.; Tambrallimath, V.; Ramaiah, K.; Khan, T. M. Y.; Bhutto, J. K.; Ali, M. A. Effect of short glass fiber addition on flexural and impact behavior of 3d printed polymer composites. *ACS Omega* **2023**, *8*, 9212−9220.
(49) Chohan, J. S.; Singh, R.; Boparai, K. S.; Penna, R.; Fraternali, F. Dimensional accuracy analysis of coupled fused deposition modeling and vapour smoothing operations for biomedical applications. *Composites part B* **2017**, *117*, 138−149.
(50) Mohamed, O. A.; Masood, S. H.; Bhowmik, J. L. Optimization of fused deposition modeling process parameters: A review of current research and future prospects. *Adv. Manuf.* **2015**, *3*, 42−53.
(51) Kantaros, A.; Chatzidai, N.; Karalekas, D. 3D Printing-Assisted Design of Scaffold Structures. *International Journal of Advanced Manufacturing Technology* **2016**, *82* (1−4), 559−571.
(52) Puppi, D.; Mota, C.; Gazzarri, M.; Dinucci, D.; Gloria, A.; Myrzabekova, M.; Ambrosio, L.; Chiellini, F. Additive manufacturing of wet-spun polymeric scaffolds for bone tissue engineering. *Biomed. Microdevices* **2012**, *14*, 1115−1127.
(53) Wang, J.; Liu, Y.; Fan, Z.; Wang, W.; Wang, B.; Guo, Z. Ink-based 3d printing technologies for graphene-based materials: A review. *Adv. Compos. Hybrid Mater.* **2019**, *2*, 1−13.
(54) Eqtesadi, S.; Motealleh, A.; Miranda, P.; Pajares, A.; Lemos, A.; Ferreira, J. M. F. Robocasting of 45S5 bioactive glass scaffolds for bone tissue engineering. *J. Eur. Ceram. Soc.* **2014**, *34*, 107−118.
(55) Cámara-Torres, M.; Fucile, P.; Sinha, R.; Mota, C.; Moroni, L. Boosting bone regeneration using augmented melt-extruded additive-manufactured scaffolds. *Int. Mater. Rev.* **2023**, *68*, 755−785.
(56) Hutmacher, D. W.; Schantz, T.; Zein, I.; Ng, K. W.; Teoh, S. H.; Tan, K. C. Mechanical properties and cell cultural response of polycaprolactone scaffolds designed and fabricated via fused deposition modeling. *J. Biomed. Mater. Med.* **2001**, *55*, 203−216.
(57) Khandan, A.; Esmaeili, S. Fabrication of polycaprolactone and polylactic acid shapeless scaffolds via fused deposition modelling technology. *J. Adv. Mater. Processess* **2019**, *7*, 16−29.
(58) Little, H.; Clarke, S. A.; Cunningham, E.; Buchanan, F. Process-induced degradation of bioresorbable pdlga in bone tissue scaffold production. *J. Mater. Sci. Mater. Med.* **2018**, *29*, 14.
(59) Jeyachandran, P.; Bontha, S.; Bodhak, S.; Balla, V. K.; Doddamani, M. Material extrusion additive manufacturing of bioactive glass/high density polyethylene composites. *Compos. Sci. Technol.* **2021**, *213*, No. 108966.
(60) Du, W.; Ren, X.; Pei, Z.; Ma, C. Ceramic binder jetting additive manufacturing: A literature review on density. *J. Manuf. Sci. Eng.* **2020**, *142*, No. 040801.
(61) Qu, H. Additive manufacturing for bone tissue engineering scaffolds. *Mater. Today Commun.* **2020**, *24*, No. 101024.
(62) Ziaee, M.; Crane, N. B. Binder Jetting: A Review of Process, Materials, and Methods. *Addit. Manuf.* **2019**, *28*, 781−801.
(63) Travitzky, N.; Bonet, A.; Dermeik, B.; Fey, T.; Filbert-Demut, I.; Schlier, L.; Schlordt, T.; Greil, P. Additive manufacturing of ceramic-based materials. *Adv. Eng. Mater.* **2014**, *16*, 729−754.
(64) Moon, J.; Caballero, A. C.; Hozer, L.; Chiang, Y.-M.; Cima, M. J. Fabrication of functionally graded reaction infiltrated SiC-Si Composite by three-dimensional printing (3DP) process. *Mater. Sci. Eng., A* **2001**, *298*, 110−119.
(65) Trombetta, R.; Inzana, J. A.; Schwarz, E. M.; Kates, S. L.; Awad, H. A. 3D printing of calcium phosphate ceramics for bone tissue engineering and drug delivery. *Ann. Biomed. Eng.* **2017**, *45*, 23−44.

https://doi.org/10.1021/acsomega.4c04870
ACS Omega 2024, 9, 44042−44075

(66) Li, Y.; Feng, Z.; Huang, L.; Essa, K.; Bilotti, E.; Zhang, H.; Peijs, T.; Hao, L. Additive manufacturing high performance graphene-based composites: A review. *Composites Part A* **2019**, *124*, No. 105483.
(67) Utela, B.; Storti, D.; Anderson, R.; Ganter, M. A review of process development steps for new material systems in three-dimensional printing (3DP). *J. Manuf. Process.* **2008**, *10*, 96−104.
(68) Lee, H.; Lim, C. H. J.; Low, M. J.; Tham, N.; Murukeshan, V. M.; Kim, Y. J. Lasers in additive manufacturing: A review. *Int. J. Precis. Eng. Manuf. GT* **2017**, *4*, 307−322.
(69) Li, R.; Liu, J.; Shi, Y.; Wang, L.; Jiang, W. Balling behavior of stainless steel and nickel powder during selective laser melting process. *Int. J. Adv. Manuf. Technol.* **2012**, *59*, 1025−1035.
(70) Krakhmalev, P.; Yadroitsev, I. Microstructure and properties of intermetallic composite coatings fabricated by selective laser melting of ti-sic powder mixtures. *Intermetallics (Barking)* **2014**, *46*, 147−155.
(71) Wubneh, A.; Tsekoura, E. K.; Ayranci, C.; Uludağ, H. Current state of fabrication technologies and materials for bone tissue engineering. *Acta Biomater.* **2018**, *80*, 1−30.
(72) Zhang, B.; Jaiswal, P.; Rai, R.; Nelaturi, S. *Additive Manufacturing of Functionally Graded Objects: A Review*. International Design Engineering Technical Conferences and Computers and Information in Engineering Conference Proceedings; American Society of Mechanical Engineers; 2016, 50077:V01AT02A045/1−17.
(73) Wang, X.; Xu, S.; Zhou, S.; Xu, W.; Leary, M.; Choong, P.; Qian, M.; Brandt, M.; Xie, Y. M. Topological design and additive manufacturing of porous metals for bone scaffolds and orthopaedic implants: A review. *Biomaterials* **2016**, *83*, 127−141.
(74) Shojib Hossain, M.; Gonzalez, J. A.; Martinez Hernandez, R.; Arif, M.; Shuvo, I.; Mireles, J.; Choudhuri, A.; Lin, Y.; Wicker, R. B. Fabrication of smart parts using powder bed fusion additive manufacturing technology. *Addit. Manuf.* **2016**, *10*, 58−66.
(75) Nouri, A.; Rohani Shirvan, A.; Li, Y.; Wen, C. Additive manufacturing of metallic and polymeric load-bearing biomaterials using laser powder bed fusion: A review. *J. Mater. Sci. Technol.* **2021**, *94*, 196−215.
(76) Zhang, Y.; Jarosinski, W.; Jung, Y. G.; Zhang, J. Additive Manufacturing Processes and Equipment.. In *Additive Manufacturing: Materials, Processes, Quantifications and Applications*; Zhang, Y., Jung, Y. G., Eds.; Academic Press: London, 2018; pp 39−51. DOI: 10.1016/B978-0-12-812155-9.00002-5.
(77) Salmi, M. Additive manufacturing processes in medical applications. *Materials* **2021**, *14*, 1−16.
(78) Shanmugam, R.; Ramoni, M. O.; Chandran, J.; Mohanavel, V.; Pugazhendhi, L. A review on the significant classification of additive manufacturing. *J. Phys.: Conf. Ser.* **2021**, *2027*, No. 012026.
(79) Dhavalikar, P.; Lan, Z.; Kar, R.; Salhadar, K.; Gaharwar, A. K.; Cosgriff-Hernandez, E. *Biomedical Applications of Additive Manufacturing.. In Biomaterials Science: An Introduction to Materials in Medicine*, 4th ed.; Wagner, W. R., Sakiyama-Elbert, S. E., Zhang, G., Yaszemski, M. J., Eds.; Academic Press: London, 2021; pp 623−639.
(80) Svetlizky, D.; Das, M.; Zheng, B.; Vyatskikh, A. L.; Bose, S.; Bandyopadhyay, A.; Schoenung, J. M.; Lavernia, E. J.; Eliaz, N. Directed energy deposition (DED) additive manufacturing: Physical characteristics, defects, challenges and applications. *Mater. Today* **2021**, *49*, 271−295.
(81) Justin, D. F.; Brent, E. S.; Fallin, T. W.; Gabbita, D. J. Laser based metal deposition (LBMD) of implant structures. United State Patents, Appl No. US7666522, Filed 2010.
(82) Negi, S.; Nambolan, A. A.; Kapil, S.; Joshi, P. S.; R, M.; Karunakaran, K. P.; Bhargava, P. Review on electron beam based additive manufacturing. *Rapid Prototyp. J.* **2020**, *26*, 485−498.
(83) Bhardwaj, T.; Shukla, M. Laser additive manufacturing- direct energy deposition of Ti-15Mo biomedical alloy: Artificial neural network based modeling of track dilution. *Lasers Manuf. Mater. Process.* **2020**, *7*, 245−258.
(84) Wysocki, B.; Maj, P.; Sitek, R.; Buhagiar, J.; Kurzydłowski, K. J.; Świeszkowski, W. Laser and electron beam additive manufacturing methods of fabricating titanium bone implants. *Appl. Sci.* **2017**, *7*, 657.
(85) Wysocki, B.; Maj, P.; Sitek, R.; Buhagiar, J.; Kurzydłowski, K. J.; Świeszkowski, W. Laser and electron beam additive manufacturing methods of fabricating titanium bone implants. *Appl. Sci.* **2017**, *7*, 657.
(86) Sahasrabudhe, H.; Harrison, R.; Carpenter, C.; Bandyopadhyay, A. Stainless Steel to Titanium bimetallic structure using LENS. *Addit. Manuf.* **2015**, *5*, 1−8.
(87) Selemani, M. A.; Castiaux, A. D.; Martin, R. S. PolyJet-based 3D printing against micromolds to produce channel structures for microchip electrophoresis. *ACS Omega* **2022**, *7*, 13362−13370.
(88) Yap, Y. L.; Wang, C.; Sing, S. L.; Dikshit, V.; Yeong, W. Y.; Wei, J. Material jetting additive manufacturing: An experimental study using designed metrological benchmarks. *Precis. Eng.* **2017**, *50*, 275−285.
(89) Cui, X.; Boland, T.; D'lima, D. D.; Lotz, M. K. Thermal inkjet printing in tissue engineering and regenerative medicine. *Recent. Pat. Drug Delivery Formul.* **2017**, *6*, 149−155.
(90) Derby, B. Inkjet printing of functional and structural materials: fluid property requirements, feature stability, and resolution. *Annu. Rev. Mater. Res.* **2010**, *40*, 395−414.
(91) Calvert, P. Inkjet printing for materials and devices. *Chem. Mater.* **2001**, *13*, 3299−3305.
(92) Singh, M.; Haverinen, H. M.; Dhagat, P.; Jabbour, G. E. Inkjet printing-process and its applications. *Adv. Mater.* **2010**, *22*, 673−685.
(93) Bikas, H.; Stavropoulos, P.; Chryssolouris, G. Additive manufacturing methods and modeling approaches: A critical review. *Int. J. Adv. Manuf. Technol.* **2016**, *83*, 389−405.
(94) Zhu, F.; Macdonald, N. P.; Skommer, J.; Wlodkowic, D. Biological implications of lab-on-a-chip devices fabricated using multi-jet modelling and stereolithography processes. *Bio-MEMS Med. Microdevices II* **2015**, *9518*, No. 951808.
(95) Yap, Y. L.; Tan, Y. S. E.; Tan, H. K. J.; Peh, Z. K.; Low, X. Y.; Yeong, W. Y.; Tan, C. S. H.; Laude, A. 3D printed bio-models for medical applications. *Rapid Prototyp. J.* **2017**, *23*, 227−235.
(96) Yap, Y. L.; Lai, Y. M.; Zhou, H. F.; Yeong, W. Y. Compressive strength of thin-walled cellular core by inkjet-based additive manufacturing. *Proceedings of the International Conference on Progress in Additive Manufacturing*, 2014; pp 333−338..
(97) Bai, L.; Gong, C.; Chen, X.; Sun, Y.; Zhang, J.; Cai, L.; Zhu, S.; Xie, S. Q. additive manufacturing of customized metallic orthopedic implants: Materials, structures, and surface modifications. *Metals* **2019**, *9*, 1004.
(98) Jardini, A. L.; Larosa, M. A.; Macedo, M. F.; Bernardes, L. F.; Lambert, C. S.; Zavaglia, C. A. C.; Filho, R. M.; Calderoni, D. R.; Ghizoni, E.; Kharmandayan, P. Improvement in cranioplasty: Advanced prosthesis biomanufacturing. *Procedia CIRP* **2016**, *49*, 203−208.
(99) Yan, R.; Luo, D.; Huang, H.; Li, R.; Yu, N.; Liu, C.; Hu, M.; Rong, Q. Electron beam melting in the fabrication of three-dimensional mesh titanium mandibular prosthesis scaffold. *Sci. Rep.* **2018**, *8*, 750.
(100) Fan, H.; Fu, J.; Li, X.; Pei, Y.; Li, X.; Pei, G.; Guo, Z. Implantation of customized 3-D printed Titanium prosthesis in limb salvage surgery: A case series and review of the literature. *World J. Surg. Oncol.* **2015**, *13*, 308.
(101) Saikko, V.; Ahlroos, T.; Revitzer, H.; Ryti, O.; Kuosmanen, P. the effect of acetabular cup position on wear of a large-diameter metal-on-metal prosthesis studied with a hip joint simulator. *Tribol. Int.* **2013**, *60*, 70−76.
(102) Lim, H. K.; Choi, Y. J.; Choi, W. C.; Song, I. S.; Lee, U. L. Reconstruction of maxillofacial bone defects using patient-specific long-lasting titanium implants. *Sci. Rep.* **2022**, *12*, 7538.
(103) Hollander, D. A.; Von Walter, M.; Wirtz, T.; Sellei, R.; Schmidt-Rohlfing, B.; Paar, O.; Erli, H. J. Structural, mechanical and in vitro characterization of individually structured Ti-6Al-4V produced by direct laser forming. *Biomaterials* **2006**, *27*, 955−963.
(104) Yang, Y.; He, C.; Dianyu, E.; Yang, W.; Qi, F.; Xie, D.; Shen, L.; Peng, S.; Shuai, C. Mg bone implant: Features, developments and perspectives. *Mater. Des.* **2020**, *185*, No. 108259.

https://doi.org/10.1021/acsomega.4c04870
ACS Omega 2024, 9, 44042−44075

(105) Taniguchi, N.; Fujibayashi, S.; Takemoto, M.; Sasaki, K.; Otsuki, B.; Nakamura, T.; Matsushita, T.; Kokubo, T.; Matsuda, S. Effect of pore size on bone ingrowth into porous Titanium implants fabricated by additive manufacturing: An in vivo experiment. *Mater. Sci. Eng., C* **2016**, *59*, 690−701.
(106) Rama, M.; Vijayalakshmi, U. Synergism of silver/CEM drug on novel proteinaceous silk fibroin/mesoporous silica based sandwich-layered nanofibrous scaffolds for osteoregenerative applications. *Ceram. Int.* **2023**, *49*, 17032−17051.
(107) Anandan, D.; Mary Stella, S.; Arunai Nambiraj, N.; Vijayalakshmi, U.; Jaiswal, A. K. Development of mechanically compliant 3D composite scaffolds for bone tissue engineering applications. *J. Biomed. Mater. Res., Part A* **2018**, *106*, 3267−3274.
(108) Nie, L.; Chen, D.; Suo, J.; Zou, P.; Feng, S.; Yang, Q.; Yang, S.; Ye, S. Physicochemical characterization and biocompatibility in vitro of biphasic calcium phosphate/polyvinyl alcohol scaffolds prepared by freeze-drying method for bone tissue engineering applications. *Colloids Surf., B* **2012**, *100*, 169−176.
(109) Hallgren, C.; Reimers, H.; Chakarov, D.; Gold, J.; Wennerberg, A. An in vivo study of bone response to implants topographically modified by laser micromachining. *Biomaterials* **2003**, *24*, 701−710.
(110) Chen, Y.; Xu, W.; Shafiq, M.; Tang, J.; Hao, J.; Xie, X.; Yuan, Z.; Xiao, X.; Liu, Y.; Mo, X. Three-dimensional porous gas-foamed electrospun nanofiber scaffold for cartilage regeneration. *J. Colloid Interface Sci.* **2021**, *603*, 94−109.
(111) Gide, K. M.; Islam, S.; Bagheri, Z. S. Polymer-based materials built with additive manufacturing methods for orthopedic applications: A review. *J. Compos. Sci.* **2022**, *6*, 262.
(112) Dhandapani, R.; Krishnan, P. D.; Zennifer, A.; Kannan, V.; Manigandan, A.; Arul, M. R.; Jaiswal, D.; Subramanian, A.; Kumbar, S. G.; Sethuraman, S. Additive manufacturing of biodegradable porous orthopaedic screw. *Bioact. Mater.* **2020**, *5*, 458−467.
(113) Espalin, D.; Arcaute, K.; Rodriguez, D.; Medina, F.; Posner, M.; Wicker, R. Fused deposition modeling of patient-specific polymethylmethacrylate implants. *Rapid Prototyp. J.* **2010**, *16*, 164−173.
(114) Mota, C.; Wang, S.-Y.; Puppi, D.; Gazzarri, M.; Migone, C.; Chiellini, F.; Chen, G.-Q.; Chiellini, E. Additive manufacturing of Poly[(R)-3-Hydroxybutyrate-Co-(R)-3-Hydroxyhexanoate] scaffolds for engineered bone development. *J. Tissue Eng. Regener. Med.* **2017**, *11*, 175−186.
(115) Mazzoli, A.; Ferretti, C.; Gigante, A.; Salvolini, E.; Mattioli-Belmonte, M. Selective laser sintering manufacturing of Polycaprolactone bone scaffolds for applications in bone tissue engineering. *Rapid Prototyp. J.* **2015**, *21*, 386−392.
(116) Kosorn, W.; Sakulsumbat, M.; Uppanan, P.; Kaewkong, P.; Chantaweroad, S.; Jitsaard, J.; Sitthiseripratip, K.; Janvikul, W. PCL/PHBV blended three dimensional scaffolds fabricated by fused deposition modeling and responses of chondrocytes to the scaffolds. *J. Biomed. Mater. Res. Part B* **2017**, *105*, 1141−1150.
(117) Singh, J. P.; Pandey, P. M.; Verma, A. K. Fabrication of three dimensional open porous regular structure of PA-2200 for enhanced strength of scaffold using selective laser sintering. *Rapid Prototyp. J.* **2016**, *22*, 752−765.
(118) Dong, L.; Wang, S. J.; Zhao, X. R.; Zhu, Y. F.; Yu, J. K. 3D-Printed Poly (ϵ-Caprolactone) scaffold integrated with cell-laden Chitosan hydrogels for bone tissue engineering. *Sci. Rep.* **2017**, *7*, 13412.
(119) Naghiesh, S.; Badrossamay, M.; Foroozmehr, E.; Kharaziha, M. Combination of PLA micro-fibers and PCL-Gelatin nano-fibers for development of bone tissue engineering scaffolds. *Int. J. Swarm Intell. Evol. Comput.* **2017**, *06*, 150.
(120) Nyberg, E.; Rindone, A.; Dorafshar, A.; Grayson, W. L. Comparison of 3D-Printed Poly-ϵ-Caprolactone scaffolds functionalized with Tricalcium Phosphate, Hydroxyapatite, Bio-Oss, or decellularized bone matrix. *Tissue Eng. Part A* **2017**, *23*, 503−514.
(121) Wang, L.; Huang, L.; Li, X.; Zhong, D.; Li, D.; Cao, T.; Yang, S.; Yan, X.; Zhao, J.; He, J.; Cao, Y.; Wang, L. Three-dimensional printing PEEK implant: A novel choice for the reconstruction of chest wall defect. *Ann. Thorac. Surg.* **2019**, *107*, 921−928.
(122) Singh, D.; Babbar, A.; Jain, V.; Gupta, D.; Saxena, S.; Dwibedi, V. Synthesis, characterization, and bioactivity investigation of biomimetic biodegradable PLA scaffold fabricated by fused filament fabrication process. *J. Braz. Soc. Mech. Sci. Eng.* **2019**, *41*, 121.
(123) Xiong, Z.; Liu, W.; Qian, H.; Lei, T.; He, X.; Hu, Y.; Lei, P. Tantalum nanoparticles reinforced PCL scaffolds using direct 3D printing for bone tissue engineering. *Front. Mater.* **2021**, *8*, No. 609779.
(124) Du, X.; Ronayne, S.; Lee, S. S.; Hendry, J.; Hoxworth, D.; Bock, R.; Ferguson, S. J. 3D-printed PEEK/Silicon Nitride scaffolds with a triply periodic minimal surface structure for spinal fusion implants. *ACS Appl. Bio. Mater.* **2023**, *6*, 3319−3329.
(125) Giubilini, A.; Messori, M.; Bondioli, F.; Minetola, P.; Iuliano, L.; Nyström, G.; Maniura-Weber, K.; Rottmar, M.; Siqueira, G. 3D-printed Poly(3-Hydroxybutyrate-Co-3-Hydroxyhexanoate)-Cellulose-based scaffolds for biomedical applications. *Biomacromolecules* **2023**, *24*, 3961−3971.
(126) Milazzo, M.; Fitzpatrick, V.; Owens, C. E.; Carraretto, I. M.; McKinley, G. H.; Kaplan, D. L.; Buehler, M. J. 3D printability of Silk/Hydroxyapatite composites for microprosthetic applications. *ACS Biomater. Sci. Eng.* **2023**, *9*, 1285−1295.
(127) Yap, T.; Heathman, N.; Phillips, T.; Beaman, J.; Tehrani, M. Additive Manufacturing of Polyaryletherketone (PAEK) polymers and their composites. *Compos. Part B* **2023**, *266*, No. 111019.
(128) Vijayalakshmi, U.; Balamurugan, A.; Rajeswari, S. Synthesis and characterization of porous Silica gels for biomedical applications. *Trends Biomat. Artif. Organs* **2005**, *18*, 101−105.
(129) Zhou, Q.; Su, X.; Wu, J.; Zhang, X.; Su, R.; Ma, L.; Sun, Q.; He, R. Additive manufacturing of bioceramic implants for restoration bone engineering: technologies, advances, and future perspectives. *ACS biomater. Sci. Eng.* **2023**, *9*, 1164−1189.
(130) Bohner, M.; Galea, L.; Doebelin, N. Calcium phosphate bone graft substitutes: Failures and hopes. *J. Eur. Ceram. Soc.* **2012**, *32*, 2663−2671.
(131) Esslinger, S.; Grebhardt, A.; Jaeger, J.; Kern, F.; Killinger, A.; Bonten, C.; Gadow, R. Additive manufacturing of β-Tricalcium phosphate components via fused deposition of ceramics (FDC). *Materials* **2021**, *14*, 156.
(132) Cipitria, A.; Reichert, J. C.; Epari, D. R.; Saifzadeh, S.; Berner, A.; Schell, H.; Mehta, M.; Schuetz, M. A.; Duda, G. N.; Hutmacher, D. W. Polycaprolactone scaffold and reduced RhBMP-7 dose for the regeneration of critical-sized defects in sheep tibiae. *Biomaterials* **2013**, *34*, 9960−9968.
(133) Fielding, G. A.; Bandyopadhyay, A.; Bose, S. Effects of Silica and Zinc oxide doping on mechanical and biological properties of 3D printed Tricalcium Phosphate tissue engineering scaffolds. *Dent. Mater.* **2012**, *28*, 113−122.
(134) Park, J. S.; Lee, S. J.; Jo, H. H.; Lee, J. H.; Kim, W. D.; Lee, J. Y.; Park, S. A. Fabrication and characterization of 3D-printed Bbone-like β-Tricalcium Pphosphate/Polycaprolactone scaffolds for dental tissue engineering. *J. Indus. Eng. Chem.* **2017**, *46*, 175−181.
(135) Dávila, J. L.; Freitas, M. S.; Inforçatti Neto, P.; Silveira, Z. C.; Silva, J. V. L.; D'Ávila, M. A. Fabrication of PCL/β-TCP scaffolds by 3D mini-screw extrusion printing. *J. Appl. Polym. Sci.* **2016**, *133*, 43031.
(136) Shim, J. H.; Won, J. Y.; Park, J. H.; Bae, J. H.; Ahn, G.; Kim, C. H.; Lim, D. H.; Cho, D. W.; Yun, W. S.; Bae, E. B.; Jeong, C. M.; Huh, J. B. Effects of 3D-printed Polycaprolactone/β-Tricalcium phosphate membranes on guided bone regeneration. *Int. J. Mol. Sci.* **2017**, *18*, 899.
(137) Lee, S.; Choi, D.; Shim, J. H.; Nam, W. Efficacy of three-dimensionally printed Polycaprolactone/β-Tricalcium phosphate scaffold on mandibular Rreconstruction. *Sci. Rep.* **2020**, *10*, 4979.
(138) Anjaneyulu, U.; Pattanayak, D. K.; Vijayalakshmi, U. Snail shell derived natural Hydroxyapatite: Effects on NIH-3T3 cells for orthopedic applications. *Mater. Manuf. Process.* **2016**, *31*, 206−216.

https://doi.org/10.1021/acsomega.4c04870
ACS Omega 2024, 9, 44042−44075

(139) Buyuksungur, S.; Endogan Tanir, T.; Buyuksungur, A.; Bektas, E. I.; Torun Kose, G.; Yucel, D.; Beyzadeoglu, T.; Cetinkaya, E.; Yenigun, C.; Tönük, E.; Hasirci, V.; Hasirci, N. 3D printed Poly(ϵ-Caprolactone) scaffolds modified with Hydroxyapatite and Poly(Propylene Fumarate) and their effects on the healing of rabbit femur defects. *Biomater. Sci.* **2017**, *5*, 2144−2158.
(140) Tcacencu, I.; Rodrigues, N.; Alharbi, N.; Benning, M.; Toumpaniari, S.; Mancuso, E.; Marshall, M.; Bretcanu, O.; Birch, M.; McCaskie, A.; Dalgarno, K. Osseointegration of porous Apatite-Wollastonite and Poly(Lactic acid) composite structures created using 3d printing techniques. *Mater. Sci. Eng. Part C* **2018**, *90*, 1−7.
(141) Ramu, M.; Ananthasubramanian, M.; Kumaresan, T.; Gandhinathan, R.; Jothi, S. Optimization of the configuration of porous bone scaffolds made of Polyamide/Hydroxyapatite composites using selective laser sintering for tissue engineering applications. *Biomed. Mater. Eng.* **2018**, *29*, 739−755.
(142) Oladapo, B. I.; Zahedi, S. A.; Adeoye, A. O. M. 3D printing of bone scaffolds with hybrid biomaterials. *Composites Part B* **2019**, *158*, 428−436.
(143) Oladapo, B. I.; Ismail, S. O.; Bowoto, O. K.; Omigbodun, F. T.; Olawumi, M. A.; Muhammad, M. A. Lattice design and 3D-printing of PEEK with $Ca_{10}(OH)(PO_4)_3$ and in-vitro bio-composite for bone implant. *J. Biol. Macromol.* **2020**, *165*, 50−62.
(144) Nazeer, M. A.; Onder, O. C.; Sevgili, I.; Yilgor, E.; Kavakli, I. H.; Yilgor, I. 3D Printed Poly(Lactic acid) scaffolds modified with Chitosan and Hydroxyapatite for bone repair applications. *Mater. Today Commun.* **2020**, *25*, No. 101515.
(145) Manzoor, F.; Golbang, A.; Jindal, S.; Dixon, D.; McIlhagger, A.; Harkin-Jones, E.; Crawford, D.; Mancuso, E. 3D Printed PEEK/HA composites for bone tissue engineering applications: Effect of material formulation on mechanical performance and bioactive potential. *J. Mech. Behav. Biomed. Mater.* **2021**, *121*, No. 104601.
(146) Zhang, B.; Wang, L.; Song, P.; Pei, X.; Sun, H.; Wu, L.; Zhou, C.; Wang, K.; Fan, Y.; Zhang, X. 3D printed bone tissue regenerative PLA/HA scaffolds with comprehensive performance optimizations. *Mater. Des.* **2021**, *201*, No. 109490.
(147) Park, S.; Kim, J. E.; Han, J.; Jeong, S.; Lim, J. W.; Lee, M. C.; Son, H.; Kim, H. B.; Choung, Y.-H.; Seonwoo, H.; Chung, J. H.; Jang, K.-J. 3D-printed Poly(ε-Caprolactone)/Hydroxyapatite scaffolds modified with alkaline hydrolysis enhance osteogenesis in vitro. *Polymer* **2021**, *13*, 257.
(148) Zafeiris, K.; Brasinika, D.; Karatza, A.; Koumoulos, E.; Karoussis, I. K.; Kyriakidou, K.; Charitidis, C. A. Additive manufacturing of Hydroxyapatite−Chitosan−Genipin composite scaffolds for bone tissue engineering applications. *Mater. Sci. Eng.Part C* **2021**, *119*, No. 111639.
(149) Xia, Y.; Zhou, P. Y.; Cheng, X. S.; Xie, Y.; Liang, C.; Li, C.; Xu, S. G. selective laser sintering fabrication of nano-Hydroxyapatite/Poly-ε-Caprolactone scaffolds for bone tissue engineering applications. *Int. J. Nanomedicine* **2013**, *8*, 4197−4213.
(150) Li, J.; Li, K.; Du, Y.; Tang, X.; Liu, C.; Cao, S.; Zhao, B.; Huang, H.; Zhao, H.; Kong, W.; Xu, T.; Shao, C.; Shao, J.; Zhang, G.; Lan, H.; Xi, Y. Dual-nozzle 3D printed nnano-Hydroxyapatite scaffold loaded with Vancomycin sustained-release microspheres for enhancing bone regeneration. *Int. J. Nanomedicine* **2023**, *18*, 307−322.
(151) Priyadarshini, B.; Rama, M.; Chetan; Vijayalakshmi, U. Bioactive coating as a surface modification technique for biocompatible metallic implants: A review. *J. Asian Ceram. Soc.* **2019**, *7*, 397−406.
(152) Hench, L. L. Bioactive Glasses and Glass-Ceramics. *Mater. Sci. Forum* **1998**, *293*, 37−64.
(153) Yang, S.; Wang, J.; Tang, L.; Ao, H.; Tan, H.; Tang, T.; Liu, C. Mesoporous bioactive glass doped-Poly (3-Hydroxybutyrate-Co-3-Hydroxyhexanoate) composite scaffolds with 3-dimensionally hierarchical pore networks for bone regeneration. *Colloids Surf. Part B* **2014**, *116*, 72−80.
(154) Sun, M.; Liu, A.; Shao, H.; Yang, X.; Ma, C.; Yan, S.; Liu, Y.; He, Y.; Gou, Z. Systematical evaluation of mechanically strong 3d printed diluted Magnesium doping Wollastonite scaffolds on osteogenic capacity in rabbit calvarial defects. *Sci. Rep.* **2016**, *6*, 34029.
(155) Wu, C.; Luo, Y.; Cuniberti, G.; Xiao, Y.; Gelinsky, M. *3D*-printing of hierarchical and tough mesoporous bioactive glass scaffolds with controllable pore architecture, excellent mechanical strength and mineralization ability. *Acta Biomater.* **2011**, *7*, 2644−2650.
(156) Abdal-hay, A.; Raveendran, N. T.; Fournier, B.; Ivanovski, S. Fabrication of biocompatible and bioabsorbable Polycaprolactone/Magnesium hydroxide 3D printed scaffolds: Degradation and in vitro osteoblasts interactions. *Composites Part B* **2020**, *197*, No. 108158.
(157) Wu, Y.-H. A.; Chiu, Y.-C.; Lin, Y.-H.; Ho, C.-C.; Shie, M.-Y.; Chen, Y.-W. 3D-Printed bioactive Calcium Silicate/Poly-ε-Caprolactone bioscaffolds modified with biomimetic extracellular matrices for bone regeneration. *Int. J. Mol. Sci.* **2019**, *20*, 942.
(158) Shan, Y.; Bai, Y.; Yang, S.; Zhou, Q.; Wang, G.; Zhu, B.; Zhou, Y.; Fang, W.; Wen, N.; He, R.; Zhao, L. 3D-printed Strontium-incorporated β-TCP bioceramic triply periodic minimal surface scaffolds with simultaneous high porosity, enhanced strength, and excellent bioactivity. *J. Adv.Ceram.* **2023**, *12*, 1671−1684.
(159) Bobbert, F. S. L.; Lietaert, K.; Eftekhari, A. A.; Pouran, B.; Ahmadi, S. M.; Weinans, H.; Zadpoor, A. A. Additively manufactured metallic porous biomaterials based on minimal surfaces: A unique combination of topological, mechanical, and mass transport properties. *Acta Biomater.* **2017**, *53*, 572−584.
(160) Tilton, M.; Borjali, A.; Isaacson, A.; Varadarajan, K. M.; Manogharan, G. P. On structure and mechanics of biomimetic meta-biomaterials fabricated via metal additive manufacturing. *Mater. Des.* **2021**, *201*, No. 109498.
(161) Zhang, L. C.; Klemm, D.; Eckert, J.; Hao, Y. L.; Sercombe, T. B. Manufacture by selective laser melting and mechanical behavior of a biomedical Ti-24Nb-4Zr-8Sn alloy. *Scr. Mater.* **2011**, *65*, 21−24.
(162) Mahjouri-Samani, M.; Fathi-Hafshejani, P.; Johnson, H.; Ahmadi, Z.; Roach, M.; Shamsaei, N. Phase-selective and localized TiO_2 coating on additive and wrought Titanium by a direct laser surface modification approach. *ACS Omega* **2020**, *5*, 16744−16751.
(163) Galarraga, H.; Warren, R. J.; Lados, D. A.; Dehoff, R. R.; Kirka, M. M.; Nandwana, P. Effects of heat treatments on microstructure and properties of Ti-6Al-4V ELI Alloy Fabricated by Electron Beam melting (EBM). *Mater. Sci. Eng. Part A* **2017**, *685*, 417−428.
(164) Nune, K. C.; Kumar, A.; Misra, R. D. K.; Li, S. J.; Hao, Y. L.; Yang, R. Functional response of osteoblasts in functionally gradient Titanium alloy mesh arrays processed by 3D additive manufacturing. *Colloids Surf. Part B* **2017**, *150*, 78−88.
(165) Van Bael, S.; Chai, Y. C.; Truscello, S.; Moesen, M.; Kerckhofs, G.; Van Oosterwyck, H.; Kruth, J. P.; Schrooten, J. The effect of pore geometry on the in vitro biological behavior of human periosteum-derived cells seeded on selective laser-melted Ti6Al4V bone scaffolds. *Acta Biomater.* **2012**, *8*, 2824−2834.
(166) Sobral, J. M.; Caridade, S. G.; Sousa, R. A.; Mano, J. F.; Reis, R. L. Three-dimensional plotted scaffolds with controlled pore size gradients: Effect of scaffold geometry on mechanical performance and cell seeding efficiency. *Acta Biomater.* **2011**, *7*, 1009−1018.
(167) Amin Yavari, S.; van der Stok, J.; Chai, Y. C.; Wauthle, R.; Tahmasebi Birgani, Z.; Habibovic, P.; Mulier, M.; Schrooten, J.; Weinans, H.; Zadpoor, A. A. Bone regeneration performance of surface-treated porous Titanium. *Biomaterials* **2014**, *35*, 6172−6181.
(168) Surmeneva, M. A.; Surmenev, R. A.; Chudinova, E. A.; Koptioug, A.; Tkachev, M. S.; Gorodzha, S. N.; Rännar, L. E. Fabrication of multiple-layered gradient cellular metal scaffold via electron beam melting for segmental bone reconstruction. *Mater. Des.* **2017**, *133*, 195−204.
(169) Arabnejad, S.; Burnett Johnston, R.; Pura, J. A.; Singh, B.; Tanzer, M.; Pasini, D. High-strength porous biomaterials for bone replacement: A strategy to assess the interplay between cell morphology, mechanical properties, bone ingrowth and manufacturing constraints. *Acta Biomater.* **2016**, *30*, 345−356.

https://doi.org/10.1021/acsomega.4c04870
ACS Omega 2024, 9, 44042−44075

(170) Zhang, S.; Wei, Q.; Cheng, L.; Li, S.; Shi, Y. Effects of Scan line spacing on pore characteristics and mechanical properties of porous Ti6Al4V implants fabricated by selective laser melting. *Mater. Des.* **2014**, *63*, 185−193.
(171) Wang, X.; Xu, S.; Zhou, S.; Xu, W.; Leary, M.; Choong, P.; Qian, M.; Brandt, M.; Xie, Y. M. Topological design and additive manufacturing of porous metals for bone scaffolds and orthopaedic implants: A review. *Biomaterials* **2016**, *83*, 127−141.
(172) Davidson, J. A.; Mishra, A. K.; Kovacs, P.; Poggie, R. A. New surface-hardened, low-modulus, corrosion-resistant Ti-13Nb-13Zr alloy for total hip arthroplasty. *Biomed. Mater. Eng.* **1994**, *4*, 231−241.
(173) Kuroda, D.; Niinomi, M.; Morinaga, M.; Kato, Y.; Yashiro, T. Design and mechanical properties of New β type Titanium alloys for implant materials. *Mater. Sci. Eng. Part A* **1998**, *243*, 244−249.
(174) Okazaki, Y.; Ito, Y.; Kyo, K.; Tateishi, T. A. corrosion resistance and corrosion fatigue strength of new Titanium alloys for medical implants without V and Al. *Mater. Sci. Eng., A* **1996**, *213*, 138−147.
(175) Chai, Y. C.; Kerckhofs, G.; Roberts, S. J.; Van Bael, S.; Schepers, E.; Vleugels, J.; Luyten, F. P.; Schrooten, J. Ectopic bone formation by 3D porous Calcium phosphate-Ti6Al4V hybrids produced by perfusion electrodeposition. *Biomaterials* **2012**, *33*, 4044−4058.
(176) Simonelli, M.; Tse, Y. Y.; Tuck, C. Effect of the build orientation on the mechanical properties and fracture modes of SLM Ti-6Al-4V. *Mater. Sci. Eng.Part A* **2014**, *616*, 1−11.
(177) Parthasarathy, J.; Starly, B.; Raman, S. A design for the additive manufacture of functionally graded porous structures with tailored mechanical properties for biomedical applications. *J. Manuf. Process.* **2011**, *13*, 160−170.
(178) Croes, M.; Bakhshandeh, S.; van Hengel, I. A. J.; Lietaert, K.; van Kessel, K. P. M.; Pouran, B.; van der Wal, B. C. H.; Vogely, H. C.; Van Hecke, W.; Fluit, A. C.; Boel, C. H. E.; Alblas, J.; Zadpoor, A. A.; Weinans, H.; Amin Yavari, S. Antibacterial and immunogenic behavior of Silver coatings on additively manufactured porous Titanium. *Acta Biomater.* **2018**, *81*, 315−327.
(179) Vandenbroucke, B.; Kruth, J.-P. Selective laser melting of biocompatible metals for rapid manufacturing of medical parts. *Rapid Prototyp. J.* **2007**, *13*, 196−203.
(180) Lee, B. S.; Lee, H. J.; Lee, K. S.; Kim, H. G.; Kim, G. H.; Lee, C. W. Enhanced Oosseointegration of Ti6Al4V ELI screws built-up by electron beam additive manufacturing: An experimental study in rabbits. *Appl. Surf. Sci.* **2020**, *508*, No. 145160.
(181) van Hengel, I. A. J.; Putra, N. E.; Tierolf, M. W. A. M.; Minneboo, M.; Fluit, A. C.; Fratila-Apachitei, L. E.; Apachitei, I.; Zadpoor, A. A. Biofunctionalization of selective laser melted porous titanium using Silver and Zinc nanoparticles to prevent infections by antibiotic-resistant bacteria. *Acta Biomater.* **2020**, *107*, 325−337.
(182) Yao, Y.; Wang, L.; Li, J.; Tian, S.; Zhang, M.; Fan, Y. A novel auxetic structure-based bone screw design: Tensile mechanical characterization and pullout fixation strength evaluation. *Mater. Des.* **2020**, *188*, No. 108424.
(183) Yao, Y.; Yuan, H.; Huang, H.; Liu, J.; Wang, L.; Fan, Y. Biomechanical design and analysis of auxetic pedicle screw to resist loosening. *Comput. Biol. Med.* **2021**, *133*, No. 104386.
(184) Arabnejad, S.; Johnston, B.; Tanzer, M.; Pasini, D. Fully porous 3D printed Titanium femoral stem to reduce stress-shielding following total hip arthroplasty. *J. Orthopaed. Res.* **2017**, *35*, 1774−1783.
(185) Polak, S.; Beever, L.; Wade, A.; Fukuoka, M.; Worth, A. J. Biomechanical comparison of Titanium alloy additively manufactured and conventionally manufactured plate-screw constructs. *N Z. Vet. J.* **2024**, *72*, 17−27.
(186) Chakraborty, A.; Das, A.; Datta, P.; Majumder, S.; Barui, A.; Roychowdhury, A. 3D printing of Ti-6Al-4V-based porous-channel dental implants: Computational, biomechanical, and cytocompatibility analyses. *ACS Appl. Bio. Mater.* **2023**, *6*, 4178.
(187) Wang, P.; Li, X.; Luo, S.; Nai, M. L. S.; Ding, J.; Wei, J. Additively Manufactured Heterogeneously Porous Metallic Bone with Biostructural Functions and Bone-like Mechanical Properties. *J. Mater. Sci. Technol.* **2021**, *62*, 173−179.
(188) Long, T.; Zhang, X.; Huang, Q.; Liu, L.; Liu, Y.; Ren, J.; Yin, Y.; Wu, D.; Wu, H. Novel Mg-based alloys by selective laser melting for biomedical applications: Microstructure evolution, microhardness and in vitro degradation behaviour. *Virtual Phys. Prototyp.* **2018**, *13*, 71−81.
(189) Hort, N.; Huang, Y.; Fechner, D.; Stormer, M.; Blawert, C.; Witte, F.; Vogt, C.; Drucker, H.; Willumeit, R.; Kainer, K.U. Magnesium alloys as implant materials-Principles of property design for Mg-RE alloys. *Acta Biomater.* **2010**, *6*, 1714−1725.
(190) Ng, C. C.; Savalani, M. M.; Man, H. C.; Gibson, I. Layer manufacturing of Magnesium and its alloy structures for future applications. *Virtual Phys. Prototyp.* **2010**, *5*, 13−19.
(191) Wang, Y.; Fu, P.; Wang, N.; Peng, L.; Kang, B.; Zeng, H.; Yuan, G.; Ding, W. Challenges and solutions for the additive manufacturing of biodegradable Magnesium implants. *Engineering* **2020**, *6*, 1267−1275.
(192) Farag, M. M.; Yun, H. S. Effect of Gelatin addition on fabrication of Magnesium phosphate-based scaffolds prepared by additive manufacturing system. *Mater. Lett.* **2014**, *132*, 111−115.
(193) Li, Y.; Zhou, J.; Pavanram, P.; Leeflang, M. A.; Fockaert, L. I.; Pouran, B.; Tümer, N.; Schröder, K. U.; Mol, J. M. C.; Weinans, H.; Jahr, H.; Zadpoor, A. A. Additively manufactured biodegradable porous Magnesium. *Acta Biomater.* **2018**, *67*, 378−392.
(194) Antoniac, I.; Popescu, D.; Zapciu, A.; Antoniac, A.; Miculescu, F.; Moldovan, H. Magnesium filled Polylactic acid (PLA) material for filament based 3D printing. *Materials* **2019**, *12*, 719.
(195) Ho, Y. H.; Joshi, S. S.; Wu, T. C.; Hung, C. M.; Ho, N. J.; Dahotre, N. B. In-vitro bio-corrosion behavior of friction stir additively manufactured AZ31B Magnesium alloy-Hydroxyapatite composites. *Mater. Sci. Eng.Part C* **2020**, *109*, No. 110632.
(196) Golafshan, N.; Vorndran, E.; Zaharievski, S.; Brommer, H.; Kadumudi, F. B.; Dolatshahi-Pirouz, A.; Gbureck, U.; van Weeren, R.; Castilho, M.; Malda, J. Tough Magnesium phosphate-based 3D-printed implants induce bone regeneration in an equine defect model. *Biomaterials* **2020**, *261*, No. 120302.
(197) Xie, K.; Wang, N.; Guo, Y.; Zhao, S.; Tan, J.; Wang, L.; Li, G.; Wu, J.; Yang, Y.; Xu, W.; Chen, J.; Jiang, W.; Fu, P.; Hao, Y. Additively manufactured biodegradable porous Magnesium implants for elimination of implant-related infections: An in vitro and in vivo study. *Bioact. Mater.* **2022**, *8*, 140−152.
(198) Dong, J.; Tümer, N.; Leeflang, M. A.; Taheri, P.; Fratila-Apachitei, L. E.; Mol, J. M. C.; Zadpoor, A. A.; Zhou, J. Extrusion-based additive manufacturing of Mg-Zn alloy scaffolds. *J. Magnesium Alloys* **2022**, *10*, 2491−2509.
(199) Lee, J.; Farag, M. M.; Park, E. K.; Lim, J.; Yun, H. S. A simultaneous process of 3D Magnesium phosphate scaffold fabrication and bioactive substance loading for hard tissue regeneration. *Mater. Sci. Eng.Part C* **2014**, *36*, 252−260.
(200) Meininger, S.; Moseke, C.; Spatz, K.; März, E.; Blum, C.; Ewald, A.; Vorndran, E. Effect of Strontium substitution on the material properties and osteogenic potential of 3D powder printed Magnesium phosphate Scaffolds. *Mater. Sci. Eng.Part C* **2019**, *98*, 1145−1158.
(201) Kopp, A.; Derra, T.; Müther, M.; Jauer, L.; Schleifenbaum, J. H.; Voshage, M.; Jung, O.; Smeets, R.; Kröger, N. Influence of design and postprocessing parameters on the degradation behavior and mechanical properties of additively manufactured Magnesium scaffolds. *Acta Biomater.* **2019**, *98*, 23−35.
(202) Bakhshi, R.; Mohammadi-Zerankeshi, M.; Mehrabi-Dehdezi, M.; Alizadeh, R.; Labbaf, S.; Abachi, P. Additive manufacturing of PLA-Mg composite scaffolds for hard tissue engineering applications. *J. Mech. Behav. Biomed. Mater.* **2023**, *138*, No. 105655.
(203) Wang, Y.; Fu, P.; Wang, N.; Peng, L.; Kang, B.; Zeng, H.; Yuan, G.; Ding, W. Challenges and solutions for the additive manufacturing of biodegradable Magnesium implants. *Engineering* **2020**, *6*, 1267−1275.

https://doi.org/10.1021/acsomega.4c04870
ACS Omega 2024, 9, 44042−44075

(204) Qin, Y.; Wen, P.; Guo, H.; Xia, D.; Zheng, Y.; Jauer, L.; Poprawe, R.; Voshage, M.; Schleifenbaum, J. H. Additive manufacturing of biodegradable metals: Current research status and future perspectives. *Acta Biomater.* **2019**, *98*, 3−22.
(205) Oriňáková, R.; Oriňák, A.; Bučková, L. M.; Giretová, M.; Medvecký, Ľ.; Labbanczová, E.; Kupková, M.; Hrubovčáková, M.; Kovaľ, K. Iron based degradable foam structures for potential orthopedic applications. *Int. J. Electrochem. Sci.* **2013**, *8*, 12451−12465.
(206) Chou, D. T.; Wells, D.; Hong, D.; Lee, B.; Kuhn, H.; Kumta, P. N. Novel processing of Iron-Manganese alloy-based biomaterials by inkjet 3-D printing. *Acta Biomater.* **2013**, *9*, 8593−8603.
(207) Zhang, J.; Zhao, S.; Zhu, M.; Zhu, Y.; Zhang, Y.; Liu, Z.; Zhang, C. 3D-printed Magnetic Fe_3O_4 /MBG/PCL composite scaffolds with multifunctionality of bone regeneration, local anticancer drug delivery and hyperthermia. *J. Mater. Chem. Part B* **2014**, *2*, 7583−7595.
(208) Yang, C.; Huan, Z.; Wang, X.; Wu, C.; Chang, J. 3D printed Fe scaffolds with HA nanocoating for bone regeneration. *ACS Biomater. Sci. Eng.* **2018**, *4*, 608−616.
(209) Li, Y.; Jahr, H.; Lietaert, K.; Pavanram, P.; Yilmaz, A.; Fockaert, L. I.; Leeflang, M. A.; Pouran, B.; Gonzalez-Garcia, Y.; Weinans, H.; Mol, J. M. C.; Zhou, J.; Zadpoor, A. A. Additively manufactured biodegradable porous Iron. *Acta Biomater.* **2018**, *77*, 380−393.
(210) Putra, N. E.; Leeflang, M. A.; Minneboo, M.; Taheri, P.; Fratila-Apachitei, L. E.; Mol, J. M. C.; Zhou, J.; Zadpoor, A. A. Extrusion-based 3D printed biodegradable porous Iron. *Acta Biomater.* **2021**, *121*, 741−756.
(211) Wen, P.; Voshage, M.; Jauer, L.; Chen, Y.; Qin, Y.; Poprawe, R.; Schleifenbaum, J. H. Laser additive manufacturing of Zn metal parts for biodegradable applications: Processing, formation quality and mechanical properties. *Mater. Des.* **2018**, *155*, 36−45.
(212) Cockerill, I.; Su, Y.; Sinha, S.; Qin, Y. X.; Zheng, Y.; Young, M. L.; Zhu, D. Porous Zinc scaffolds for bone tissue engineering applications: A novel additive manufacturing and casting approach. *Mater. Sci. Eng.Part C* **2020**, *110*, No. 110738.
(213) Wen, P.; Qin, Y.; Chen, Y.; Voshage, M.; Jauer, L.; Poprawe, R.; Schleifenbaum, J. H. Laser additive manufacturing of Zn porous scaffolds: Shielding gas flow, surface quality and densification. *J. Mater. Sci. Technol.* **2019**, *35*, 368−376.
(214) Qin, Y.; Wen, P.; Voshage, M.; Chen, Y.; Schückler, P. G.; Jauer, L.; Xia, D.; Guo, H.; Zheng, Y.; Schleifenbaum, J. H. Additive manufacturing of biodegradable Zn-XWE43 porous scaffolds: Formation quality, microstructure and mechanical properties. *Mater. Des.* **2019**, *181*, No. 107937.
(215) Voshage, M.; Megahed, S.; Schückler, P. G.; Wen, P.; Qin, Y.; Jauer, L.; Poprawe, R.; Schleifenbaum, J. H. Additive manufacturing of biodegradable Zn-XMg alloys: Effect of Mg content on manufacturability, microstructure and mechanical properties. *Mater. Today Commun.* **2022**, *32*, No. 103805.
(216) Feng, J.; Tang, Y.; Liu, J.; Zhang, P.; Liu, C.; Wang, L. Bio-high entropy alloys: Progress, challenges, and opportunities. *Front. Bioeng. Biotechnol.* **2022**, *10*, No. 977282.
(217) Yeh, J. W.; Chen, S. K.; Lin, S. J.; Gan, J. Y.; Chin, T. S.; Shun, T. T.; Tsau, C. H.; Chang, S. Y. Nanostructured high-entropy alloys with multiple principal elements: Novel alloy design concepts and outcomes. *Adv. Eng. Mater.* **2004**, *6*, 299−303.
(218) Yeh, J. W. Recent progress in high-entropy alloys. *Annales de Chimie: Science des Materiaux* **2006**, *31*, 633−648.
(219) Akmal, M.; Hussain, A.; Afzal, M.; Lee, Y. I.; Ryu, H. J. Systematic Study of (MoTa)XNbTiZr medium- and high-entropy alloys for biomedical implants- in vivo biocompatibility examination. *J. Mater. Sci. Technol.* **2021**, *78*, 183−191.
(220) Nagase, T.; Iijima, Y.; Matsugaki, A.; Ameyama, K.; Nakano, T. Design and fabrication of Ti−Zr-Hf-Cr-Mo and Ti−Zr-Hf-Co-Cr-Mo high-entropy alloys as metallic biomaterials. *Mater. Sci. Eng. Part C* **2020**, *107*, No. 110322.
(221) Ishimoto, T.; Ozasa, R.; Nakano, K.; Weinmann, M.; Schnitter, C.; Stenzel, M.; Matsugaki, A.; Nagase, T.; Matsuzaka, T.; Todai, M.; Kim, H. S.; Nakano, T. Development of TiNbTaZrMo bio-high entropy alloy (BioHEA) super-solid solution by selective laser melting, and its improved mechanical property and biocompatibility. *Scr. Mater.* **2021**, *194*, No. 113658.
(222) Deng, C.; Wang, C.; Chai, L.; Wang, T.; Luo, J. Mechanical and chemical properties of CoCrFeNiMo0.2 high entropy alloy coating fabricated on Ti6Al4V by laser cladding. *Intermetallics (Barking)* **2022**, *144*, No. 107504.
(223) Feng, J.; Wei, D.; Zhang, P.; Yu, Z.; Liu, C.; Lu, W.; Wang, K.; Yan, H.; Zhang, L.; Wang, L. Preparation of TiNbTaZrMo high-entropy alloy with tunable young's modulus by selective laser melting. *J. Manuf. Process.* **2023**, *85*, 160−165.
(224) Kumar, P.; Jain, N. K.; Jaiswal, S.; Gupta, S. Development of Ti-Ta-Nb-Mo-Zr high entropy alloy by μ-plasma arc additive manufacturing process for knee implant applications and its biocompatibility evaluation. *J. Mater. Res. Technol.* **2023**, *22*, 541−555.
(225) Gokcekaya, O.; Ishimoto, T.; Nishikawa, Y.; Kim, Y. S.; Matsugaki, A.; Ozasa, R.; Weinmann, M.; Schnitter, C.; Stenzel, M.; Kim, H. S.; Miyabayashi, Y.; Nakano, T. Novel single crystalline-like non-equiatomic TiZrHfNbTaMo bio-high entropy alloy (BioHEA) developed by laser powder bed fusion. *Mater. Res. Lett.* **2023**, *11*, 274−280.
(226) Zhao, G.; Shao, X.; Zhang, Q.; Wu, Y.; Wang, Y.; Chen, X.; Tian, H.; Liu, Y.; Liu, Y.; Lu, B. Porous bio-high entropy alloy scaffolds fabricated by direct ink writing. *J. Mater. Sci. Technol.* **2023**, *157*, 21−29.
(227) Balla, V. K.; Bodhak, S.; Bose, S.; Bandyopadhyay, A. Porous Tantalum structures for bone implants: Fabrication, mechanical and in vitro biological properties. *Acta Biomater.* **2010**, *6* (8), 3349−3359.
(228) Habijan, T.; Haberland, C.; Meier, H.; Frenzel, J.; Wittsiepe, J.; Wuwer, C.; Greulich, C.; Schildhauer, T. A.; Köller, M. The biocompatibility of dense and porous Nickel-Titanium produced by selective laser melting. *Mater. Sci. Eng. Part C* **2013**, *33*, 419−426.
(229) Stenlund, P.; Kurosu, S.; Koizumi, Y.; Suska, F.; Matsumoto, H.; Chiba, A.; Palmquist, A. osseointegration enhancement by Zr doping of Co-Cr-Mo implants fabricated by electron beam melting. *Addit. Manuf.* **2015**, *6*, 6−15.
(230) Jahadakbar, A.; Moghaddam, N. S.; Amerinatanzi, A.; Dean, D.; Karaca, H. E.; Elahinia, M. Finite element simulation and additive manufacturing of stiffness-matched NiTi fixation hardware for mandibular reconstruction surgery. *Bioengineering* **2016**, *3*, 36.
(231) Shah, F. A.; Omar, O.; Suska, F.; Snis, A.; Matic, A.; Emanuelsson, L.; Norlindh, B.; Lausmaa, J.; Thomsen, P.; Palmquist, A. Long-term osseointegration of 3D printed CoCr constructs with an interconnected open-pore architecture prepared by electron beam melting. *Acta Biomater.* **2016**, *36*, 296−309.
(232) Tai, B. L.; Kao, Y. T.; Payne, N.; Zheng, Y.; Chen, L.; Shih, A. J. 3D printed composite for simulating thermal and mechanical responses of the cortical bone in orthopaedic surgery. *Med. Eng. Phys.* **2018**, *61*, 61−68.
(233) Bartolomeu, F.; Costa, M. M.; Alves, N.; Miranda, G.; Silva, F. S. Additive manufacturing of NiTi-Ti6Al4V multi-material cellular structures targeting orthopedic implants. *Opt. Lasers Eng.* **2020**, *134*, No. 106208.
(234) Peto, M.; Ramírez-Cedillo, E.; Hernández, A.; Siller, H. R. Structural design optimization of knee replacement implants for additive manufacturing. *Procedia Manuf.* **2019**, *34*, 574−583.
(235) Tilton, M.; Lewis, G. S.; Bok Wee, H.; Armstrong, A.; Hast, M. W.; Manogharan, G. Additive manufacturing of fracture fixation implants: Design, material characterization, biomechanical modeling and experimentation. *Addit. Manuf.* **2020**, *33*, No. 101137.
(236) Jung, H. Do; Jang, T. S.; Lee, J. E.; Park, S. J.; Son, Y.; Park, S. H. Enhanced bioactivity of Titanium-coated Polyetheretherketone implants created by a high-temperature 3D printing process. *Biofabrication* **2019**, *11*, No. 045014.

https://doi.org/10.1021/acsomega.4c04870
ACS Omega 2024, 9, 44042−44075

(237) Shin, J. H.; Kim, S. H.; Kwon, S. S.; Park, W. Il. Direct CVD growth of Graphene on three-dimensionally-shaped dielectric substrates. *Carbon* **2018**, *129*, 785−789.
(238) Dutta, R. C.; Dey, M.; Dutta, A. K.; Basu, B. Competent processing techniques for scaffolds in tissue engineering. *Biotechnol. Adv.* **2017**, *35*, 240−250.
(239) Chen, Q.; Mangadlao, J. D.; Wallat, J.; De Leon, A.; Pokorski, J. K.; Advincula, R. C. 3D printing biocompatible Polyurethane/Poly (lactic acid)/Graphene oxide nanocomposites: Anisotropic properties. *ACS Appl. Mater. Interfaces* **2017**, *9*, 4015−4023.
(240) Oladapo, B. I.; Zahedi, S. A.; Adeoye, A. O. M. 3D printing of bone scaffolds with hybrid biomaterials. *Composites Part B* **2019**, *158*, 428−436.
(241) Arif, M. F.; Alhashmi, H.; Varadarajan, K. M.; Koo, J. H.; Hart, A. J.; Kumar, S. Multifunctional performance of Carbon nanotubes and Graphene nanoplatelets reinforced PEEK composites enabled via FFF additive manufacturing. *Composites Part B* **2020**, *184*, No. 107625.
(242) Larsson, L.; Marattukalam, J. J.; Paschalidou, E.-M.; Hjorvarsson, B.; Ferraz, N.; Persson, C. Biocompatibility of a Zr-based metallic glass enabled by additive manufacturing. *ACS Appl. Bio. Mater.* **2022**, *5*, 5741−5753.
(243) Nadammal, N.; Rajput, M.; Gupta, S. K.; Ivanov, E.; Reddy, A. S.; Suwas, S.; Chatterjee, K. Laser powder bed fusion additive manufacturing of a low-modulus Ti-35Nb-7Zr-5Ta alloy for orthopedic applications. *ACS Omega* **2022**, *7*, 8506−8517.
(244) Grubova, I. Y.; Surmenev, R. A.; Neyts, E. C.; Koptyug, A. V.; Volkova, A. P.; Surmeneva, M. A. Combined first-principles and experimental study on the microstructure and mechanical characteristics of the multicomponent additive-manufactured Ti-35Nb-7Zr-5Ta alloy. *ACS Omega* **2023**, *8*, 27519−27533.
(245) Corona-Castuera, J.; Rodriguez-Delgado, D.; Henao, J.; Castro-Sandoval, J. C.; Poblano-Salas, C. A. Design and fabrication of a customized partial hip prosthesis employing CT-scan data and lattice porous structures. *ACS Omega* **2021**, *6*, 6902−6913.
(246) Rama, M.; Mohan, S. G.; Sridhar, T. M.; Nambi Raj, N. A.; Vijayalakshmi, U. Comparative Analysis of Electrospun Silk Fibroin/Chitosan Sandwich-Structured Scaffolds for Osteo Regeneration: Evaluating Mechanical Properties, Biological Performance, and Drug Release. *ACS Omega* **2024**, *9*, 28072−28092.
(247) Xue, J.; Wu, T.; Dai, Y.; Xia, Y. Electrospinning and Electrospun Nanofibers: Methods, Materials, and Applications. *Chem. Rev.* **2019**, *119*, 5298−5415.
(248) Mushtaq Alam, M.; Kumar, S.; Gopan, G.; Mani, M.; Kannan, S. Fabrication, mechanical, finite element and in vitro evaluation of 3D printed Polylactide/Biphasic Calcium phosphate composite blends. *Mater. Chem. Phys.* **2024**, *318*, No. 129306.
(249) Mushtaq Alam, M.; Sugail, M.; Kannan, S. Development, physiochemical characterization, mechanical and finite element analysis of 3D printed Polylactide-β-TCP/α-Al2O3 composite. *J. Mech. Behav. Biomed. Mater.* **2023**, *147*, No. 106161.
(250) Alam, M. M.; Ezhilan, M.; Saha, S.; Gopan, G.; Mani, M.; Kannan, S. Design, fabrication, mechanical, and in vitro evaluation of 3D printed ZrO2 reinforced Polylactide scaffolds through fused deposition modeling. *Mater. Chem. Front.* **2023**, *7*, 464−475.
(251) Alam, M.; Manivannan, E.; Rizwan, M.; Gopan, G.; Mani, M.; Kannan, S. 3D printed Polylactide-based Zirconia-toughened Alumina composites: Fabrication, mechanical, and in vitro evaluation. *Int. J. Appl. Ceram. Technol.* **2024**, *21*, 957−971.
(252) Madar Saheb, M. A.; Kanagaraj, M.; Kannan, S. Exploring the biomedical potential of PLA/Dysprosium phosphate composites via extrusion-based 3D printing: Design, morphological, mechanical, and multimodal imaging and finite element modeling. *ACS Appl. Bio. Mater.* **2023**, *6*, 5414−5425.
(253) Thangavel, M.; Elsen Selvam, R. Review of physical, mechanical, and biological characteristics of 3D-printed bioceramic scaffolds for bone tissue engineering applications. *ACS Biomater. Sci. Eng.* **2022**, *8*, 5060−5093.
(254) Meng, M.; Wang, J.; Huang, H.; Liu, X.; Zhang, J.; Li, Z. 3D printing metal implants in orthopedic surgery: Methods, applications and future prospects. *J. Orthopaed. Translat.* **2023**, *42*, 94−112.
(255) Kumawat, S.; Deshmukh, S. R.; Ghorpade, R. R. Fabrication of Ti-6Al-4v cellular lattice structure using selective laser melting for orthopedic use: A review. *Mater. Today Proc.* **2023**, DOI: 10.1016/j.matpr.2023.08.053.
(256) Kang, J.; Dong, E.; Li, D.; Dong, S.; Zhang, C.; Wang, L. Anisotropy characteristics of microstructures for bone substitutes and porous implants with application of additive manufacturing in orthopaedic. *Mater. Des.* **2020**, *191*, No. 108608.
(257) Ni, J.; Ling, H.; Zhang, S.; Wang, Z.; Peng, Z.; Benyshek, C.; Zan, R.; Miri, A. K.; Li, Z.; Zhang, X.; Lee, J.; Lee, K. J.; Kim, H. J.; Tebon, P.; Hoffman, T.; Dokmeci, M. R.; Ashammakhi, N.; Li, X.; Khademhosseini, A. Three-dimensional printing of metals for biomedical applications. *Mater. Today Bio.* **2019**, *3*, No. 100024.
(258) Kulcsár, K.; Buzgo, M.; Costa, P. F.; Zsoldos, I. Optimal microstructure and mechanical properties of open-cell porous Titanium structures produced by selective laser melting. *Front Bioeng. Biotechnol.* **2022**, *10*, No. 1022310.
(259) Palmquist, A.; Jolic, M.; Hryha, E.; Shah, F. A. Complex geometry and integrated macro-porosity: Clinical applications of electron beam melting to fabricate bespoke bone-anchored implants. *Acta Biomater.* **2023**, *156*, 125−145.
(260) Chua, K.; Khan, I.; Malhotra, R.; Zhu, D. Additive manufacturing and 3D printing of metallic biomaterials. *Eng. Regen.* **2021**, *2*, 288−299.
(261) Abbas, M.K.G.; Ramesh, S.; Lee, K.Y. S.; Wong, Y.H.; Ganesan, P.; Ramesh, S.; Alengaram, U. J.; Teng, W.D.; Purbolaksono, J. Effects of Sintering additives on the densification and properties of Alumina-toughened Zirconia ceramic composites. *Ceram. Int.* **2020**, *46*, 27539−27549.
(262) Gupta, K.; Meena, K. Artificial bone scaffolds and bone joints by additive manufacturing: A review. *Bioprinting* **2023**, *31*, No. e00268.
(263) Wu, S. Q.; Lu, Y. J.; Gan, Y. L.; Huang, T. T.; Zhao, C. Q.; Lin, J. J.; Guo, S.; Lin, J. X. Microstructural evolution and microhardness of a selective-laser-melted Ti-6Al-4V alloy after post heat treatments. *J. Alloys Compd.* **2016**, *672*, 643−652.
(264) Bandyopadhyay, A.; Zhang, Y.; Bose, S. Recent developments in metal additive manufacturing. *Curr. Opin. Chem.l Eng.* **2020**, *28*, 96−104.
(265) Bhuvanesh Kumar, M.; Sathiya, P. Methods and materials for additive manufacturing: A critical review on advancements and challenges. *Thin-Walled Struct.* **2021**, *159*, No. 107228.
(266) Chaudhary, S.; Avinashi, S. K.; Rao, J.; Gautam, C. Recent advances in additive manufacturing, applications and challenges for dentistry: A review. *ACS Biomater. Sci. Eng.* **2023**, *9*, 3987−4019.
(267) Javaid, M.; Haleem, A. Current status and challenges of additive manufacturing in orthopaedics: An overview. *J. Clin. Orthop. Trauma* **2019**, *10*, 380−386.
(268) Wu, Y.; Liu, J.; Kang, L.; Tian, J.; Zhang, X.; Hu, J.; Huang, Y.; Liu, F.; Wang, H.; Wu, Z. An overview of 3D printed metal implants in orthopedic applications: Present and future perspectives. *Heliyon* **2023**, *9*, e17718.
(269) Zhao, Y.; Wang, Z.; Zhao, J.; Hussain, M.; Wang, M. Additive manufacturing in orthopedics: A review. *ACS Biomater. Sci. Eng.* **2022**, *8*, 1367−1380.
(270) Balou, S.; Ahmed, I.; Priye, A. From waste to filament: Development of biomass-derived activated Carbon-reinforced PETG composites for sustainable 3D Printing. *ACS Sustain. Chem. Eng.* **2023**, *11*, 12667−12676.
(271) Paramatti, M.; Romani, A.; Pugliese, G.; Levi, M. PLA feedstock filled with spent coffee grounds for new product applications with large-format material extrusion additive manufacturing. *ACS Omega* **2024**, *9*, 6423−6431.
(272) Papadopoulos, L.; Pezzana, L.; Malitowski, N. M.; Sangermano, M.; Bikiaris, D. N.; Robert, T. UV-curing additive manufacturing of bio-based thermosets: Effect of diluent concen-

https://doi.org/10.1021/acsomega.4c04870
ACS Omega 2024, 9, 44042−44075

tration on printing and material properties of itaconic acid-based materials. *ACS Omega* **2023**, *8*, 31009−31020.
(273) Voet, V. S. D.; Strating, T.; Schnelting, G. H. M.; Dijkstra, P.; Tietema, M.; Xu, J.; Woortman, A. J. J.; Loos, K.; Jager, J.; Folkersma, R. Biobased Acrylate photocurable resin formulation for stereolithography 3D printing. *ACS Omega* **2018**, *3*, 1403−1408.
(274) Zhou, W.; Dong, X.; He, Y.; Zheng, W.; Leng, J. In-vitro and in-vivo studies of 4D printed shape memory scaffolds with bioactive fillers and coating for enhanced bone tissue regeneration. *Smart Mater. Struct.* **2022**, *31*, No. 105002.
(275) Haleem, A.; Javaid, M.; Vaishya, R. 5D printing and its expected applications in orthopaedics. *J. Clin. Orthopaed. Trauma* **2019**, *10*, 809−810.
(276) Brown, T. D.; Dalton, P. D.; Hutmacher, D. W. Direct writing by way of melt electrospinning. *Adv. Mater.* **2011**, *23*, 5651−5657.
(277) O'Neill, K. L.; Dalton, P. D. A Decade of Melt Electrowriting. *Small Methods* **2023**, *7*, No. 2201589.
(278) Kade, J. C.; Dalton, P. D. Polymers for melt electrowriting. *Adv. Healthc. Mater.* **2021**, *10*, No. 2001232.
(279) Großhaus, C.; Bakirci, E.; Berthel, M.; Hrynevich, A.; Kade, J. C.; Hochleitner, G.; Groll, J.; Dalton, P. D. Melt electrospinning of nanofibers from medical-grade Poly(ε-Caprolactone) with a modified nozzle. *Small* **2020**, *16*, No. 2003471.
(280) Shahverdi, M.; Seifi, S.; Akbari, A.; Mohammadi, K.; Shamloo, A.; Movahhedy, M. R. Melt electrowriting of PLA, PCL, and composite PLA/PCL scaffolds for tissue engineering application. *Sci. Rep.* **2022**, *12*, 19935.
(281) Darroch, C.; Asaro, G. A.; Gréant, C.; Suku, M.; Pien, N.; van Vlierberghe, S.; Monaghan, M. G. Melt electrowriting of a biocompatible photo-crosslinkable Poly(D,L-Lactic Acid)/Poly(ε-Caprolactone)-based material with tunable mechanical and functionalization properties. *J. Biomed. Mater. Res. Part A* **2023**, *111*, 851−862.
(282) Saidy, N. T.; Shabab, T.; Bas, O.; Rojas-González, D. M.; Menne, M.; Henry, T.; Hutmacher, D. W.; Mela, P.; De-Juan-Pardo, E. M. Melt electrowriting of complex 3D anatomically relevant scaffolds. *Front. Bioeng. Biotechnol.* **2020**, *8*, 793.
(283) Luposchainsky, S.; Jörissen, S.; Nüchter, A.; Dalton, P. D. Melt electrowriting of Poly(Dioxanone) filament using a multi-axis robot. *Macromol. Mater. Eng.* **2022**, *307*, No. 2200450.
(284) Zhou, X.; Hou, Y.; Lin, J. A review on the processing accuracy of two-photon polymerization. *AIP Adv.* **2015**, *5*, No. 030701.
(285) Faraji Rad, Z.; Prewett, P. D.; Davies, G. J. High-resolution two-photon polymerization: The most versatile technique for the fabrication of microneedle arrays. *Microsys. Nanoeng.* **2021**, *7*, 71.
(286) Marschner, D. E.; Pagliano, S.; Huang, P. H.; Niklaus, F. A methodology for two-photon polymerization micro 3D printing of objects with long overhanging structures. *Addit. Manuf.* **2023**, *66*, No. 103474.
(287) Chen, J.; Zhou, H.; Fan, Y.; Gao, G.; Ying, Y.; Li, J. 3D printing for bone repair: Coupling infection therapy and defect regeneration. *Chem. Eng. J.* **2023**, *471*, No. 144537.
(288) Ovsianikov, A.; Chichkov, B.; Adunka, O.; Pillsbury, H.; Doraiswamy, A.; Narayan, R. J. Rapid prototyping of ossicular replacement prostheses. *Appl. Surf. Sci.* **2007**, *253*, 6603−6607.
(289) Kampleitner, C.; Changi, K.; Felfel, R. M.; Scotchford, C. A.; Sottile, V.; Kluger, R.; Hoffmann, O.; Grant, D. M.; Epstein, M. M. Preclinical biological and physicochemical evaluation of two-photon engineered 3D biomimetic copolymer scaffolds for bone healing. *Biomater. Sci.* **2020**, *8*, 1683−1694.
(290) Momeni, F.; Hassani, N. S.; Liu, X.; Ni, J. A review of 4D printing. *Mater. Des.* **2017**, *122*, 42−79.
(291) Miao, S.; Castro, N.; Nowicki, M.; Xia, L.; Cui, H.; Zhou, X.; Zhu, W.; Lee, S. J.; Sarkar, K.; Vozzi, G.; Tabata, Y.; Fisher, J.; Zhang, L. G. 4D printing of polymeric materials for tissue and organ regeneration. *Mater. Today* **2017**, *20*, 577−591.
(292) Haleem, A.; Javaid, M. Expected role of four-dimensional (4D) CT and four-dimensional (4D) MRI for the manufacturing of smart orthopaedics implants using 4D printing. *J. Clin. Orthopaed.-Trauma* **2019**, *10*, S234−S235.
(293) Sahafnejad-Mohammadi, I.; Karamimoghadam, M.; Zolfagharian, A.; Akrami, M.; Bodaghi, M. 4D printing technology in medical engineering: A narrative review. *J. Braz. Soc. Mech. Sci. Eng.* **2022**, *44*, 233.
(294) Grinberg, D.; Siddique, S.; Le, M. Q.; Liang, R.; Capsal, J. F.; Cottinet, P. J. 4D printing based piezoelectric composite for medical applications. *J. Polym. Sci. Part B* **2019**, *57*, 109−115.
(295) Ghalayaniesfahani, A.; Oostenbrink, B.; van Kasteren, H.; Gibson, I.; Mehrpouya, M. 4D printing of biobased shape memory sandwich structures. *Polymer* **2024**, *307*, No. 127252.
(296) Liu, X.; Chen, W.; Shao, B.; Zhang, X.; Wang, Y.; Zhang, S.; Wu, W. Mussel patterned with 4D biodegrading elastomer durably recruits regenerative macrophages to promote regeneration of craniofacial bone. *Biomaterials* **2021**, *276*, No. 120998.
(297) Fu, P.; Li, H.; Gong, J.; Fan, Z.; Smith, A. T.; Shen, K.; Khalfalla, T. O.; Huang, H.; Qian, X.; McCutcheon, J. R.; Sun, L. 4D printing of polymers: Techniques, materials, and prospects. *Prog. Polym. Sci.* **2022**, *126*, No. 101506.
(298) Zeijderveld, J. V. 5D Printing: A New Branch of Additive Manufacturing. https://www.sculpteo.com/blog/2018/05/07/5d-printing-a-new-branch-of-additive-manufacturing. Accessed 7 May 2018.
(299) Nandagopal, R. Bangalore startup Ethereal Machines holds India flag high at CES 2018 with innovation prize. http://indianexpress.com/article/technology/tech-news-technology/bangalore-startup-ethereal-machines-holds-india-flag-high-at-ces-2018-with-innovation-prize-5018964. Accessed on 11 January 2018.
(300) Reddy, P. R.; Devi, P. A review on the advancements to additive manufacturing-4D and 5D printing. *Int. J. Mech. Prod. Eng. Res. Dev.* **2018**, *8*, 397−402.
(301) Das, M.; Alam, R.; Das, M.; Biswal, B.; Samal, B. P.; Patnaik, A.; Panda, S. K.; Owuor, P. S.; Patra, P.; Tiwary, C. S. Management of hard tissue abnormalities and digital orthopaedics using additive manufacturing techniques. *Oxf. Open Mater. Sci.* **2022**, *2*, 009.
(302) Vasiliadis, A. V.; Koukoulias, N.; Katakalos, K. From three-dimensional (3D)- to 6D-printing technology in orthopedics: Science fiction or scientific reality? *J. Funct. Biomater.* **2022**, *13*, 101.
(303) Georgantzinos, S. K.; Giannopoulos, G. I.; Bakalis, P. A. Additive manufacturing for effective smart structures: The idea of 6D printing. *J. Compos. Sci.* **2021**, *5*, 119.

https://doi.org/10.1021/acsomega.4c04870
ACS Omega 2024, 9, 44042−44075